INVESTIGATIONS OF OPEN-FRAMEWORK METAL OXALATES AND PHOSPHATES

A PROJECT REPORT SUBMITTED IN PARTIAL FULFILMENT OF THE REQUIREMENTS OF THE DEGREE OF MASTER OF SCIENCE AS A PART OF THE INTEGRATED Ph.D PROGRAMME

BY

R.VAIDHYANATHAN

TO

MANIPAL ACADEMY OF HIGHER EDUCATION

THROUGH

JAWAHARLAL NEHRU CENTRE FOR ADVANCED SCIENTIFIC RESEARCH, BANGALORE

MARCH 2000

STATEMENT

Certified that the work described here has been done under our supervision at Jawaharlal Nehru Centre for Advanced Scientific Research, Jakkur.

Prof.C.N.R. Rao,

Dr.S. Natarajan

CONTENTS

STATEMENT

ACKNOWLEDGEMENT

SUMMARY

1. AN OVERVIEW OF MICROPOROUS SOLIDS

1.1 Introduction

1.2 Zeolite and zeolite-like systems

1.3 open-framework phosphates

1.4 Microporous aluminophosphates

1.5 Open-framework metal phosphates and related systems

1.6 Carboxylates as open-frameworks

1.7 Synthetic considerations

1.8 Applications

2. SCOPE OF THE PRESENT INVESTIGATIONS

3. EXPERIMENTAL

3.1 Synthesis and characterization of zinc oxalate

3.2 Synthesis and characterization of microporous tin oxalate

3.3 Synthesis and characterization of amine oxalates and hierarchy of zinc oxalates

3.4 Synthesis and characterization of a zinc phosphate

3.5 Synthesis and characterization of tin phosphates

3.6 Characterization techniques

4. RESULTS AND DISCUSSION

4.1 Zinc oxalates with open-architectures

4.2 Tin (II) oxalate with open-architecture

4.3 Amine oxalates and their reaction with Zn^{II} ions

4.4 A zinc phosphate with open-architecture

4.5 Open-framework tin(II) phosphates

ACKNOWLEDGEMENTS

I wish to express my sincere gratitude to Prof.C.N.R.Rao, FRS for suggesting the problems, invaluable guidance and moral support, which have been instrumental in shaping me as a research student. He has taught me the art of science, the way of analyzing a problem, tackling it and how to be patient when things do not work.

I am very grateful to Dr.S.Natarajan for his invaluable suggestions, day to day guidance and continuous encouragement. He has provided much attention to me through out my work. More importantly, for allowing me to work in his lab. I am thankful to the faculties of JNCASR for the knowledge they offered me through the course work. I offer my sincere thanks to Prof.V.Krishnan and Dr.W.H.Madhusudhan. I am thankful to all the professors of Chemical Sciences Division, IISc the ample help, suggestions and constant encouragement.

I thank my colleagues S.Neeraj, A.Choudhury, G.Gautam, K.Jayaraman, S.Shivashankar and P.A.Prasad for being so nice to me and helping me in many ways, whenever I needed it. Without them my stay could not have been so pleasant. I am very grateful to my seniors especially S.Gopalan, S.Neeraj, Anupama and Sachin for the great help offered to me during my course work.

I am thankful to Sreenivas, Anil Kumar, Vasudevan, Ranganathan and the library staffs for all the help they have done to me in various aspects of my work. Finally I thank all my other friends in the hostel, who have made my hostel life a heavenly one.

SUMMARY

A variety of microporous open-framework materials have been synthesized employing hydrothermal methods in the presence of structure directing amines and characterized by X-ray crystallography and other techniques. The materials include, two zinc oxalates, a tin(II) oxalate, a zinc phosphate and a tin(II) phosphate. In another, reaction of amine oxalates with Zn^{2+} ions has been investigated as a route to synthesize the formation of hierarchy of oxalate structures.

Two novel zinc oxalates have been made by hydrothermal methods using 1,3-diamino propane and propylamine as structure directing agents. In $[H_3N(CH_2)_3NH_3]^{2+}[Zn_2(C_2O_4)_3]^{2-}3H_2O$, the linkages between the Zn and oxalate units gives rise to a layered architecture with 12-membered (6 Zn and 6 oxalates) honeycomb-like apertures wherein the amine and water molecules are located. In $2[C_3H_7NH_3]^{+}[Zn_2(C_2O_4)_3]^{2-}3H_2O$, the Zn-oxalate layers are crosslinked by another oxalate unit giving rise to a 3-D structure with two distinct channels where the amine and water molecules reside; the largest aperture in this 3-D structure involves a 20-membered ring (10 Zn and 10 oxalates). There is extensive hydrogen bonding between the amine, water and the framework. Adsorption studies indicate that water can be reversibly adsorbed in $2[C_3H_7NH_3]^{+}[Zn_2(C_2O_4)_3]^{2-}3H_2O$.

A layered tin (II) oxalate has been prepared by hydrothermal methods in the presence of structure-directing organic amines. In this

tin(II) oxalate, pseudo-pentagonal bipyramidal SnO_6 units form a puckered layered structure by sharing oxygens with the oxalate anions. The layers contain 8- and 12-membered apertures, and the amine (protonated N,N,N'N'-tetramethyl-1,2-diaminoethane) and water molecules are in the inter-lamellar region where they interact with the framework and with each other by hydrogen bonding. The lone pairs of the Sn (II) atoms point into the inter-lamellar region.

It is shown, for the first time, that open-framework zinc oxalates possessing linear chain, two-dimensional layer and three-dimensional structures are formed, in addition to monomeric and dimeric oxalates, by the reaction of amine oxalates with Zn^{2+} ions. On reacting the different amine oxalates (synthesized for the first time) with Zn^{2+} ions under different conditions, a variety of zinc oxalate structures were obtained. With guanidinium oxalate a monomeric zinc oxalate stabilized by hydrogen bonds with the guanidinium cations was formed. In another reaction, piperazine oxalate formed dimeric zinc oxalate structure hydrogen bonded with the amine molecules. With DABCO oxalate a chin-like zinc oxalate was obtained. While piperazine oxalate under a different reaction condition yielded a layered zinc oxalate with amine residing in the inter-lamellar regions. More importantly, a three-dimensional zinc oxalate has been made from a reaction between propylamine oxalate and Zn^{2+} ions, under hydrothermal conditions. The structure is identical to that of the zinc oxalate described in the section 4.1.1.

The hydrothermal synthesis and single crystal structure determination of a new open-framework zinc phosphate, $[NH_3(CH_2)_3NH_3]_2[NH_3(CH_2)_3NH_2]_2[Zn_{12}(OH_2)_2(PO_4)_{10}]H_2O$, is reported. The structure is made-up of tetrahedral linkages between ZnO_4, ZnO_3N and PO_4 moieties forming distinct channels. The structure-directing amine is present in two distinct forms, in the free state and as a ligand to zinc, the two species occurring in distinct channels.

Two new Sn(II) phosphate materials have been synthesized hydrothermally using 1,3-diaminopropane and 1,3-diamino-2-hydroxy propane as structure-directing organic amines. The solids have layered architecture and are isostructural. The structures consist of vertex sharing trigonal-pyramidal SnO_3 and tetrahedral PO_4 moieties forming infinite layers possessing 4- and 8-membered apertures. The interlamellar space is occupied by the protonated amine molecules, which interact with the framework through hydrogen bonding.

Papers based on the work have appeared in *Chem. Mater.*, 1999, **11**, 1633; *Chem. Mater.*, 1999, **11**, 3636; *J. Mater. Chem.*, 1999, **9**, 2789; *J.Mater. Chem.*, 1999, **9**, 1807.

INVESTIGATION OF OPEN-FRAMEWORK METAL OXALATES AND METAL PHOSPHATES

1. An Overview of Microporous Solids

1.1 Introduction

Designing porous materials exhibiting open-architectures has emerged as an active area of research owing to their potential use in catalysis and separation processes[1]. Microporous materials have pore sizes ranging from 5-20Å and include zeolites and other zeolite-like solids[2] (Fig.1.1). Various synthetic strategies have been employed in an attempt to synthesize novel materials with such open-architectures.

1.2 Zeolite and Zeolite-like systems

Zeolites are essentially aluminosilicates formed of basic TO_4 tetrahedra (T= Al, Si, P etc). The tetrahedra are linked in such a way as to form pores, channels and cages within the material such that significant portion of the material is literally empty space (Fig.1.2a&b). Thus zeolites are hydrated aluminosilicates constructed from AlO_4 and SiO_4 tetrahedra as shown, with the general formula $M^{n+}_{x/n}[(AlO_2)_X\ (SiO_2)]^{X-}$, where M= metal cations like Na^+, K^+ etc. Pure silica zeolites are neutral frameworks. On partially replacing the Si^{4+}ion by an Al^{3+} ion, a negative charge is introduced, resulting in an anionic framework. Interstitial cations or protons balance the negative charge of the framework. These

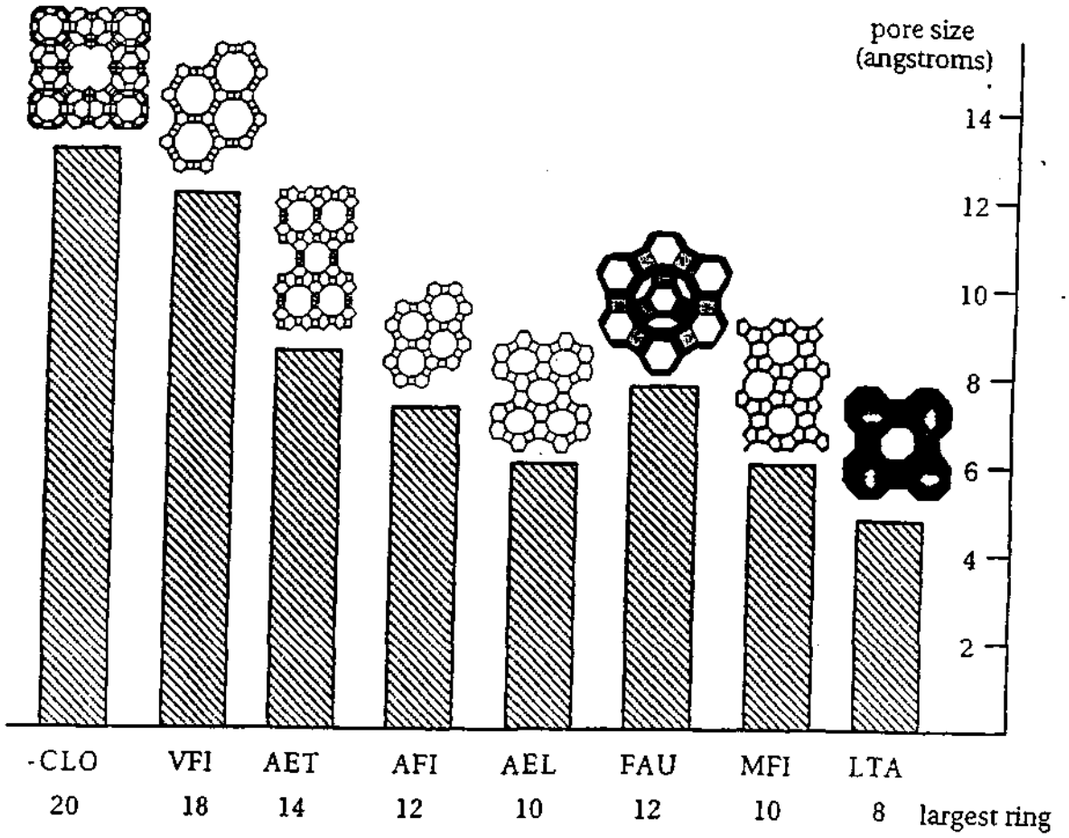

Figure 1.1

Correlation between the pore size of molecular sieves as measure from crystal structure and adsorption studies.

cations reside in the channels and cages present in the zeolitic framework. Apertures circumscribed by more than six tetrahedral (or oxygen) atoms are generally referred to as channels; whereas smaller openings are simply considered to form windows connecting larger cavities. A zeolitic channel can be described by a number of parameters. For example, its direction relative to the crystallographic axes, the number of tetrahedral atoms in the ring, and the free diameter of the channel. The channels present in these structures can be of different shapes and sizes. In ferrierite structure, the channel has an elliptical shape, whereas in ZSM-5 the channels are more circular (Fig.1.2a). Many zeolites contain different channel systems within a single structure. For example, ZSM-5 has two channel systems, a ten-ring sinusoidal channel running parallel to the a-axis and a ten-ring straight channel parallel to the b-axis.

Isomorphous substitutions as a part of the zeolitic framework by aluminium, gallium, germanium, beryllium, boron, iron, chromium, phosphorus, magnesium have been proposed by Barrer[3]. Such substitutions create a situation, wherein the numbers of occupiable sites are important. For example in $CaAl_2Si_2O_8$, replacement of Ca^{+2} with Na^+ ion would require twice the sites. Possible substitution would then be to replace Ca^{+2} and Al^{+3} simultaneously by Na^+ and Si^{+4}. This ensures that the number of cations and the available sites are the same. But in many zeolites, the number extra-framework cationic sites are far more than the number of cations usually required for balancing the framework charge.

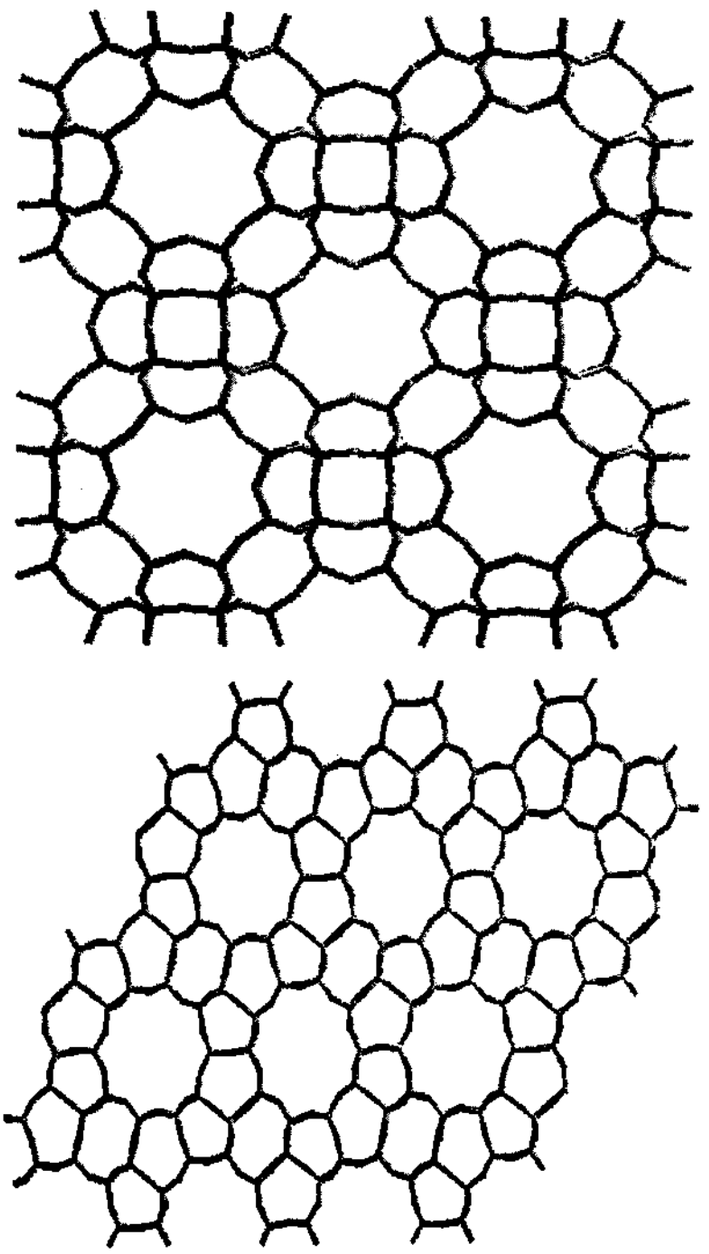

Figure 1.2

a) A polyhedral representation of zeolite ZSM-5 (MFI) viewed down the straight channel (no cations are shown for clarity).

b) A polyhedral representation of zeolite RHO with circular channels (no cations are shown for clarity).

This permits variations in Si/Al ratio in zeolites. However, Lowenstein's Rule[4], states that there can be no Al-O-Al or Si-O-Si linkages permissible within aluminosilicates and this limits the Si/Al ratio to be ≥ 1. Thus, aluminosilicates generally have strictly alternating AlO_4 and SiO_4 tetrahedra.

1.3 Open-framework Phosphates

Phosphorus, one of the highly electronegative elements, forms many oxygen compounds, which are based on the $[PO_4]^{3-}$ tetrahedra. This fact becomes obvious when one looks into the naturally occurring forms of both the silica and the aluminophosphate solids.

SiO_2	$AlPO_4$
Quartz	Berlinite
⇅ 867°	⇅ 815°±4°
Tridymite	Tridymite type
⇅ 1470°	⇅ 1025°±50°
Crystobalite	Crystobalite type

Inspite of the isomorphism between $AlPO_4$, BPO_4, $FePO_4$ and certain of the crystalline silica, there is little evidence of silica-bearing $AlPO_4$, BPO_4, $FePO_4$ in which a substitution of the kind $2\ Si^{+4} \rightleftharpoons P^{+5} + Al^{+3}$ and $Si^{+4} \rightleftharpoons P^{+5} + OH^-$ has been observed.[5,6] Nevertheless two

naturally occurring phosphate minerals viseite and kehoite have the structure of aluminosilicate analcime.

1.4 Microporous Aluminophosphates

Flanigen and co-workers performed the first systematic study of zeolite synthesis in the presence of phosphorus. Their study revealed the formation of analcime, phillipsite, chabazite, zeolite-A and zeolite-L frameworks with 5-25% phosphorus content[7]. Based on this, the synthesis of new family of microporous materials, which are silica-free, designated as $AlPO_4$-n have been reported[8]. These microporous phosphates have been synthesized by employing hydrothermal methods in the temperature range of 100°- 250°C, and using amines or quartenary ammonium salts as templates (all designated R). About 20 new structures were reported with the composition $AlPO_4.xR.yH_2O$, where x and y represent the number of template and water molecules required to fill the intra-crystalline voids respectively. Out of the twenty structures, six were layered structures, which collapsed on heating to 400°-600°C, due to the decomposition of interlayer template amines. On the other hand the remaining 3D-structures were stable even at temperatures above 1600°C. It is to be noted that many of the 3-D aluminophosphates are analogous to aluminosilicates.

These $AlPO_4$ molecular sieves exhibit intra-crystalline pore volume in the range of 0.04 to 0.35cm^3/g and adsorption pore sizes from 0.3-0.8nm. The AlPOs exhibit good molecular recognition properties. For

example, $AlPO_4$-20 admits only water but not methanol, $AlPO_4$-14 and $ALPO_4$-33 adsorb Xe (0.40nm) selectively over n-butane (0.43nm), while $AlPO_4$-17 and $AlPO_4$-18 adsorb parrafins (0.46nm) and excludes isoparaffins. $AlPO_4$-11 adsorbs cyclohexane (0.6nm) and rejects 2,2-dimethyl propane (0.62nm). The $AlPO_4$-11, like many silicates, is made up of 10-membered rings or 12-membered puckered rings. As a representative example the porous structure of $AlPO_4$-5 and VPI-5 are shown in figure 1.3a&b.

1.5 Open-framework Metal Phosphates and Related Systems

During the last two decades open-framework structures involving as much as 25 chemical elements have been synthesized and characterized. In addition to aluminosilicates and phosphates there are structures based on other elements such as oxides, oxyfluorides, nitrides, chalcogenides, germenates etc. Looking at the structural aspect of these novel materials one can realize that unlike zeolites and early AlPOs where it is essentially a corner-sharing ($[SiO_4]$,$[AlO_4]$etc) tetrahedra, these new architectures involve other complex polyhedra like $[XO_3]$, $[XO_4]$,$[XO_5]$ or $[XO_6]$ units, where X= Sn, Al, Zn etc. Investigations were then performed on the incorporation into the AlPO frameworks of elements with different valences in order to modify the chemical properties for catalysis, ion-exchange and so on. This led the Union Carbide researchers to synthesize several new series of materials, in particular the silicoaluminophosphates (SAPO-n),[9] metalaluminophosphates (MeAPO-n) and

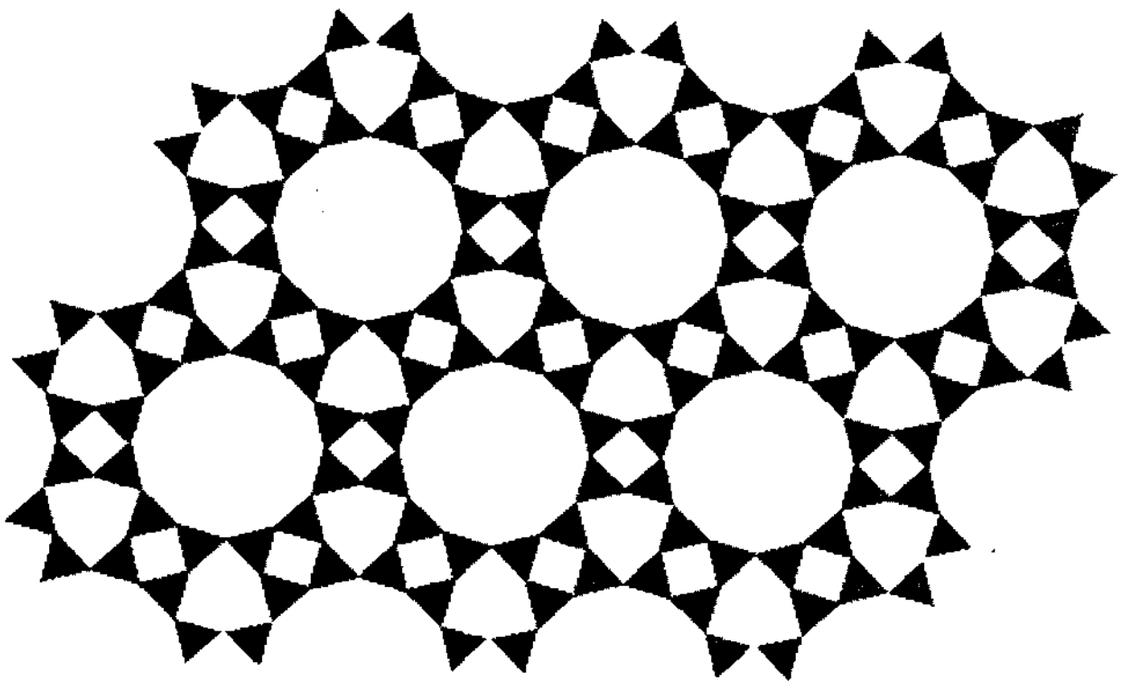

Figure 1.3

a) As a representative example the structure of $AlPO_4$-5 (no cations are shown for clarity). As can be seen the structure is formed by 4-, 6- and 12- membered rings.

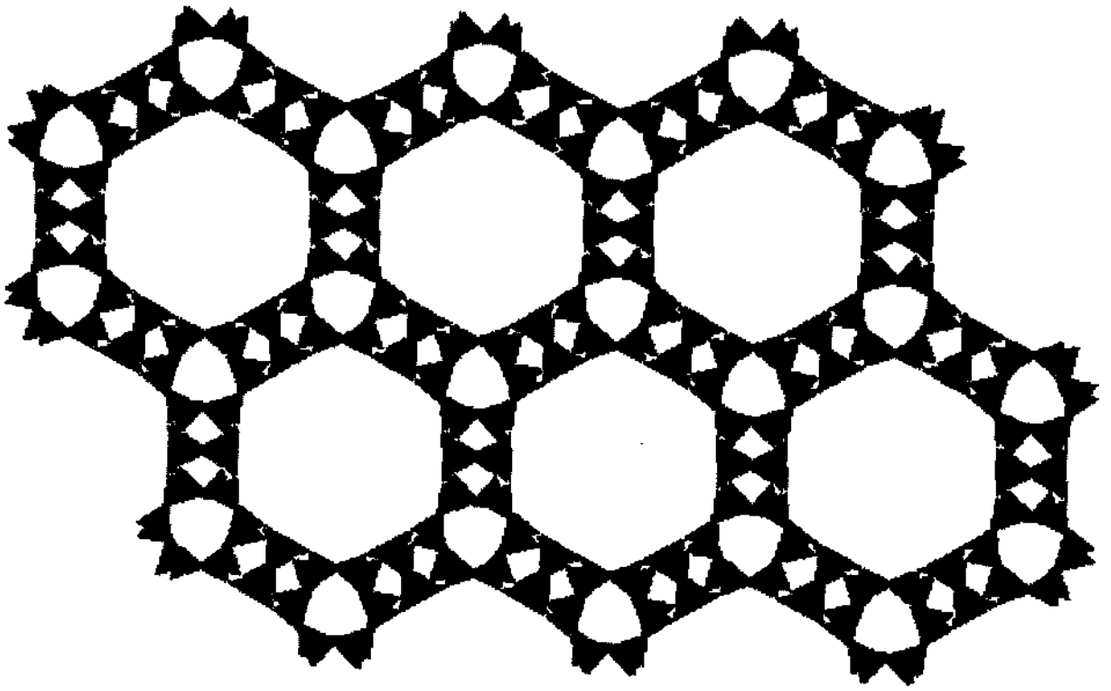

Figure 1.3

b) The structure of VPI-5 (VFI). The apertures are made up of 4-, 6- and 18- membered windows. VPI-5 has the largest pore dimensions of all the AlPO's known (no cations are shown for clarity).

metalsilicoaluminophosphates (MeAPSO-n).[10] The strategy was first to explore the divalent cations of the periodic table which can adopt tetrahedral coordination (e.g. Me = Mg^{2+}, Mn^{2+}, Fe^{2+}, Co^{2+} and Zn^{2+}). The weakly acidic pH of the reaction prevents the precipitation of the metal into hydroxides or oxides and facilitates their partial incorporation into the inorganic framework. These phases have framework compositions of general formula $(Si_xMe_wAl_yP_z)O_2$, where x varies from 0.0 to 0.2 and w from 0.0.25. The silicon substitutes preferentially at the phosphorus site whereas the metal substitutes exclusively for the aluminium. The introduction of these elements renders the framework negative and therefore requires charge-compensating cations, as in the aluminosilicates. When these cations are protons, the material exhibit acid catalytic properties which vary as a function of the structural type and the nature of the substituting element.[11] The incorporation of other elements, such as monovalent (Li), divalent (Be), trivalent (B, Cr, Fe, Ga), tetravalent (Ti, Ge) and pentavalent (As) into the AlPO framework has also been reported[12].

Hence, in combination with the molecular sieving property and Brönsted acidity that is present in these materials, they act as shape-selective acid catalysts.

1.5.1 Open-Framework Zinc and Tin phosphates

Zinc phosphates are the second largest metal phosphates that have been studied in the literature[13-17], after the phosphates of aluminium,

probably due to its predominant formation of ZnO_4 tetrahedra both in acidic and basic conditions. These structures are essentially made up of MO_4 and PO_4 tetrahedra and generally have M:P ratio less than unity. Harrison and Phillips[18,19] have made frameworks employing guanidinium cation as template. In these compounds the apertures are large inspite of the smaller size of the amine and also they do not have any M-O-M linkages though their M:P ratio is greater than unity. On the basis of the structures of $CN_3H_6.Zn_2(HPO_4)_2H_2PO_4$ and $(CN_3H_6)_2.Zn(HPO_4)_2$, they tentatively proposed the structure-directing effect for the guanidinium cations with respect to the zincophosphate networks. This cation appears to preferentially template a tetrahedral 12-ring framework motif and adopts a side-on orientation and presumably forms longish, but structurally significant N-H...O hydrogen bonding linkages. However, they stress that intra-framework hydrogen bonds, and the constraints imposed by the fixed Zn:P ratio in terms of preference for Zn-O-P and avoidance of Zn-O-Zn and P-O-P bonds are also clearly important in determining the three-dimensional frameworks of these materials. This distinctly relates to the Lowenstein's rule[4] for the avoidance of Al-O-Al linkages in aluminophosphates, but the similarity should not be overstressed, because zincophosphates never show any long range Zn/P site mixing akin to Al/Si disorder commonly observed in aluminosilicates. Thus, the local templating effect of the guanidinium cation cannot be simply correlated with the resulting overall crystal structures. In the

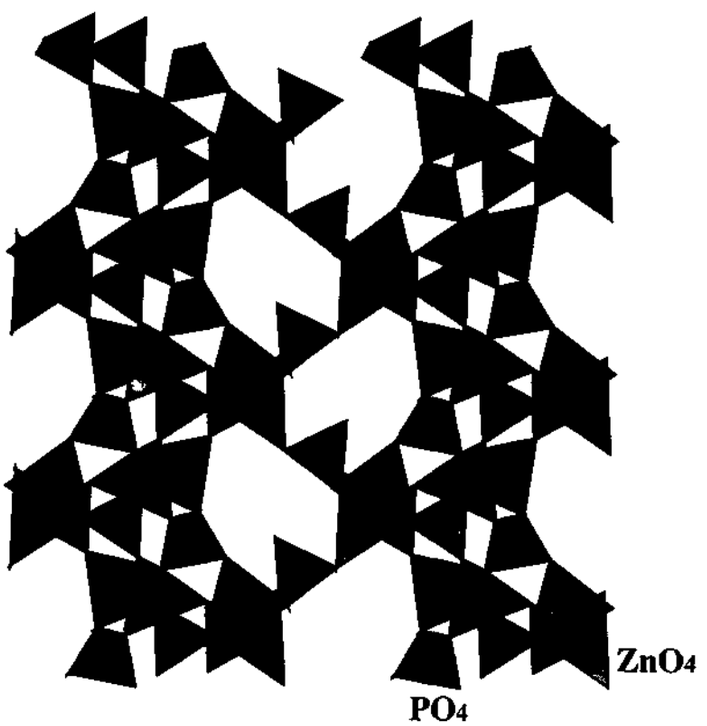

Figure 1.4

A polyhedral representation of the intersecting helical channel present in a chiral Zinc Phosphate.

novel phases $(CN_3H_6)_3.Zn_7(H2O)_4(PO4)6.H_3O$ the guanidinium cations also template 12-rings via structurally important N-H...O hydrogen bonding linkages, but also show remarkable "cooperative" effect to result in a group of three $CN_3H_6^+$ cations templating an 18-ring cavity in 'side-by-side" configuration.[18] Recently, Sevov *et al.*[20] reported the synthesis of a zinc phosphate with largest number of tetrahedral atoms in it. Neeraj *et al.*[21] made a chiral zinc phosphate using diethylenetriamine as structure directing agent (Fig.1.4). In addition, it is observed that the same SDA forms two more novel zinc phosphate structures, one possessing ladder-like layers[22] and another in which the amine acts as a ligand and forms a ten-membered ring, resulting in one-dimensional channels (Fig.1.5)[23].

Tin(II) phosphates have been studied in recent years because of the interest generated by the presence of lone pair of electrons in them[24-26]. In tin phosphates, unlike zinc phosphates the tin has three coordinations, with respect to oxygens (Fig.1.6). The fourth coordination, presumably being occupied by the lone-pair of electrons[27]. The presence of lone-pairs and their location in the structure, especially in layered materials, are so as to avoid repulsive interactions, resulting unique frameworks in the tin(II) phosphates. Tin(II) phosphate system, like the aluminophosphates forms chain, layered and three-dimensional architectures.[28]

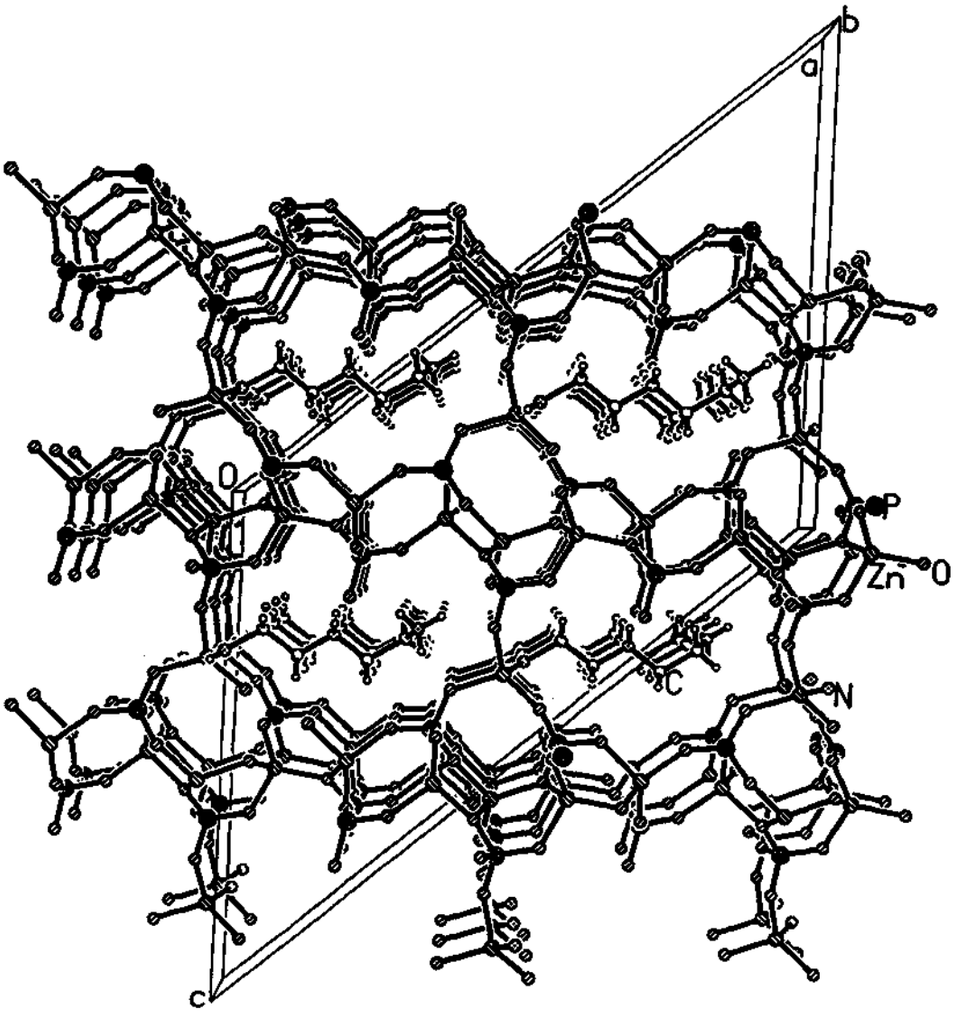

Figure 1.5

A perspective view of a zinc phosphate. The amine acts a ligand and forms one-dimensional channels made up of 10- membered rings.

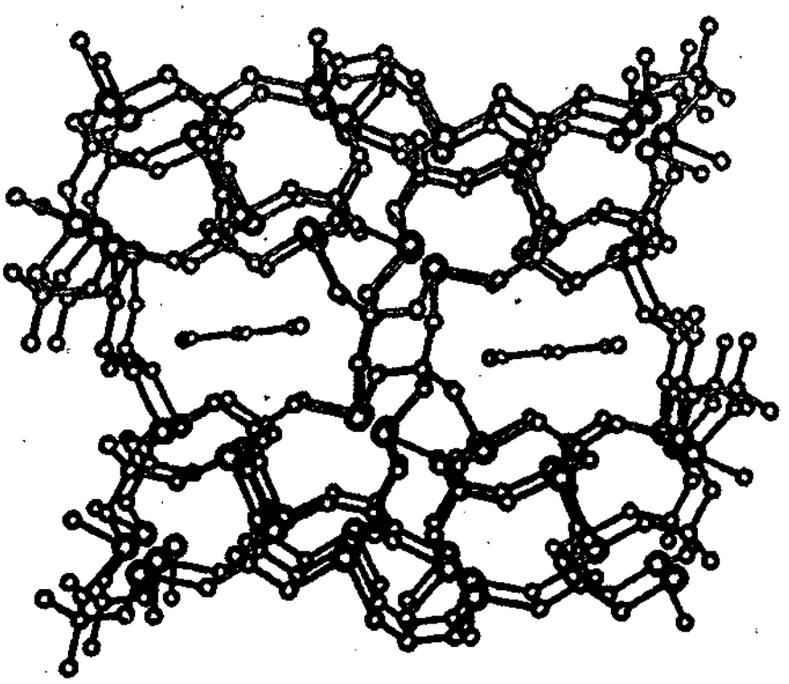

Figure 1.6

A tin(II) phosphate viewed along the b-axis exhibiting uniform 8-membered apertures.

1.6 Carboxyaltes as Open-frameworks

Following the successful use of mono- and diphosphonate in synthesis of three-dimensional open-architectures attempts were made to use carboxylates instead of phosphonates.[65,66,76] Lanthanides are known to form rigid links with dicaboxylates. Open-framework dicarboxylates of rare-earth metals, containing water in its channels have been reported during the last few years by Ferey *et al.*[29,30] The neodymium glutarate, made by them, consists of chains of edge-sharing $NdO_8(H_2O)$ polyhedra, along the a-axis. These chains are linked by two types of carboxylates, the first type bridges only between two Nd atoms along the [101] direction and the second type links the chains along the [010] direction.

Recently, a cobalt succinate[31] containing water in its channels has been synthesized hydrothermally. The structure consists of an infinite two-dimensional array of edge-sharing cobalt octahedra in the *bc-plane* covalently linked by two succinate anions. Cobalt atoms occupy three different crystallographic sites with an octahedral coordination of oxygen atoms arising from the two succinate ions and one hydroxyl group. The hydroxide oxygen atom is shared between three distinct cobalt atoms, establishing Co-μ_3-O(H) type of linkages. There are two distinct succinate units, the first is in the layers while the second acts as a pillar between the layers leading to a three-dimensional network. Magnetic susceptibility measured in the range of 2K to 300K indicates that the

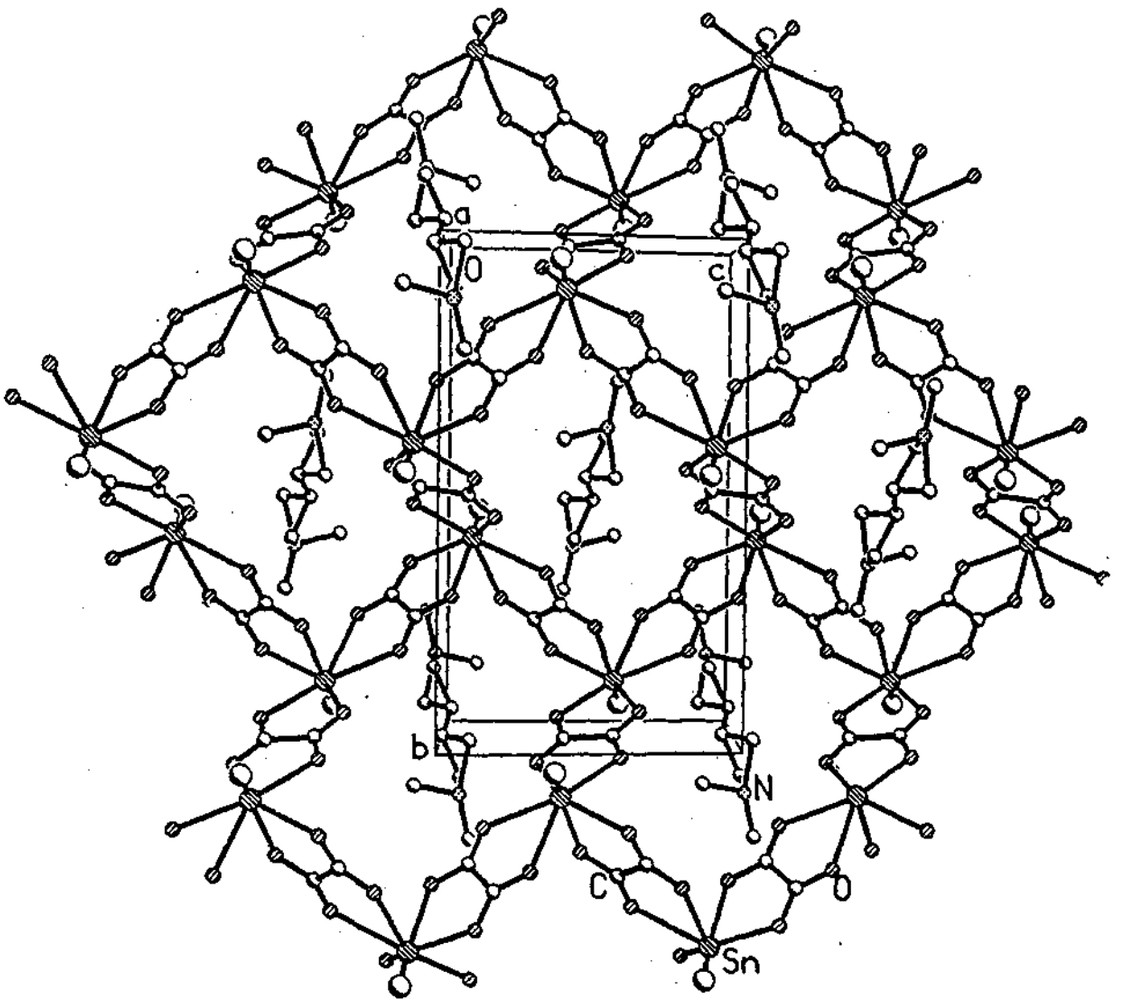

Figure 1.7

Structure of a layered tin(II) oxalate made in the presence of structure directing amines.

material has a ferrimagnetic behavior. The origin of magnetism in this compound is devised from the presence of infinite Co-O-Co linkages.

Recently Ayappan *et al.*[32] made a new layered framework structure of tin(II) oxalate in the presence of structure directing amines (Fig.1.7). In this compound Sn(II) with oxygen and along with lone pair of electrons forms a pentagonal bipyramid arrangement, akin to that seen in the classic 14 electron system. In addition to this, a tin(II) oxalate with monomeric structure has been made, in which the monomer is stabilized by hydrogen bond interaction with the amine. Till now no tin(II) oxalate with three-dimensional structure has been isolated. In addition to the phosphates and oxalates that have been made, the synthesis of hybrid structures involving both inorganic phosphates and organic oxalates has also been achieved, with the oxalate in many cases acting as a bridge between the inorganic metal phosphate layers (Fig.1.8).[79]

1.7 Synthetic Considerations

All these open-framework materials are metastable structures stabilized under hydrothermal conditions in the presence of organic amines. According to Davis and Lobo[33] the amine acts as a template if the framework is flexible and as a "structure directing agent" if the framework is related to the structure of the cation molecule. It is to be noted that, many of the large pore phosphate based open-framework structures have been synthesized by using very small organic amines (e.g. VPI-5[34] (Fig.3b), JDF-20[35], $AlPO_4$-8[36], Cloverite[37], ULM-5[38] and ULM-

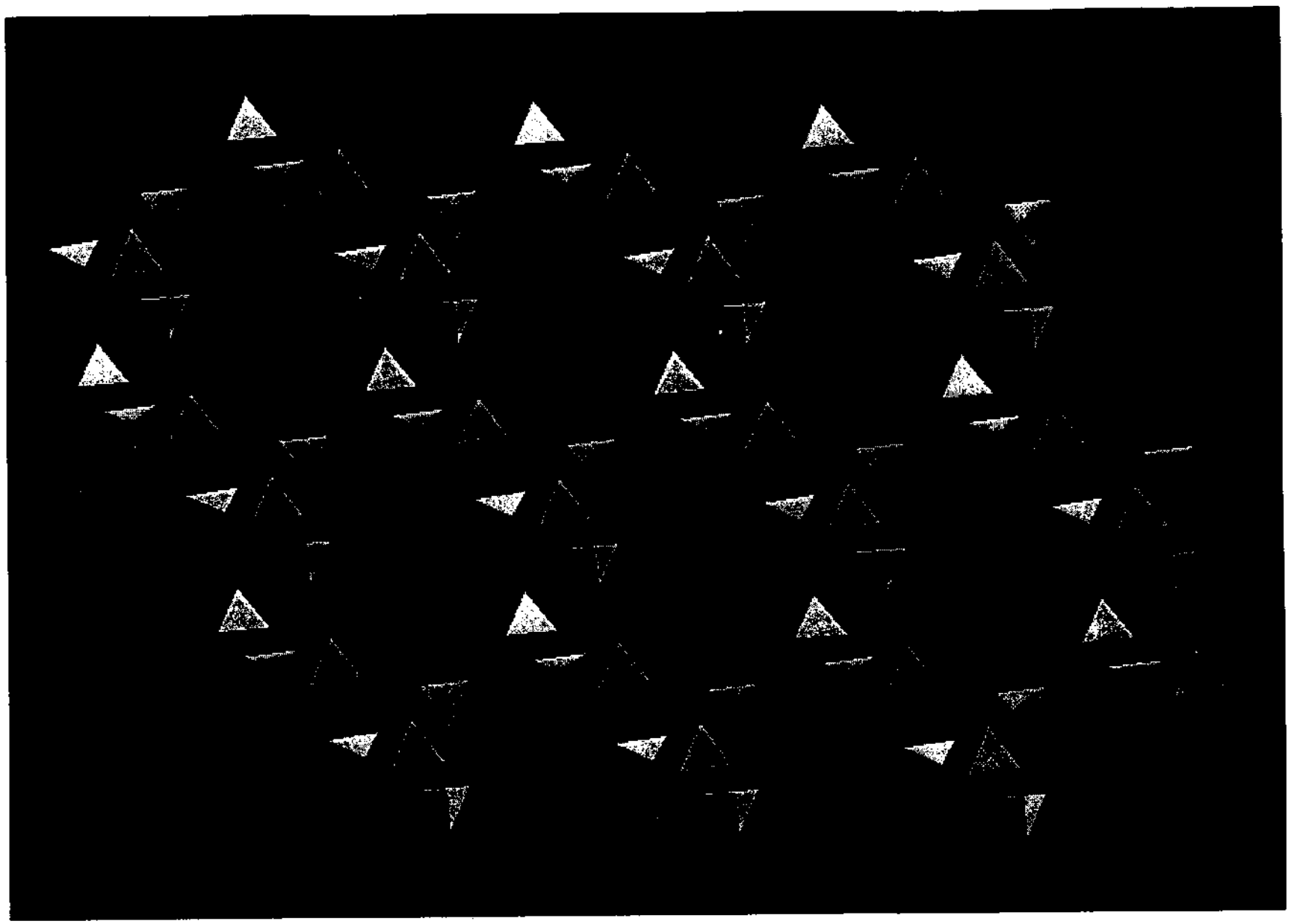

Figure 1.8
Structure of an iron phosphatooxalate viewed down the c-axis showing 12-membered apertures (amine and water molecules are not shown for clarity).

16[39]. Therefore, in open-framework materials the pores can be designed to form in an ordered fashion and also the pore size and shape can be controlled, by employing molecular units or hydrated alkali or alkaline earth cations or amines/diamines as templates or structure directing agents.

Inspite of the progress made, one is not able to adequately rationalize the formation of such a variety of open-framework metal phosphates and metal oxalates structures. In the case of aluminophosphates it is believed that linear chains of corner-shared metal phosphates are progressively transformed into ladder, layer and three-dimensional structures.[40-42] In tin phosphates, four-rings of metal phosphate are believed to be the basic building unit, which transform into larger rings and give rise to layer and other complex structures.[26] During the formation of initial chain or layer structures of metal phosphates, the amine and its interaction with the phosphoric acid has been investigated recently. Thus, the amine-phosphates are found to be key intermediates responsible in the formation of open-framework metal phosphates.[43] It has been shown that by the reaction of amine phosphates with suitable metal ions new open-framework metal phosphates are formed along with some already known phases.[15,44]

In case of open-framework metal oxalates not much attention has been given to understand their formation, probably due to the limited number of compounds that are known in this family. In the light of the

observation that amine phosphates are the key intermediates it is worthwhile to study the interaction of metal ions with amine oxalates. Such a study has been performed and the results are presented in the chapter 3.

1.8 Applications

1.8.1 Heterogeneous Catalysis

One of the most important applications of zeolites is in the field of industrial catalysis.[1] Zeolites catalyze a wide variety of reactions involving organic molecules. There are several methods by which zeolite structure is able to catalyze reactions. Firstly, their large surface area (typically 300-700 m^2g^{-1} or more than 98% of the total surface area) provides a high concentration of active sites, usually the Brönsted acid sites found in protonated zeolites.

Table 1.2: Experimental techniques for diffusion studies in zeolites

Method	Subject	Scale	Time Scale
NMR (line shape, relaxation)	elementary processes	≤ nm	10^{-10}-10^{-1}
Neutron Scattering	elementary processes	≤ nm	≤ 10^{-8}s
Tracer technique	self-diffusion	≥ μm	≥ min
PFR NMR	self-diffusion	μm-mm	ms-s
Transient and steady state measurements	transport diffusion	≥ μm	≥ s

These are generally located as hydroxyl groups, although the small concentration of defect sites undoubtedly contributes to the reactivity. These sites are able to protonate organic molecules such as alkenes to form carbonium ions, or basic groups such as hydroxyl moieties or amines. The high thermal stability of many zeolite structures makes them ideal for use in an industrial environment where many processes operate in conditions of high temperature and high pressure. The shape selective properties of zeolites can enable them control the outcome of many reactions inside the pore, either by allowing reactant product molecules to selectively diffuse through the channels, or by stabilizing the transition state (Fig1.9). Protonated forms of faujasite are widely used for catalytic cracking in petroleum industries.[45] The process converts the predominantly long chain hydrocarbons that are present in crude oil into smaller hydrocarbon molecules useful for gasoline and as feed stocks for synthesis of fine chemicals. Coke is frequently the by-product of this reaction, and causes the deactivation of the catalyst by blocking the pore structure over a period of time. Rare-earth ions, such as La^{3+}, are often added to give the catalyst extra stability as well as providing extra Brönsted acid sites formed by hydrolysis of the cation. Recently, ferrierite has been shown to be an excellent shape selective catalyst for the isomerization of butene to iso-butene[46]. The latter is an important feed stock for the production of methyl tertiary butyl ether (MTBE), which is commercial, oxygenate additive in lead-free motor fuel.

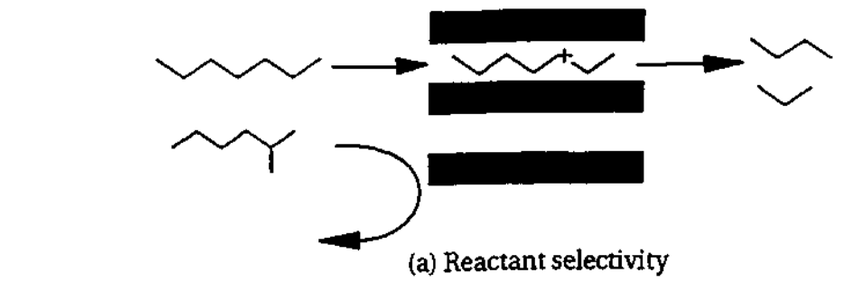

(a) Reactant selectivity

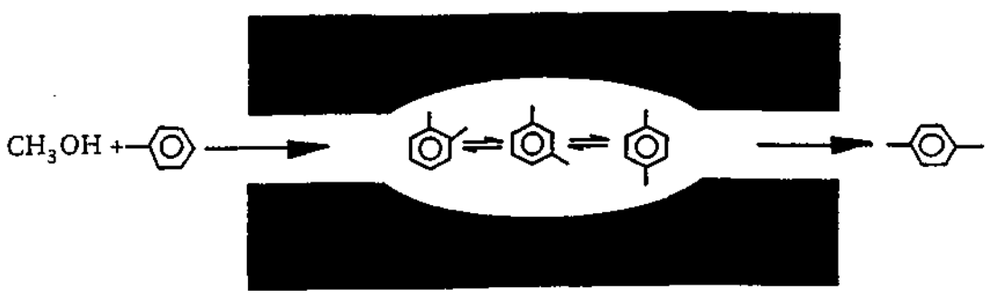

(b) Product selectivity

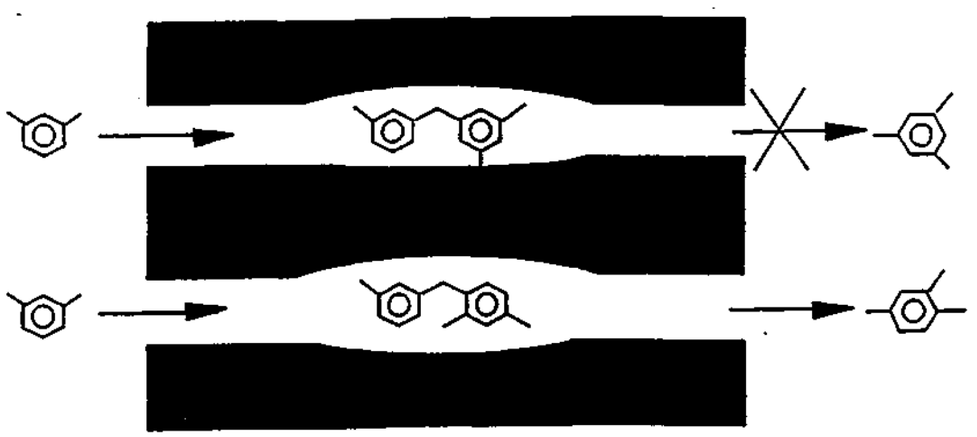

(c) Transition state selectivity

Figure 1.9

Shape selectivity exhibited by zeolites.

The addition of metal cations to a structure, either as framework species or extra-framework cations, can modify the catalytic activity. For example the addition of Cu^{2+} ions into the ZSM-5 makes it active in the conversion of NO and NO_2, which are common in automobile exhaust gases, to nitrogen and oxygen[47]. A titanosilicate ETS-1 (MFI) which contains framework titanium, exhibit redox activity and are being used for the partial oxidation reactions involving phenols and hydrogen peroxide.[48] The process is recently commercialized to produce catechol and hydroquinone from phenol.

The conversion of alcohols to alkenes in zeolite 5A structure relies on reactant shape-selectivity for its action. Only primary alcohols, rather than branched isomers, can enter the small pores of the zeolite and reach the active sites. Under normal conditions, the secondary alcohols that form the more stable carbonium ion intermediates would be converted selectively.

Product shape-selectivity is a vital characteristic in the use of ZSM-5 in the isomerization of xylenes. The p-isomer of xylene is an important starting material in the synthesis of polyesters. The isomerization reaction is known to proceed via a carbonium ion intermediate, creating a thermodynamic equilibrium between the isomers. However, although p-xylene is not the thermodynamically favored isomer in an equilibrium mixture. It has a much higher diffusivity than the

o- and m-isomers in the pore structure of ZSM-5 on account of its relatively linear shape and can escape from the catalyst more rapidly.

The methanol-to-gasoline (MTG) process[49] is an important method of obtaining gasoline in locations with no direct source of crude oil. In New Zealand it is used routinely as a step in converting the natural gas reserves into petrol for transportation. Mechanistic studies on this system have shown that the important intermediate is dimethylether. The smaller channel of the ZSM-5 pore structure prohibits the formation of aromatic species larger than C_9 and C_{10}, thus reducing the amount of coking.

The majority of zeolite catalytic applications are based on zeolites acting as shape selective acid catalyst. However, there have been reports on the base catalytic activity of these materials. Hathaway and Davis have synthesized nanophase cesium oxide stabilized in the pores of zeolites, forming very good base catalysts.[50] Gortsema and co-workers have also commercialized a process using cesium-loaded zeolites to catalyze the formation of 4-methylthiazole, which is an intermediate in the synthesis of an important fungicide.[51]

The chiral crystal structure of polymorph A of zeolite-β[52] offers the possibility of asymmetric synthesis. Indeed it has been shown that the use of chiral amines as templates can enhance the yield of these chiral phases.[33]

1.8.2 Ion Exchange

The presence of extra framework cations in the structure allows efficient ion-exchange to occur in aqueous solutions.[53] This is exploited in many commercial applications. For example, Na-A and Na-P as water softeners, owing to their ability to exchange Na^+ ions for Ca^{2+} and Mg^{2+} ions in hard water. This is also a major constituent of concentrated detergents and washing powder formulations, where it replaces sodium tripolyphosphate to reduce the environmentally hazardous phosphate concentration. Ammonium and potassium exchanged porous materials are frequently added to soil to improve crop yields. Recently, an important use of porous solids as ion-exchangers has been as radioactive decontaminants.[54] In the dehydrated form many of the zeolites have a high affinity for water, making them effective drying agents, for example in drying of organic solvents during synthesis and in double-glazing.

1.8.3 Sorption and Gas separation

The shape selectivity of zeolites can also be used to separate gases. Two modes of operation can be envisaged. In the first, which is essentially a thermodynamic effect, the diffusion affinity of the porous material for each sorbate effects the separation procedure. In this regard, the discovery of Li-LSX[55] has made the non-cryogenic separation of O_2 and N_2 from air possible. The affinity of lithium ions for the N_2 molecule, which has a quadrupolar moment three times larger than the O_2 molecule, is exploited efficiently in this process. Alternatively, the

kinetics of transport through the channels in these zeolitic solids can be used to achieve the separation. The Asahi process operates in this principle to separate mixtures of C_8 aromatic isomers (xylenes and ethyl benzene).[56]

The present day challenge lies in synthesizing new microporous materials with novel properties beyond catalysis and separation. In these lines search is in progress for making materials that has magnetically aligned channels (ferromagnetic/ferrimagnetic channels etc.) by use of which one can isolate N_2 and O_2 from air, through non-cryogenic method. Likewise making materials with chiral channels can enable the separation of enantiomers from racemic mixtures, better known as enantio-selective processes.

2. SCOPE OF THE PRESENT INVESTIGATION

In what follows, the scope of the investigations reported in this thesis are presented.

2.1 Synthesis and characterization of open-framework zinc oxalates

Inorganic open-framework materials are generally synthesized hydrothermally in the presence of organic amines. In the last few years there has been considerable effort in designing open-framework inorganic materials other than phosphates. There has been some success with open-framework structures formed by metal carboxylates[29-31] wherein the carboxylates cross-link the extended metal-oxygen networks made from

edge- and/or corner-shared polyhedra, giving rise to a three-dimensional connectivity possessing channels. These materials somewhat resemble the channel structures formed by the phosphates, but they have been prepared in the absence of any organic amines. The recent report of novel tin(II) oxalates with open architecture synthesized in the presence of structure-directing amines (SDA's)[32], led us to explore the possibility of designing new open-framework carboxylate structures, by carrying out hydrothermal synthesis in the presence of SDA's. In this direction, we have carried out the synthesis of zinc oxalates in the presence of organic amines. Although, transition metal oxalates with layered and other architectures containing amines have been reported[58,59], to our knowledge, open-framework zinc oxalates of well-defined structures have not been reported hitherto. It is generally assumed that zinc oxalates may also form honeycomb structures. We, also decided to explore if such oxalate based open-architectures can also exhibit interesting properties like reversible hydration/dehydration, ion-exchange etc, similar to their phosphate counterparts[60].

2.2 Synthesis and characterization of open-framework tin oxalates

The synthesis of novel open-framework structures has emerged as an important area of research because of their potential use in separation processes and catalysis[1,2]. Synthesis of these materials generally makes use of structure-directing agents (SDAs), as is common in the preparation of zeolitic materials[2]. A large number of open-framework solids based on

metal phosphates and phosphonates have been synthesized and characterized in the last decade[61-66]. Interestingly, organic porous solids mimicking the behavior of inorganic porous solids have been synthesized only in the last two or three years.[67-69] Rigid bidentate ligands linked with metal centers are known to form open networks,[70] and carboxylates of metals with new open architectures, possessing interesting physical properties (e.g. reversible hydration/ dehydration) have been reported in the last three to four years.[29-31,71-73] A new family of tin oxalates containing SDAs was reported a few months ago, including two monomers having 4-coordinated Sn(II) and one sheet structure having 6-coordinated Sn(II)[32]. Based on our experience with open-framework tin phosphates,[24-28,74] it appeared to us that the tin oxalates may well form a wide variety of open-framework solids with different aperture sizes as well as interesting structural features. We have therefore attempted to synthesize further tin oxalates in the presence of structure-directing amines by hydrothermal methods.

2.3 Investigation of the role of amine oxalates in the formation of open-framework metal oxalates

Among the novel open-framework materials not based on phosphates, those of phosphonates[65,66,76] and carboxylates[29-31] are noteworthy. A new family of tin oxalates containing SDAs was reported a few months ago, including two monomers having 4-coordinated Sn(II) and one sheet structure having 6-coordinated Sn(II)[32]. In the tin phosphate

family, the isolation of materials having one- $[C_6N_2H_{18}]^{2+}2[SnPO_4]^-$ (ladder-like chains)[26], two- $[C_2N_2H_{10}]^{2+}[Sn_2(PO_4)_2]^{2-}H_2O$[25], (layers, intercalated with amine) and three- dimensionally[27] $\{0.5[H_3N(CH_2)_2NH_3]^{2+}[Sn_4P_3O_{12}]^-\}$, $\{0.5[H_3N(CH_2)_4NH_3]^{2+}[Sn_4P_3O_{12}]^-\}$. $\{0.5[H_3NCH_2CH_2CH(NH_3)CH_2CH_3]^{2+}\ [Sn_4P_3O_{12}]^-H_2O\}$ extended networks clearly indicate that the system is very versatile like the aluminophosphate family of open-framework materials. One of the basic structural building block, present in most of these materials, a four-membered ring made of $[Sn_2P_2O_4]$ moiety has also been isolated and characterized[77].

Recently it has been pointed out that amine-phosphates may act as potential intermediates in the formation of open-framework metal phosphates and provide a convenient route for the synthesis of these materials[43]. The reaction of amine phosphate with metal ions yields a variety metal phosphates with diverse structures and dimensions[43]. Pertaining to these observations we wanted to examine the potential of amine-oxalates in acting as the intermediate in the formation metal carboxylate based open-architectures. We have, therefore investigated the reaction of amine-oxalate with Zn^{II} ions.

2.4 Synthesis and characterization of zinc phosphate with open-architecture

A large variety of open-framework metal phosphates have been synthesized over the years by employing organic amines as templates[2].

The role of the amines in the formation of these fascinating structures, however, remains somewhat mysterious. It has been suggested that factors such as the shape of the amine and its pKa may be of significance[30]. Davis and Lobo[33] propose that the amine act as a space-filling agent if the open-framework structure is flexible, and acts as a structure-directing agent when the shape of the amine and the framework are related. During the course of our investigations of open-framework zinc phosphates, we have found even more curious roles of the organic amines. Thus, we have recently shown that in some zinc phosphates, the organic amine acts as a ligand to Zn, at the same time forming the open-framework structure[23]. In the light of these observations we decided to probe more on understanding the dual role of the amine in the open-framework chemistry.

2.5 Synthesis and characterization of low-dimensional framework tin phosphate

Open framework materials are of considerable interest due to the wide structural diversity and potential applications in catalysis and other areas[1]. The continued research in this area has shown that new materials with novel architectures can be made in the presence of structure-directing organic amines[2]. Recently, it is established that open-framework tin(II) phosphates can be made under hydrothermal conditions[24-28]. The chemistry of bivalent tin and its related compounds, especially the phosphates[74] and phosphonates[63,66] continues to yield

unexpected results. In the tin phosphate family, the isolation of materials having one- $[C_6N_2H_{18}]^{2+}2[SnPO_4]^-$ (ladder-like chains)[26], two- $[C_2N_2H_{10}]^{2+}[Sn_2(PO_4)_2]^{2-}H_2O$, (layers, intercalated with amine)[25] and three- dimensionally $\{0.5[H_3N(CH_2)_2NH_3]^{2+}[Sn_4P_3O_{12}]^-\}$[24], $\{0.5[H_3N(CH_2)_4NH_3]^{2+}[Sn_4P_3O_{12}]^-\}$,$\{0.5[H_3NCH_2CH_2CH(NH_3)CH_2CH_3]^{2+}$ $[Sn_4P_3O_{12}]^-H_2O$[27] extended networks clearly indicate that the system is very versatile like the aluminophosphate family of open-framework materials. One of the basic structural building block, present in most of these materials, a 4-membered ring made of $[Sn_2P_2O_4]$ moiety has also been isolated and characterized[77]. The main structural features present in all the tin phosphate and phosphonate materials are the presence of either three- and/or four- coordinated Sn^{II} atoms that are vertex linked to PO_4 tetrahedra, forming channels and cavities. In general, it is observed that the Sn : P ratio in these tin phosphates is greater than 1.

3. EXPERIMENTAL

3.1 Synthesis and characterization of the zinc oxalates

The zinc oxalates, $[H_3N(CH_2)_3NH_3]^{2+}[Zn_2(C_2O_4)_3]^{2-}3H_2O$ and $2[C_3H_7NH_3]^+[Zn_2(C_2O_4)_3]^{2-}3H_2O$, were synthesized starting from a mixture containing 1,3-diaminopropane (DAP) and n-propylamine (PA), respectively, as the SDAs. In a typical synthesis, for $[H_3N(CH_2)_3NH_3]^{2+}[Zn_2(C_2O_4)_3]^{2-}3H_2O$, 1.273g of oxalic acid was

dissolved in 5 ml of deionized water and 0.41g of ZnO was added to the above under constant stirring. To this mixture 0.42 ml of DAP was added and homogenized for 10 min. The final composition of the mixture was ZnO: $2H_2C_2O_4$: DAP: $55H_2O$. For $2[C_3H_7NH_3]^+[Zn_2(C_2O_4)_3]^{2-}3H_2O$, zinc oxide, oxalic acid, PA and water were mixed in the ratio ZnO: $H_2C_2O_4$: 2PA: $55H_2O$. The mixtures with an initial pH of 8.0 were transferred into a 23-mL (fill factor = 40%) PTFE bottle, and sealed in a stainless steel autoclave (Parr, Moline, IL). The sealed pressure bombs were heated at 110 °C for 168 h for $[H_3N(CH_2)_3NH_3]^{2+}[Zn_2(C_2O_4)_3]^{2-}3H_2O$ and 65 h for $2[C_3H_7NH_3]^+[Zn_2(C_2O_4)_3]^{2-}3H_2O$ under autogeneous pressure. The mixtures after the reaction had a pH of 6.5. The resulting products, which contained large quantity of transparent single crystals, were filtered and washed thoroughly with deionized water. Initial characterizations were performed with powder x-ray diffraction (PWDXRD) The powder X-ray diffraction pattern of the powdered single crystals indicated that the products were new materials; the pattern was entirely consistent with the structure determined by single-crystal X-ray diffraction. The powder X-ray diffraction pattern of the powdered single crystals indicated that the product was a new material; the pattern was entirely consistent with the structure determined by single-crystal X-ray diffraction. Thermogravimetric analysis (TGA) was carried out in static air in the range between 25 and 600°C using a heating rate of 10°C/min. The final

characterization was done using single crystal XRD. The crystal structure data are presented in Table 4.1.1.

3.2 Synthesis and characterization of the microporous tin oxalate

The tin(II) oxalate, $[(CH_3)_2NH(CH_2)_2NH(CH_3)_2]^{2+}$ $[Sn_2(C_2O_4)_3]^{2-}$ H_2O was synthesized starting from a mixture containing N,N,N',N'-tetramethyl ethylenediamine (TMED), as the SDAs. In a typical synthesis, tin(II) oxalate, phosphoric acid (85 wt%), TMED and water in the ratio SnC_2O_4: H_3PO_4: TMED: 55 H_2O were taken in the starting mixture. The starting mixture was stirred to attain homogeneity, transferred into a 23 ml (fill-factor = 40%) PTFE bottle, and sealed in a stainless steel autoclave (Parr, USA). The sealed pressure bombs were heated at 150° C for 48h. The resulting product, which contained a small quantity of crystals along with white powder, was filtered and washed thoroughly with de-ionized water. The single crystals were easily separated from the white powder under an optical microscope. Powder X-ray diffraction (XRD) and thermogravimetric analysis (TGA) were done for initial characterization (TGA was carried out in static air in the range between 25° and 900° C). The final characterization was done using single crystal XRD. The tables containing crystal structure details are presented in Table 4.2.1.

3.3 Synthesis and Characterization of amine oxalates and hierarchy of zinc oxalates

3.3.1 Preparation of amine oxalates

As precursor in metal oxalate synthesis, oxalates of some amines including those of propylamine (PRO), guanidine (GUO), piperazine (PIPO) and 1,4-diazabicyclo[2,2,2]octane (DABCO-O) were first synthesized. In a typical experiment amine was added drop-by-drop to an aqueous solution of oxalic acid under continuous stirring. In all cases the acid: amine ratio is maintained either as 2:1 or 1:1. The resulting gel/solution was heated at 85°C for 12h and left at room temperature to obtain single crystals of amine oxalates. The initial characterizations were done using powder XRD, thermogravimetric analysis (TGA) and IR-spectroscopy. Finally, structure was determined by single crystal XRD. The crystal structure data are given in tables IV.3.1-IV.3.6.

3.3.2 Reaction of amine oxalates with Zn^{II} ions

The precursor, amine oxalates were reacted with Zn^{II} ions under hydrothermal environment. Typically, 0.137g of ZnO was dispersed in 3ml of water and 2g of GUO were added to it under continuous stirring. The contents were homogenized, transferred to a PTFE-lined stainless steel acid digestion bombs (Parr, USA) and heated to 85°C for a fortnight. The final composition of the mixture was ZnO: 5GUO: $100H_2O$.

In another reaction PIPO was reacted with aqueous suspension of ZnO in the ratio ZnO: 2.035PIPO: $100H_2O$, at 50°C for 5days following

the same procedure as that of above reaction involving GUO. In yet another reaction DABCO-O was stirred with ZnO aqueous solution in the ratio ZnO: DABCO-O: $200H_2O$, and was heated under hydrothermal conditions at 150°C for 3days. The reaction of PRO with Zn ions was carried out at 150°C for 3days starting from an initial composition of ZnO: PRO: $25H_2O$. In all cases single crystals suitable for single crystal XRD were obtained. Initial characterizations were performed using powder X-ray diffraction (PWDXRD) and thermogravimetric analysis (TGA). TGA was carried out under nitrogen atmosphere from room temperature to 600°C at a rate of 5°C/min. In all cases the final characterization was done using single crystal diffraction. The crystal data are presented in tables 4.3.1-4.3.4.

3.4 Synthesis and characterization of the zinc phosphate

The $[NH_3(CH_2)_3NH_3]_2[NH_3(CH_2)_3NH_2]_2[Zn_{12}(OH_2)_2(PO_4)_{10}]H_2O$ was synthesized hydrothermally starting from a zinc phosphate gel containing 1,3-diaminopropane (DAP) as the structure-directing agents. In a typical synthesis, 0.7 g of the oxalic acid and 0.251 g of zinc oxide was dispersed in 4 ml of deionized water. 1.0 ml of DAP was added to the mixture and stirred for 15 min. 0.08 ml of H_3PO_4 was added to the above and the stirring continued to attain homogeneity. The final composition of the mixture was ZnO: $0.4H_3PO_4$: $3.0H_2C_2O_4$: 4.7DAP: $72H_2O$. The mixture was sealed in a Teflon lined stainless steel autoclave (Parr, USA) and heated initially at 170°C for 48h and then finally at 180°C for 48h.

The resulting product had the composition and contained predominantly large cube-like single crystals, suitable for single crystal X-ray diffraction, was filtered and washed thoroughly with deionized water.

The EDAX analysis indicated that Zn: P ratio of 55: 45 which also in excellent agreement with the stated composition. The powder X-ray diffraction pattern of the powdered single crystals indicated that the product was a new material; the pattern was entirely consistent with the structure determined by single-crystal X-ray diffraction. A least squares fit of the powder XRD lines gave the following cell: a = 13.075(1), b = 14.282(1), c = 14.202(2) Å, β = 93.4°, which is in agreement with that determined by single crystal XRD. Thermogravimetric analysis (TGA) was carried out under a flow of nitrogen (40ml min^{-1}) in the range from room temperature to 700°C using a heating rate of 5°C/min. Finally the structure was determined performing a single crystal XRD. The structural data are presented in Table 4.4.1.

3.5 Synthesis and characterization the tin phosphate

Both the $[NH_3(CH_2)_3NH_3]^{2+}2[SnPO_4]^-$ and the $[NH_3(CH_2CHOHCH_2)NH_3]^{2+}2[SnPO_4]^-$ were synthesized by hydrothermal methods starting from a tin phosphate gel containing DAP and DAHP as the structure-directing agents. In a typical synthesis, 2.088g of tin(II) oxalate (Aldrich) was dispersed in 10ml of water and 1.38ml of 85wt% aqueous H_3PO_4 (Aldrich) was added to the mixture under continuous stirring. 1.314ml of DAP (I) and 1.821g of DAHP (II) was added

respectively to the above and stirred until homogeneous. The final composition of the mixture was SnC_2O_4: 2.0 H_3PO_4: 1.5DAP/2.0DAHP: $55H_2O$. The mixture was sealed in a Teflon lined stainless steel autoclave (Parr, USA) and heated initially at 150°C for 48h and then finally at 180°C for 36h for the one with DAP and at 150°C for 120h for the one with DAHP. The resulting product, containing predominantly large plate-like single crystals and a small quantity of powder was filtered and washed thoroughly with deionised water.

The powder X-ray diffraction pattern for both the compounds were identical and indicated that the product was a new material; the pattern is entirely consistent with the structure determined by single-crystal X-ray diffraction. Thermogravimetric analysis (TGA) was carried out under an oxygen atmosphere in the range from room temperature to 600°C at a rate of 5°C/min. The final characterization was done by performing single crystal XRD. The crystal structure informations are presented in Table 4.5.1.

3.6 Characterization techniques

3.6.1 Initial characterizations

The powder X-ray diffraction patterns were recorded for all the samples on a Rich Seifert-3000TT X-ray powder diffractometer. The thermogravimetric analysis (TGA) of all the compounds were performed on a Mettler-Toledo TG850 instrument. The reversible hydration/dehydration studies were done on the zinc oxalate using the

adsorption set up fitted with a Cahn-2000 microbalence. The energy dispersive analysis of X-rays (EDAX) was carried out on a Leica S440I scanning electron microscope fitted with a Link isis spectrometer. The IR- spectra of the amine oxalates were recorded on a Bruker spectrometer

3.6.2 Single Crystal Structure Determination

A suitable single crystal of each compound was carefully selected under a polarizing microscope and glued to a thin glass fiber with cyanoacrylate (superglue) adhesive. Single crystal structure determination by X-ray diffraction was performed on a Siemens Smart-CCD diffractometer equipped with a normal focus, 2.4 kW sealed tube x-ray source (Mo-K_α radiation, λ = 0.71073 Å) operating at 50 kV and 40mA. A hemisphere of intensity data was collected at room temperature in 1321 frames with ω scans (width of 0.30° and exposure time of 20s per frame) in the 2θ range 3 to 48.0°.

The structure was solved by direct methods using SHELXS-86[19] and difference Fourier syntheses. Whenever the amine molecule in the structure was heavily disordered, restraints for the bond distances have been used to keep the molecule intact and within reasonable limits. All the hydrogen positions for I were initially located in the difference Fourier maps, but for the final refinement the hydrogen atoms were placed geometrically and held in the riding mode. No absorption corrections were applied. The last cycles of refinement included atomic positions for all the atoms, anisotropic thermal parameters for all the non-hydrogen

atoms and isotropic thermal parameters for all the hydrogen atoms. Full-matrix-least-squares structure refinement against $|F^2|$ was carried out using SHELXTL-PLUS[20] package of programs.

4. RESULTS AND DISCUSSION

4.1 Zinc oxalates with open-architectures

4.1.1 Structure of the open-framework zinc oxalates

a) $[H_3N(CH_2)_3NH_3]^{2+}[Zn_2(C_2O_4)_3]^{2-}3H_2O$

The asymmetric unit of $[H_3N(CH_2)_3NH_3]^{2+}[Zn_2(C_2O_4)_3]^{2-}3H_2O$ contains 28 non-hydrogen atoms (Fig.4.1.1). $[H_3N(CH_2)_3NH_3]^{2+}[Zn_2(C_2O_4)_3]^{2-}3H_2O$ consists of macroanionic sheets of formula $[Zn_2(C_2O_4)_3]^{2-}$ with interlamellar $[H_3N(CH_2)_3NH_3]^{2+}$ ions, the individual layers involving a network of ZnO_6 octahedra and C_2O_4 units. Each Zn atoms is crosslinked to six oxalate oxygens, forming a honeycomb network as shown in Fig.4.1.2a. This type of network results in a 12-membered pore within the layers, which stack one over the other, along the c axis. Such perforated sheets have been observed earlier in layered aluminophosphates[78] and iron phosphate-oxalates[79]. The protonated organic amine molecules sit in the middle of the 12-membered pores. There are three water molecules present in the material occupying the pores along with the amine (Fig.4.1.2b). Along the b axis the layers stack one over the other with the water molecules situated in between the layers as shown in Fig.4.1.3. The amine and the water molecules

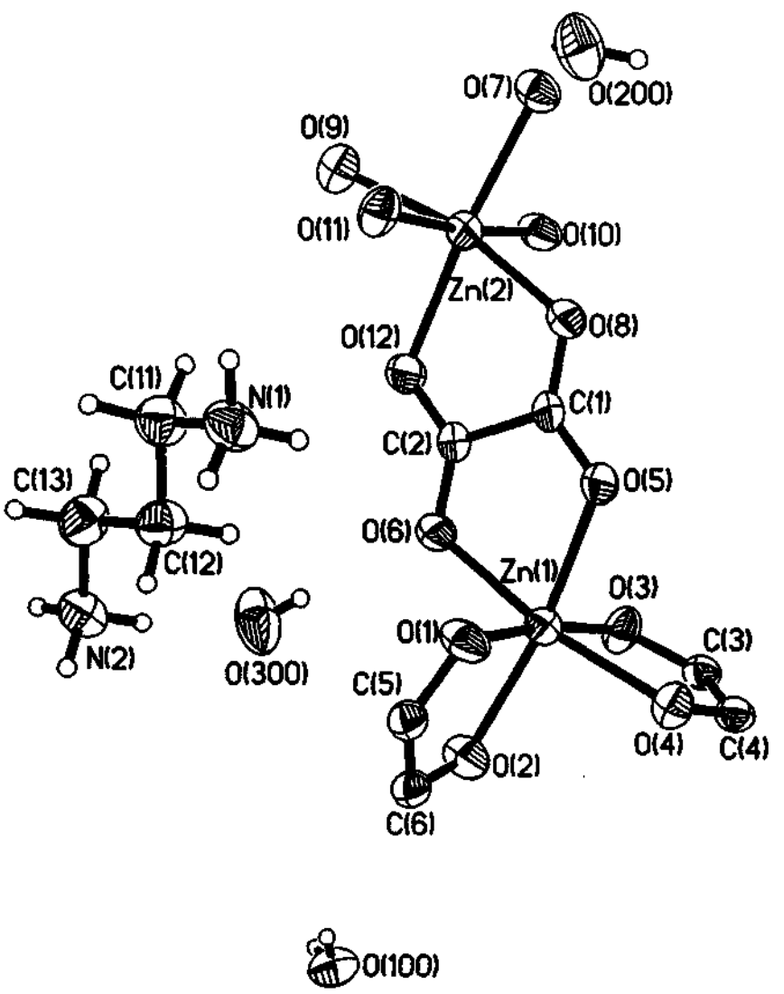

Figure 4.1.1

ORTEP plot of $[H_3N(CH_2)_3NH_3]^{2+}[Zn_2(C_2O_4)_3]^{2-}3H_2O$. Thermal ellipsoids are given at 50% probability.

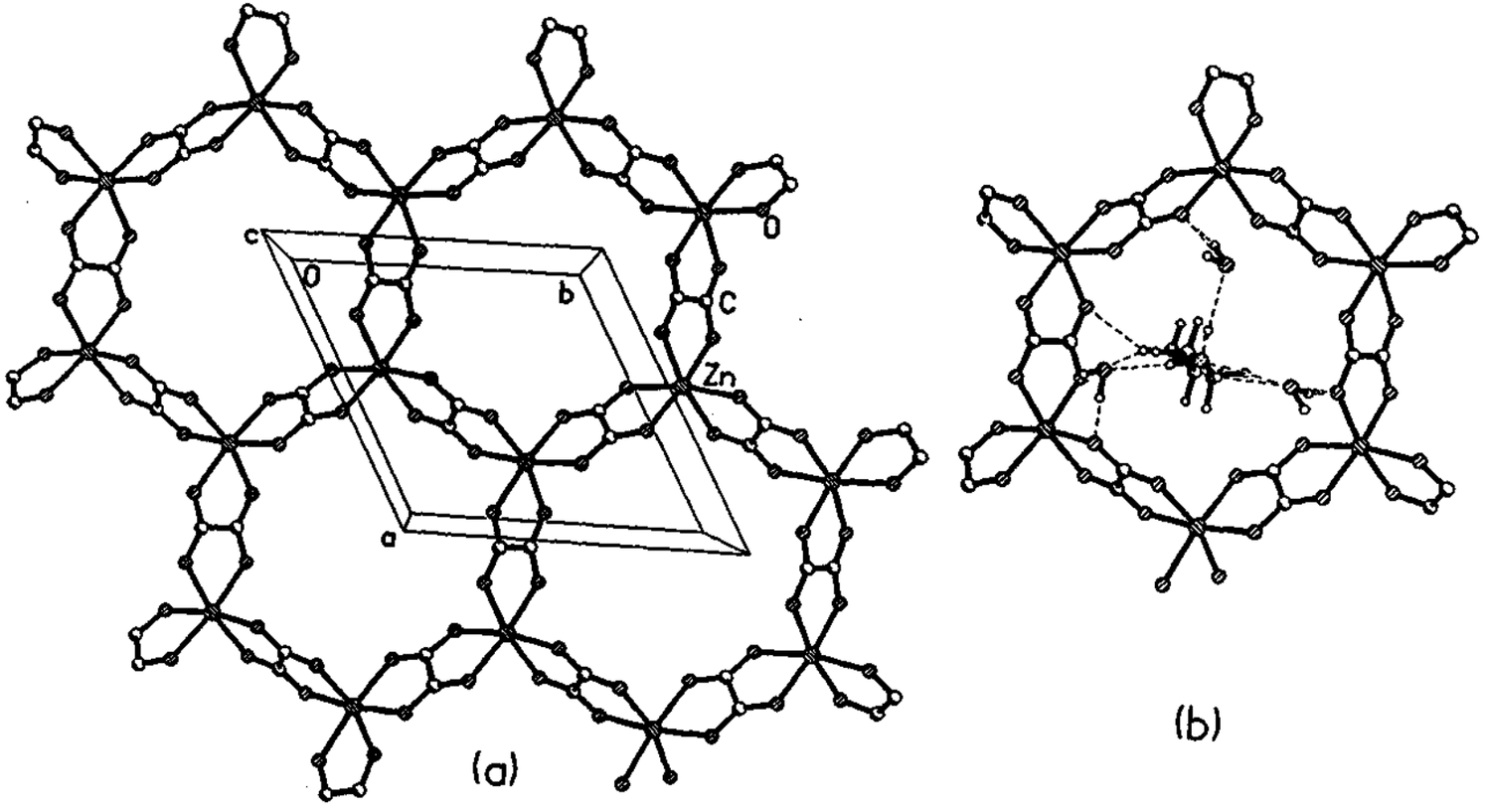

Figure 4.1.2

(a) Structure of $[H_3N(CH_2)_3NH_3]^{2+}[Zn_2(C_2O_4)_3]^{2-}3H_2O$ in the ab plane showing the honeycomb architecture.

(b) Structure showing a single 12-membered aperture with the amine and water molecules. Dotted lines represent the hydrogen bond interactions.

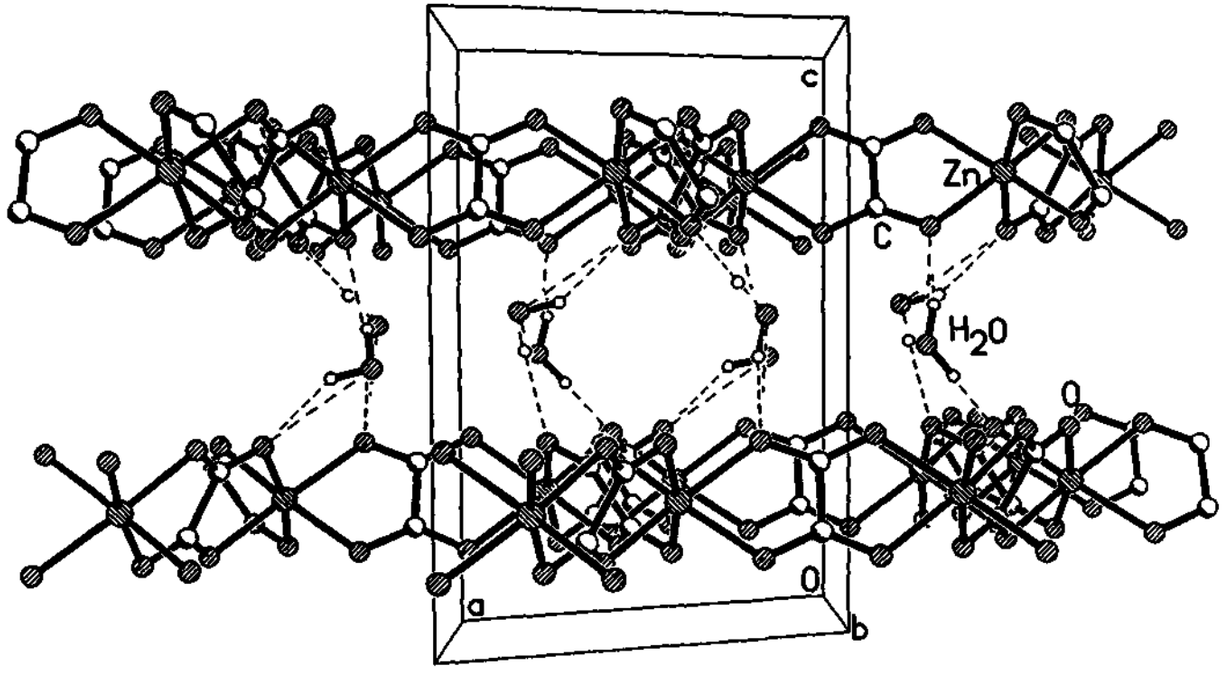

Figure 4.1.3

Structure of $[H_3N(CH_2)_3NH_3]^{2+}[Zn_2(C_2O_4)_3]^{2-}3H_2O$ along the ac plane showing the layer arrangement. Amine molecules are not shown for clarity. Note that the water molecules involve in hydrogen bonding (dotted lines).

participate in extensive hydrogen bonding, lending structural stability to this material. The various hydrogen bond interactions between the sheets and the guest molecules can be seen in Figs. 4.1.2b and 4.1.3. In Table 4.1.7, we list the important hydrogen bond interactions.

The Zn – O distances in $[H_3N(CH_2)_3NH_3]^{2+}[Zn_2(C_2O_4)_3]^{2-}3H_2O$ are in the range 2.068 – 2.121 Å (ave. 2.093 Å), with the longer distances being associated with the oxygens that are double-bonded to the carbon atoms. The variations in the distances are reflected in the C – O bonding, as well (Table 4.1.3). The O – Zn – O and O – C – O bond angles are in the range 79.9 – 173.2 and 125.2 – 127.2°, respectively (Table 4.1.4).

b) $2[C_3H_7NH_3]^{+}[Zn_2(C_2O_4)_3]^{2-}3H_2O$

The asymmetric unit of $2[C_3H_7NH_3]^{+}[Zn_2(C_2O_4)_3]^{2-}3H_2O$ contains 19 non-hydrogen atoms and is shown in Fig. 4.1.4. The structure of $2[C_3H_7NH_3]^{+}[Zn_2(C_2O_4)_3]^{2-}3H_2O$ also consists of a network of ZnO_6 octahedra and oxalate units and three oxalate units connect with the Zn atoms giving rise to a three-dimensional connectivity. Of the three oxalate units, two connect via an in-plane linkage and the third one is crosslinked to the Zn atom in an out-of-plane manner resulting in a interrupted honeycomb structure with a 20-member elliptical ring, as shown in Fig. 4.1.5. This type of connectivity between the Zn and oxalate units does not appear to have been encountered earlier. The elliptical pores in this 3-D zinc oxalate is formed by the linkage between 10 Zn and 10 oxalate units lying in the same plane and the other oxalate unit connect

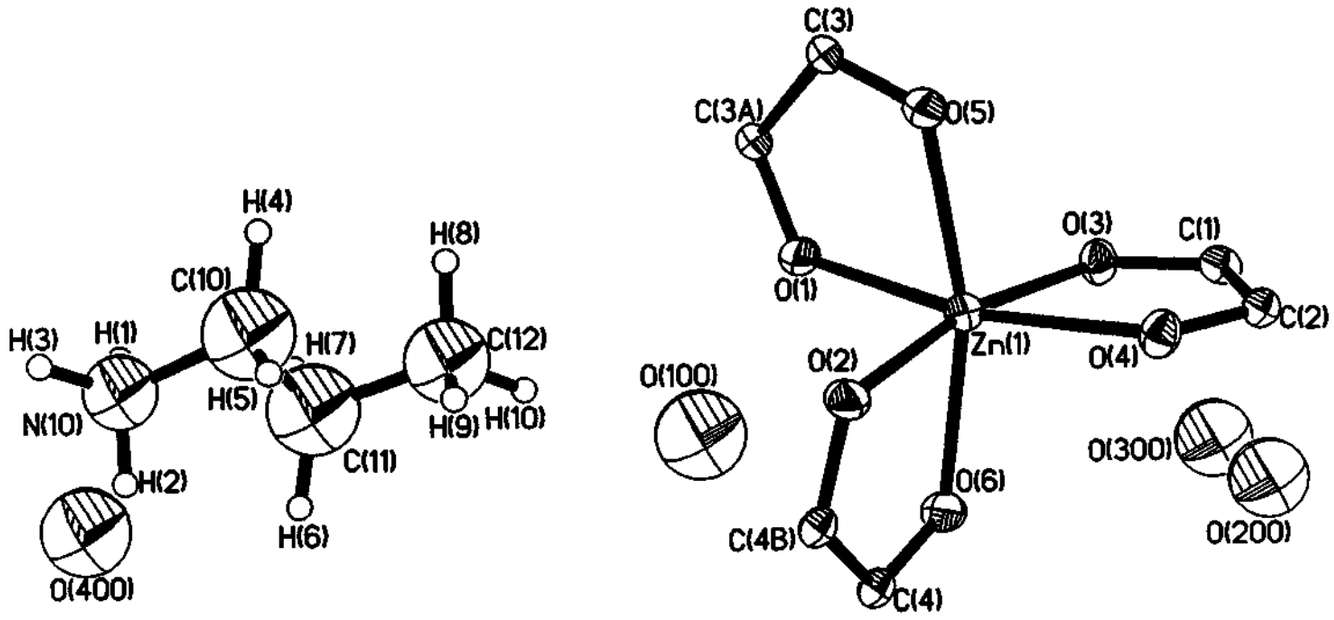

Figure 4.1.4

ORTEP plot of $2[C_3H_7NH_3]^+[Zn_2(C_2O_4)_3]^{2-}3H_2O$. Thermal ellipsoids are given at 50% probability.

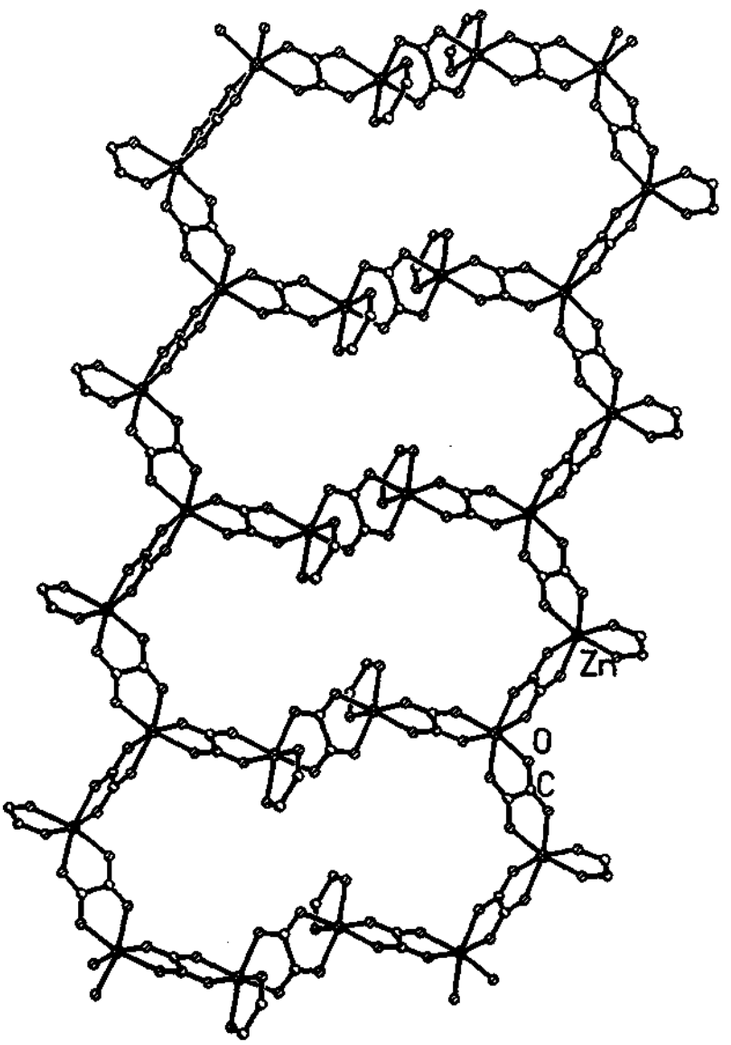

Figure 4.1.5

Structure of $2[C_3H_7NH_3]^+[Zn_2(C_2O_4)_3]^{2-}3H_2O$, showing the 20-membered aperture. Note that the one of the Zn atoms is connected by out of plane oxalate unit.

the elliptical pores such that two such rings are perpendicular to each other. Though the largest pore opening in propylamine containing zinc oxalate compound is a 20-membered one it appears smaller in projection. Thus, along the b axis, the structure has the appearance of an 12-membered square-channel system made from 6 Zn and 6 oxalate units (~8.5 x 8.2 Å; longest atom-atom contact distance not including van der Waals radii) (Fig. 4.1.6). The 20-member aperture has the dimensions ~17.2 x 6.9 Å. Along the c axis it appears to have another 12-membered channel made from 8 Zn and 4 oxalate units of 8.3 x 6.1Å diameter (Fig. 4.1.7). The organic structure-directing agent, n-propylamine, which is highly disordered, occupies these channels along with water molecules. There is considerable hydrogen bond interaction between the guest molecules and the host structure as presented in Table 4.1.7.

The Zn – O distances in $2[C_3H_7NH_3]^+[Zn_2(C_2O_4)_3]^{2-}3H_2O$ are in the range 2.068 – 2.121 Å (ave. 2.096 Å), with the longer distances being associated with the oxygens that are double-bonded to the carbon atoms. The O – Zn – O and O – C – O bond angles are in the range 79.1 – 168.4° and 126.0 – 126.5°, respectively (Table 4.1.6).

4.1.2 Initial characterization of the zinc oxalates

TGA studies of $[H_3N(CH_2)_3NH_3]^{2+}[Zn_2(C_2O_4)_3]^{2-}3H_2O$ and $2[C_3H_7NH_3]^+[Zn_2(C_2O_4)_3]^{2-}3H_2O$ were carried out in static air from room temperature to 600 °C and show weight loss in three steps. For $[H_3N(CH_2)_3NH_3]^{2+}[Zn_2(C_2O_4)_3]^{2-}3H_2O$, a sharp mass loss of about 9.3%

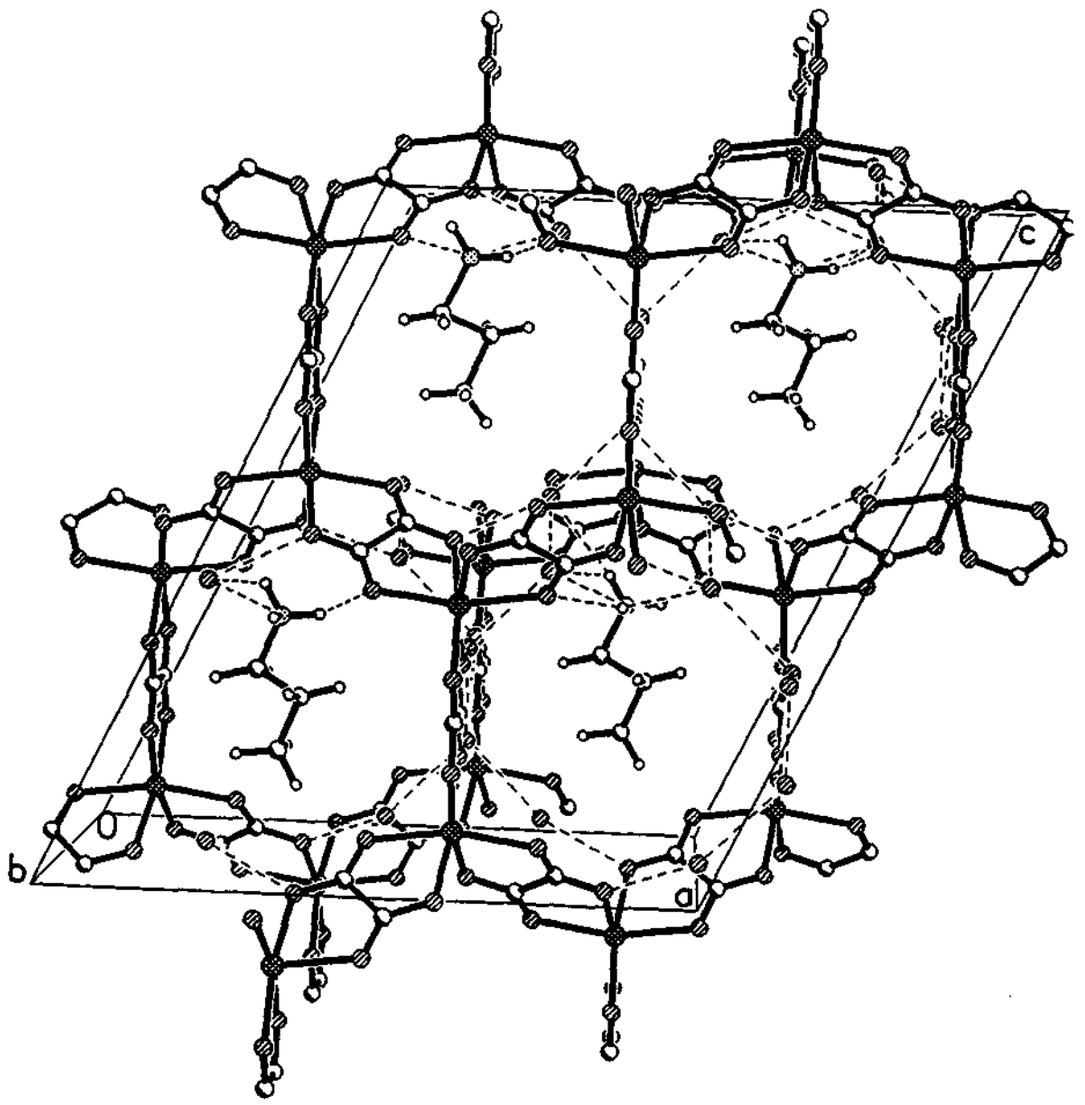

Figure 4.1.6

Structure of $2[C_3H_7NH_3]^+[Zn_2(C_2O_4)_3]^{2-}3H_2O$, along the b axis showing the 12-membered square channels. Dotted lines represent the various hydrogen bond interactions.

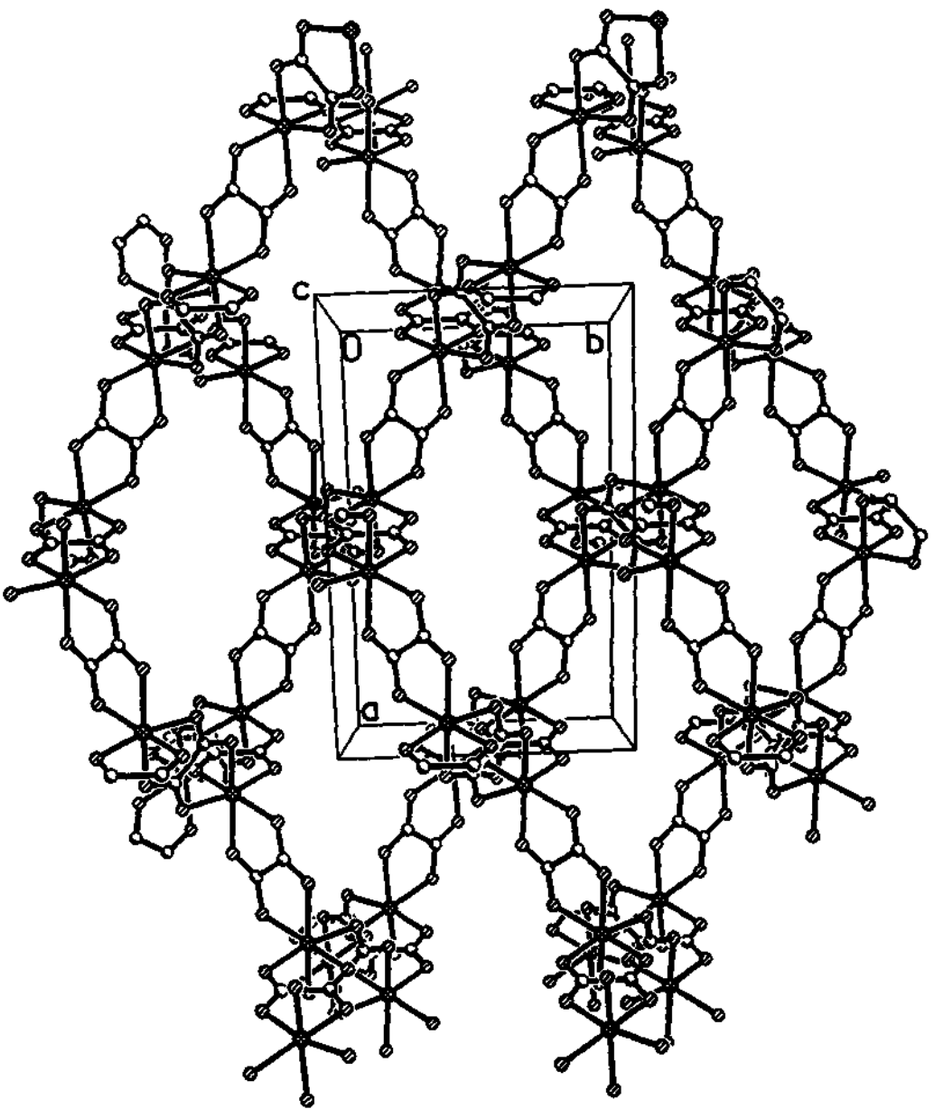

Figure 4.1.7

Structure of $2[C_3H_7NH_3]^+[Zn_2(C_2O_4)_3]^{2-}3H_2O$, along the c axis showing the 12-membered elliptical channels.

occurring at 150 °C corresponds to the loss of water molecules (calcd. 10.3%) and a continuous two step mass loss of 57.2 % 300-400 °C region corresponds to the loss of carbon dioxide and amine molecules (calcd. 55.6%). For $2[C_3H_7NH_3]^+[Zn_2(C_2O_4)_3]^{2-}3H_2O$, a sharp mass loss of about 10.2% at 65 °C corresponds to the loss of water molecules (calcd. 9.5%) and the mass loss of about 33.8% in the region 270-330 °C corresponds to the loss of carbon dioxide from the oxalate (calcd. 33%), with the loss of 24.4% in the region 360-430 °C corresponding to the loss of the amine molecules (calcd. 28%). The powder XRD patterns of the decomposed products indicated a poorly crystalline product with very weak reflections that corresponds to the mineral zincite, ZnO (JCPDS: 36-1451).

4.1.3 Adsorption studies of the zinc oxalate

Adsorption studies, carried out gravimetrically with a Cahn electric balance, show that dehydrated $2[C_3H_7NH_3]^+[Zn_2(C_2O_4)_3]^{2-}3H_2O$ adsorbs water reversibly exhibiting a Langmuir type I adsorption isotherm (Fig. 4.1.8). The observed weight changes at 25 °C correspond to 3.0 water molecules per unit cell, in agreement with the framework formula derived from crystallographic investigations. Unlike the 3-D framework, the 2-D zinc oxalate loses crystallinity on desorption of water, indicating that the hydrogen bond interactions between the water and the framework is crucial for the structural stability of this material. It is possible that such hydrogen bonding is responsible for the 20-membered aperture in $2[C_3H_7NH_3]^+[Zn_2(C_2O_4)_3]^{2-}3H_2O$.

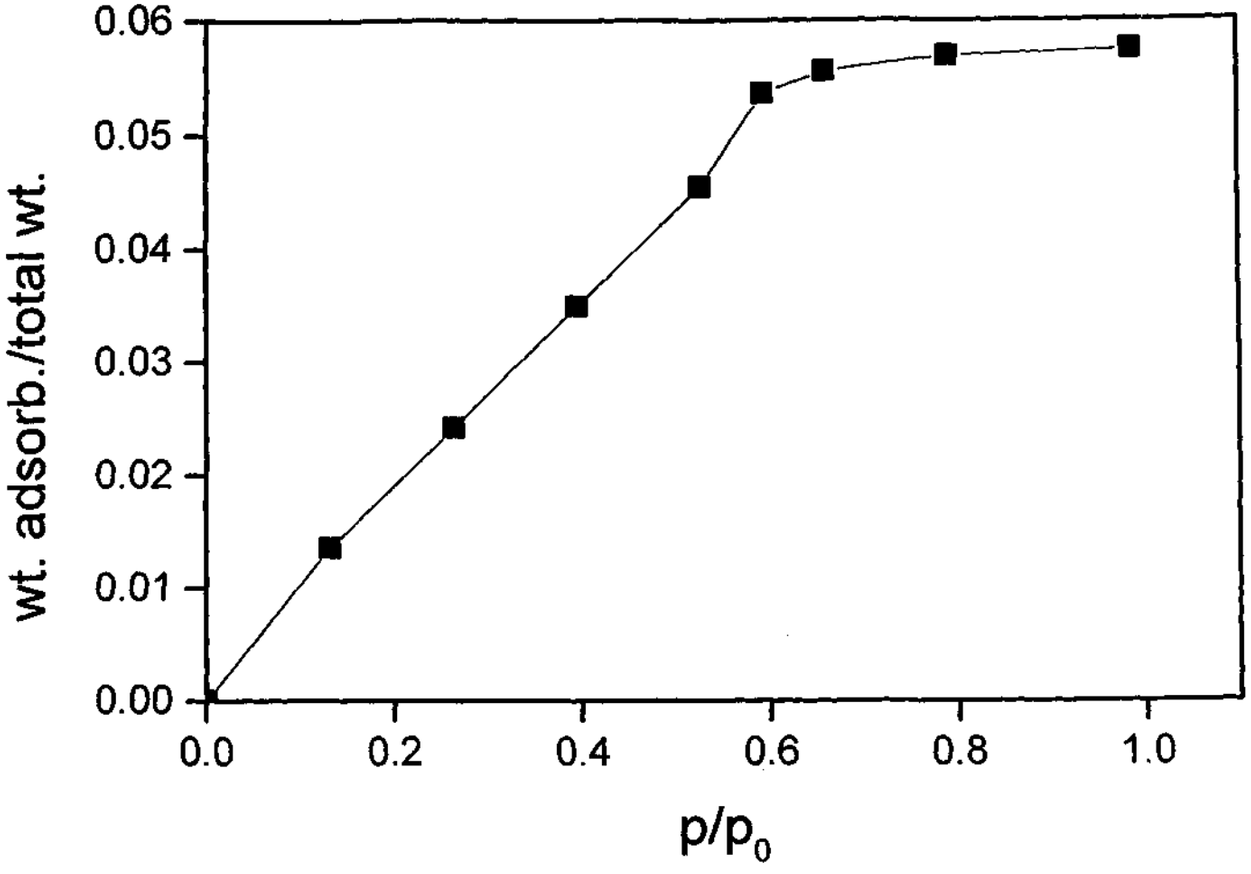

Figure 4.1.8

Room-temperature adsorption isotherm for H_2O in the dehydrated sample of $2[C_3H_7NH_3]^+[Zn_2(C_2O_4)_3]^{2-}3H_2O$.

Both are members of a new family of framework solids with an identical framework composition. The difference in their structures arises from the distinct ways the oxalate units link to the Zn atoms. Whereas $2[C_3H_7NH_3]^+[Zn_2(C_2O_4)_3]^{2-}3H_2O$ has a three-dimensional structure arising from the covalent bonding between the oxalates and Zn, $[H_3N(CH_2)_3NH_3]^{2+}[Zn_2(C_2O_4)_3]^{2-}3H_2O$ has a two-dimensional architecture containing overlapping layers.

In the layered zinc oxalate, the connectivity between the Zn and the oxalate moieties results in a 12-membered honeycomb aperture within the layer. The pores penetrate the entire structure in a direction perpendicular to the sheets, yielding a solid with unidimensional channels (~8.4 X 8.6 Å; longest atom-atom contact distance not including the van der Waals radii) containing the SDA and water molecules (Fig. 4.1.2a and 4.1.2b). The type of perforated sheets seen in $[H_3N(CH_2)_3NH_3]^{2+}[Zn_2(C_2O_4)_3]^{2-}3H_2O$ is well-known in aluminum phosphates[78] and identical honeycomb structures have been known for $[M(II)M(IV)(ox)_3]^-$ and $[M(IV)_2(ox)_3]$, where M is a transition element[58-60]. The honeycomb structures for the bimetallic transition metal oxalates have been made in the presence of ammonium cation. To our knowledge, this is the first case of a honeycomb structure in a pure zinc oxalate material. The honeycomb structure in the layered structure may be largely due to the use of the organic di-cation, $[DAPH_2]^{2+}$, in the starting

synthesis mixture, as such a di-cation might be needed for neutralizing the charge on the di-anionic oxalate sheets.

The layers formed by Zn and oxalate moieties in $[H_3N(CH_2)_3NH_3]^{2+}[Zn_2(C_2O_4)_3]^{2-}3H_2O$ are also present in $2[C_3H_7NH_3]^{+}[Zn_2(C_2O_4)_3]^{2-}3H_2O$, except that the layers get crosslinked by another oxalate as can be seen from Fig. 4.1.6. We also see large 20-membered apertures (Fig. 4.1.5) formed by the Zn and the oxalate units. Large apertures are known to occur in other framework solids, including layered materials[78,79], but 20-membered rings are indeed rare, such apertures and channels being found in very few materials[37,80]. There is three-dimensional connectivity in $2[C_3H_7NH_3]^{+}[Zn_2(C_2O_4)_3]^{2-}3H_2O$ and an examination of the connectivity patterns between the oxalates and M^{2+} ions (M = Zn) shows that the hexa-coordinated Zn atom has two in-plane connectivity and one out-of-plane connectivity with the oxalate units as shown in Figure 4.1.9. The out-of-plane connectivity is responsible for the three-dimensional nature of the structure (Figs. 4.1.6 and 4.1.7). Interesting is the similarity between the structure of $2[C_3H_7NH_3]^{+}[Zn_2(C_2O_4)_3]^{2-}3H_2O$ and of the oxalate-phosphates discovered recently[81]. Thus, the Fe oxalate-phosphates have iron phosphate sheets crosslinked by oxalate units, not unlike the structure of an iron oxalate described by Decurtins *et al.*[59].

4.1.4 Hydrogen bonds in the open-framework zinc oxalates

The importance of multi-point hydrogen bonding in these materials becomes apparent when we examine the distances and angles listed in Table 4.1.7. In $[H_3N(CH_2)_3NH_3]^{2+}[Zn_2(C_2O_4)_3]^{2-}3H_2O$, which has a layered architecture with the organic amine at the centre of the 12-membered ring along with the water molecules, hydrogen bond interactions appear to be much stronger than in the 3-D zinc oxalate, which has a more open structure. The primary hydrogen bond interactions seem to be between the framework oxygens and water molecules. The amine molecules participate in both inter- (involving amine and framework) as well as intra- (involving amine and water molecules) layer hydrogen bonding. Compound $[H_3N(CH_2)_3NH_3]^{2+}[Zn_2(C_2O_4)_3]^{2-}3H_2O$, shows a dominance of hydrogen bonding with donor-acceptor (O....H) distances in the range of 1.85 – 2.35 Å and the majority of the angles above 150°. The ideal angle for a planar architecture is 180° and this 2-D oxalate network with angles above 150° indicates the importance of hydrogen bond interactions in low dimensional solids.

The coordination environment of Zn atoms in open-framework phosphates and oxalates provides an interesting comparison. The Zn atoms, in most of the zinc phosphates with open-architectures have a tetrahedral environment (4-coordination)[21-23]. In the oxalates under discussion, we have 6 coordination for the zinc atoms. This is probably because the average charge per oxygen on the oxalate (0.5) is less than

that on the phosphate (0.75) and more oxalate oxygens are therefore needed to satisfy the valence of zinc.

4.1.5 Conclusions

The present study shows that new open-framework zinc oxalates can be obtained when the synthesis is carried out in the presence of organic amines. Of the two oxalates described here, one has a honeycomb structure and another an interrupted honeycomb structure. They possess a two-dimensional layer or three-dimensional channel structures, not unlike many of the Zn phosphates. While $Zn(C_2O_4)2H_2O$ is known to possess a chain structure[82], we are yet to obtain one-dimensional chain Zn oxalate analogues to chain phosphates in the presence of amines. The honeycomb structure observed by us for $[H_3N(CH_2)_3NH_3]^{2+}[Zn_2(C_2O_4)_3]^{2-}3H_2O$ is noteworthy as this is the first example of such an architecture for a divalent metal oxalate. This opens up the possibility of synthesizing oxalates of various divalent transition metals possibly possessing interesting magnetic properties. The interesting three-dimensional structure of $2[C_3H_7NH_3]^{+}[Zn_2(C_2O_4)_3]^{2-}3H_2O$ underscores the need for further research on open-framework oxalates prepared in the presence of structure-directing agents.

Table 4.1.1 Crystal data and structure refinement parameters for $[H_3N(CH_2)_3NH_3]^{2+}[Zn_2(C_2O_4)_3]^{2-}3H_2O$ and $2[C_3H_7NH_3]^{+}[Zn_2(C_2O_4)_3]^{2-}3H_2O$.

Parameters	$[H_3N(CH_2)_3NH_3]^{2+}[Zn_2(C_2O_4)_3]^{2-}3H_2O$	$2[C_3H_7NH_3]^{+}[Zn_2(C_2O_4)_3]^{2-}3H_2O$
Empirical formula	$Zn_2O_{15}C_9N_2H_{18}$	$Zn_2O_{15}C_{12}N_2H_{26}$
Crystal system	Triclinic	Monoclinic
Space group	P •	C2/c (No. 15)
Crystal size (mm)	0.08 x 0.08 x 0.2	0.12 x 0.12 x 0.16
a (Å)	9.261(1)	15.847(1)
b (Å)	9.455(1)	9.685(1)
c (Å)	12.487(1)	18.333(1)
α (°)	83.93(1)	90.0
β (°)	88.01(1)	115.5(1)
γ (°)	61.03(1)	90.0
Volume (Å^3)	951.1(1)	2539.1(2)
Z	2	4
Formula mass	524.8	569.1
ρ_{calc} (gcm^{-3})	1.83	1.60
λ (MoKα) Å	0.71073	0.71073
μ (mm^{-1})	2.60	1.97
θ range (°)	1.64 – 23.29	2.46 – 24.03
Total data collected	3984	5142
Index ranges	$-10 \le h \le 9$, $-10 \le k \le 10$, $-13 \le l \le 12$	$-17 \le h \le 16$, $-10 \le k \le 7$, $-20 \le l \le 20$
Unique data	2673	1849
Observed data (I >2σ(I))	2561	1460
Refinement method	Full-matrix least-squares on $\|F^2\|$	Full-matrix least-squares on $\|F^2\|$
R_{merg}	0.06	0.06
R indexes [I >2σ(I)]	$R_1 = 0.03$, $wR_2 = 0.08$	$R_1 = 0.07$, $wR_2 = 0.21$
R (all data)	$R_1 = 0.03$, $wR_2 = 0.08$	$R_1 = 0.08$, $wR_2 = 0.22$
Goodness of fit ($S_{obs.}$)	1.15	1.13
Goodness of fit ($S_{all.}$)	1.15	1.05
No. of variables	278	125
Largest difference map peak and hole eÅ^{-3}	0.579 and –0.429	0.615 and –0.671

[a] $R_1 = \bullet \||F_o|-|F_c|\| / \bullet |F_o|$; [b] $wR_2 = \{\bullet [w(F_o^2 - F_c^2)^2] / \bullet [w(F_o^2)^2]\}^{1/2}$. $w = 1/[\sigma^2(F_o)^2 + (aP)^2 + bP]$, $P = [\max.(F_o^2,0) + 2(F_c)^2]/3$, where a = 0.0383 and b = 0.608 for $[H_3N(CH_2)_3NH_3]^{2+}[Zn_2(C_2O_4)_3]^{2-}3H_2O$ and a = 0.1597 and b = 0.0 for $2[C_3H_7NH_3]^{+}[Zn_2(C_2O_4)_3]^{2-}3H_2O$.

Table 4.1.2 Atomic coordinates [x 10^4] and isotropic thermal parameters [Å x 10^3] for the non-hydrogen atoms in $[H_3N(CH_2)_3NH_3]^{2+}[Zn_2(C_2O_4)_3]^{2-}3H_2O$

Atom	X	Y	Z	U_{eq} $
Zn(1)	5730(1)	-1446(1)	-2376(1)	30(1)
Zn(2)	2432(1)	-4895(1)	-2418(1)	30(1)
O(1)	3918(3)	603(2)	-3275(2)	38(1)
O(2)	5574(2)	353(2)	-1493(2)	36(1)
O(3)	7713(2)	-3357(2)	-1501(2)	36(1)
O(4)	7710(2)	-1502(2)	-3286(2)	32(1)
O(5)	5418(3)	-2980(2)	-3323(2)	36(1)
O(6)	3955(3)	-1833(3)	-1493(2)	38(1)
O(7)	2523(3)	-6710(2)	-3272(2)	35(1)
O(8)	4082(3)	-4397(3)	-3342(2)	37(1)
O(9)	447(2)	-4715(2)	-1492(2)	35(1)
O(10)	4264(3)	-6951(2)	-1520(2)	36(1)
O(11)	450(2)	-2954(2)	-3340(2)	34(1)
O(12)	2650(3)	-3282(3)	-1475(2)	35(1)
C(1)	4443(3)	-3452(3)	-2950(2)	27(1)
C(2)	3603(3)	-2791(3)	-1869(2)	27(1)
C(3)	9086(3)	-3650(3)	-1882(2)	27(1)
C(4)	9089(3)	-2610(3)	-2936(2)	27(1)
C(5)	3575(3)	1898(3)	-2898(2)	28(1)
C(6)	4561(3)	1761(3)	-1870(2)	28(1)
O(100)	7953(3)	-41(3)	4724(2)	43(1)
O(200)	1786(4)	-5377(3)	-5443(2)	52(1)
O(300)	2055(4)	577(4)	-175(3)	69(1)
N(2)	-1064(3)	3145(3)	-536(2)	38(1)
N(1)	-1312(3)	2251(3)	-4350(2)	43(1)
C(11)	-1915(4)	2160(4)	-3242(2)	43(1)
C(12)	-1069(4)	2591(4)	-2439(2)	41(1)
C(13)	-1851(4)	2722(4)	-1353(2)	44(1)

$ U(eq) is defined as one third of the trace of the orthogonalized U_{ij} tensor.

Table 4.1.3. Selected interatomic distances in $[H_3N(CH_2)_3NH_3]^{2+}[Zn_2(C_2O_4)_3]^{2-}3H_2O$

Moiety	Distance (Å)	Moiety	Distance (Å)
Zn(1) – O(1)	2.087(2)	C(1) – O(5)	1.245(3)
Zn(1) – O(2)	2.068(2)	C(1) – O(8)	1.242(3)
Zn(1) – O(3)	2.082(2)	C(2) – O(6)	1.238(4)
Zn(1) – O(4)	2.105(2)	C(2) – O(12)	1.248(4)
Zn(1) – O(5)	2.093(2)	C(3) – O(3)	1.251(3)
Zn(1) – O(6)	2.104(2)	C(3)^b – O(9)	1.245(3)
Zn(2) – O(7)	2.080(2)	C(4) – O(4)	1.251(3)
Zn(2) – O(8)	2.084(2)	C(4)^b – O(11)	1.242(3)
Zn(2) – O(9)	2.084(2)	C(5) – O(1)	1.248(4)
Zn(2) – O(10)	2.095(2)	C(5)^a – O(7)	1.249(3)
Zn(2) – O(11)	2.121(2)	C(6) – O(2)	1.249(3)
Zn(2) – O(12)	2.110(2)	C(6)^a – O(10)	1.236(4)
C(1) – C(2)	1.566(4)	C(3) – C(4)	1.558(4)
C(5) – C(6)	1.559(4)		
		Organic Moiety	
N(1) – C(11)	1.484(4)	C(11) – C(12)	1.496(5)
C(12) – C(13)	1.503(4)	C(13) – N(2)	1.468(4)

a x, y-1, z; b x-1, y, z

Table 4.1.4. Selected bond angles in $\{H_3N(CH_2)_3NH_3\}^{2+}\{Zn_2(C_2O_4)_3\}^{2-}3H_2O$

Moiety	Angle (°)	Moiety	Angle (°)
O(2) – Zn(1) – O(3)	95.9(5)	O(2) – Zn(1) – O(1)	80.0(3)
O(3) – Zn(1) – O(1)	173.2(2)	O(2) – Zn(1) – O(5)	169.3(2)
O(3) – Zn(1) – O(5)	93.5(2)	O(1) – Zn(1) – O(5)	91.0(2)
O(2) – Zn(1) – O(6)	95.4(3)	O(3) – Zn(1) – O(6)	93.7(4)
O(1) – Zn(1) – O(6)	92.1(3)	O(5) – Zn(1) – O(6)	79.0(2)
O(2) – Zn(1) – O(4)	93.0(2)	O(3) – Zn(1) – O(4)	79.8(2)
O(1) – Zn(1) – O(4)	94.8(4)	O(5) – Zn(1) – O(4)	93.5(3)
O(6) – Zn(1) – O(4)	169.9(2)	O(7) – Zn(2) – O(9)	94.0(2)
O(7) – Zn(2) – O(8)	98.0(2)	O(9) – Zn(2) – O(8)	164.5(4)
O(7) – Zn(2) – O(10)	80.1(2)	O(9) – Zn(2) – O(10)	96.6(2)
O(8) – Zn(2) – O(10)	95.1(2)	O(7) – Zn(2) – O(12)	172.5(3)
O(9) – Zn(2) – O(12)	89.3(4)	O(8) – Zn(2) – O(12)	79.9(4)
O(10) – Zn(2) – O(12)	92.9(2)	O(7) – Zn(2) – O(11)	95.3(1)
O(8) – Zn(2) – O(11)	89.3(2)	O(9) – Zn(2) – O(11)	79.9(1)
O(10) – Zn(2) – O(11)	174.1(2)	O(12) – Zn(2) – O(11)	91.9(2)
O(8) – C(1) – O(5)	126.8(2)	O(6) – C(2) – O(12)	126.6(3)
$O(9)^a$ – C(3) – O(3)	125.2(2)	$O(11)^a$ – C(4) – O(4)	126.6(2)
O(1) – C(5) – $O(7)^b$	125.9(3)	$O(10)^b$ – C(6) – O(2)	127.2(2)
O(8) – C(1) – C(2)	117.1(2)	O(5) – C(1) – C(2)	116.1(2)
O(6) – C(2) – C(1)	116.6(2)	O(12) – C(2) – C(1)	116.8(3)
$O(9)^a$ – C(3) – C(4)	117.5(2)	O(3) – C(3) – C(4)	117.3(2)
O(4) – C(4) – C(3)	116.3(2)	$O(11)^a$ – C(4) – C(3)	117.1(2)
O(1) – C(5) – C(6)	116.8(2)	$O(7)^b$ – C(5) – C(6)	117.2(2)
$O(10)^b$ – C(6) – C(5)	116.7(2)	O(2) – C(6) – C(5)	116.1(2)
		Organic Moiety	
N(1) – C(11) – C(12)	112.2(3)	C(11) – C(12) – C(13)	111.6(3)
C(12) – C(13) – N(2)	113.7(3)		

a x+1, y, z; b x, y+1, z

Table 4.1.5 Atomic coordinates [x 10^4] and isotropic thermal parameters [Å x 10^3] for the non-hydrogen atoms in $2[C_3H_7NH_3]^+[Zn_2(C_2O_4)_3]^{2-}3H_2O$

Atom	X	Y	z	U(eq)[#]
Zn(1)	4180(1)	11249(1)	5861(1)	69(1)
O(1)	3584(3)	12847(5)	5024(3)	83(1)
O(2)	3936(3)	9650(5)	5025(2)	81(1)
O(3)	4669(3)	12626(4)	6827(2)	75(1)
O(4)	4662(3)	9861(4)	6835(2)	75(1)
O(5)	2783(3)	11145(4)	5688(3)	79(1)
O(6)	5408(3)	11355(4)	5687(3)	79(1)
C(1)	5000	12047(8)	7500	66(2)
C(2)	5000	10440(8)	7500	61(2)
C(3)	2273(4)	11993(6)	5192(3)	62(1)
C(4)	5425(3)	10499(6)	5193(3)	64(1)
O(100)[a]	4703(16)	14278(20)	4407(13)	394(10)
O(200)[a,l]	4644(14)	5548(18)	6795(11)	182(6)
O(300)[a,l]	4673(14)	6993(19)	6726(12)	189(6)
O(400)[a]	2801(13)	13183(19)	529(12)	360(9)
N(10)[a]	1721(12)	11247(10)	947(10)	222(6)
C(10)[a]	1738(18)	10745(28)	1735(12)	329(13)
C(11)[a]	2583(19)	11696(29)	2030(16)	347(13)
C(12)[a]	2645(18)	11158(19)	2833(15)	284(11)

[a] refined isotropically; [l] Site Occupancy Factor (SOF) = 0.5

[#] U(eq) is defined as one third of the trace of the orthogonalized U_{ij} tensor.

Table 4.1.6 Selected bond distances and angles in $2[C_3H_7NH_3]^+[Zn_2(C_2O_4)_3]^{2-}3H_2O$

Moiety	Distance, Å	Moiety	Distance, Å
Zn(1) – O(1)	2.096(4)	C(1) – O(3)	1.247(5)
Zn(1) – O(2)	2.093(4)	C(2) – O(4)	1.235(5)
Zn(1) – O(3)	2.082(4)	C(3) – O(1)[a]	1.250(7)
Zn(1) – O(4)	2.099(4)	C(4) – O(6)	1.237(7)
Zn(1) – O(5)	2.099(4)	C(4) – O(2)[b]	1.246(7)
Zn(1) – O(6)	2.105(4)	C(3) – O(5)	1.233(7)
C(1) – C(2)	1.557(12)	C(3) – C(3)[a]	1.554(10)
C(4) – C(4)[b]	1.559(10)		
Moiety	**Angle (°)**	**Moiety**	**Angle (°)**
O(3) – Zn(1) – O(2)	168.6(2)	O(3) – Zn(1) – O(1)	92.0(2)
O(2) – Zn(1) – O(1)	97.4(2)	O(3) – Zn(1) – O(4)	79.7(2)
O(2) – Zn(1) – O(4)	92.0(2)	O(1) – Zn(1) – O(4)	168.4(2)
O(3) – Zn(1) – O(5)	98.0(2)	O(2) – Zn(1) – O(5)	90.2(2)
O(1) – Zn(1) – O(5)	79.1(2)	O(4) – Zn(1) – O(5)	94.1(2)
O(3) – Zn(1) – O(6)	93.9(2)	O(2) – Zn(1) – O(6)	79.4(2)
O(1) – Zn(1) – O(6)	90.4(2)	O(4) – Zn(1) – O(6)	98.0(2)
O(5) – Zn(1) – O(6)	164.3(2)	O(3)[c] – C(1) – O(3)	126.5(7)
O(4)[c] – C(2) – O(4)	126.0(7)	O(5) – C(3) – O(1)[a]	126.5(5)
O(6) – C(4) – O(2)[a]	126.1(5)	O(3) – C(1) – C(2)	116.7(4)
O(4) – C(2) – C(1)	117.0(4)	O(5) – C(3) – C(3)[b]	118.0(6)
O(1)[a] – C(3) – C(3)[a]	115.5(6)	O(6) – C(4) – C(4)[b]	117.4(6)
O(2)[b] – C(4) – C(4)[b]	116.4(6)		

a -x+1/2, -y+5/2, -z+1; b -x+1, -y+2, -z+1 c -x+1, y, -z+3/2

Table 4.1.7 Important hydrogen bond distances and angles in both the compounds.

Moiety	Distance, Å	Moiety	Angle (°)
$[H_3N(CH_2)_3NH_3]^{2+}[Zn_2(C_2O_4)_3]^{2-}3H_2O$			
O(3) – H(11)	2.215(1)	O(3) – H(11) – N(2)	156.0(2)
O(12) – H(12)	1.957(1)	O(12) – H(12) – N(2)	178.2(1)
O(9) – H(11)	2.345(1)	O(9) – H(11) – N(2)	142.3(1)
O(4) – H(101)	1.930(1)	O(4) – H(101) – O(100)	175.4(2)
O(1) – H(102)	2.142(1)	O(1) – H(102) – O(100)	169.7(2)
O(7) – H(201)	2.063(1)	O(7) – H(201) – O(200)	160.6(1)
O(5) – H(202)	2.101(1)	O(5) – H(202) – O(200)	149.8(1)
O(2) – H(301)	2.166(1)	O(2) – H(301) – O(300)	175.0(1)
O(6) – H(302)	2.088(1)	O(6) – H(302) – O(300)	176.1(1)
O(100) – H(2)	1.964(1)	O(100) – H(2) – N(1)	167.7(3)
O(100) – H(3)	2.158(1)	O(100) – H(3) – N(1)	142.8(1)
O(200) – H(1)	1.887(3)	O(200) – H(1) – N(1)	164.2(1)
O(300) – H(10)	1.858(1)	O(300) – H(10) – N(2)	170.5(1)
$2[C_3H_7NH_3]^{+}[Zn_2(C_2O_4)_3]^{2-}3H_2O$			
O(6) – H(1)	2.342(1)	O(6) – H(1) – N(1)	132.6(1)
O(5) – H(2)	2.357(1)	O(5) – H(2) – N(1)	131.4(1)
O(100) – H(3)	2.424(1)	O(100) – H(3) – N(1)	158.2(1)

4.2 Tin (II) oxalate with open-architecture

4.2.1 Structure of the open-framework tin oxalate

The asymmetric unit of the tin(II) oxalate contains 15 non-hydrogen atoms (Fig. 4.2.1a) and the structure consists of macro-anionic sheets of formula $[Sn(C_2O_4)_{1.5}]^-$ with inter-lamellar $[(CH_3)_2NH(CH_2)_2NH(CH_3)_2]^{2+}$ ions. The framework is made up of a network of SnO_6 units [with pseudo-pentagonal bi-pyramidal geometry (Fig. 4.2.1(b)), assuming that one of the vertices is occupied by the lone-pair of electrons] and C_2O_4 moieties, which are linked to form puckered sheets that are stacked along a (Fig. 4.2.2-4.2.4). The lone pairs of electrons on Sn(II) project into the inter-lamellar spaces as shown in Fig. 4.2.3, and the structure contains 8- (along the a axis) and 12-membered (along the b axis) apertures. The SDA (protonated N,N,N'N'-tetramethyl-1,2-diaminoethane) resides in the 12-membered pores along with water molecules (Fig. 4.2.3), and these pores penetrate the entire structure in a direction perpendicular to the sheets, yielding a solid with uni-dimensional channels (~ 4.8 x 9.2 Å; longest atom-atom contact distance not including the van der Waals radii). The various hydrogen bonding interactions between the puckered layers and the guest species are best seen in Fig. 4.2.4.

The Sn – O distances are in the range 2.182 – 2.596 Å (ave. 2.424 Å), with the longer distances being associated with the oxygens that are double bonded to the carbon atoms. The variations in the distances are reflected in the C – O bonding, too (Table 4.2.3). The O – Sn – O and O

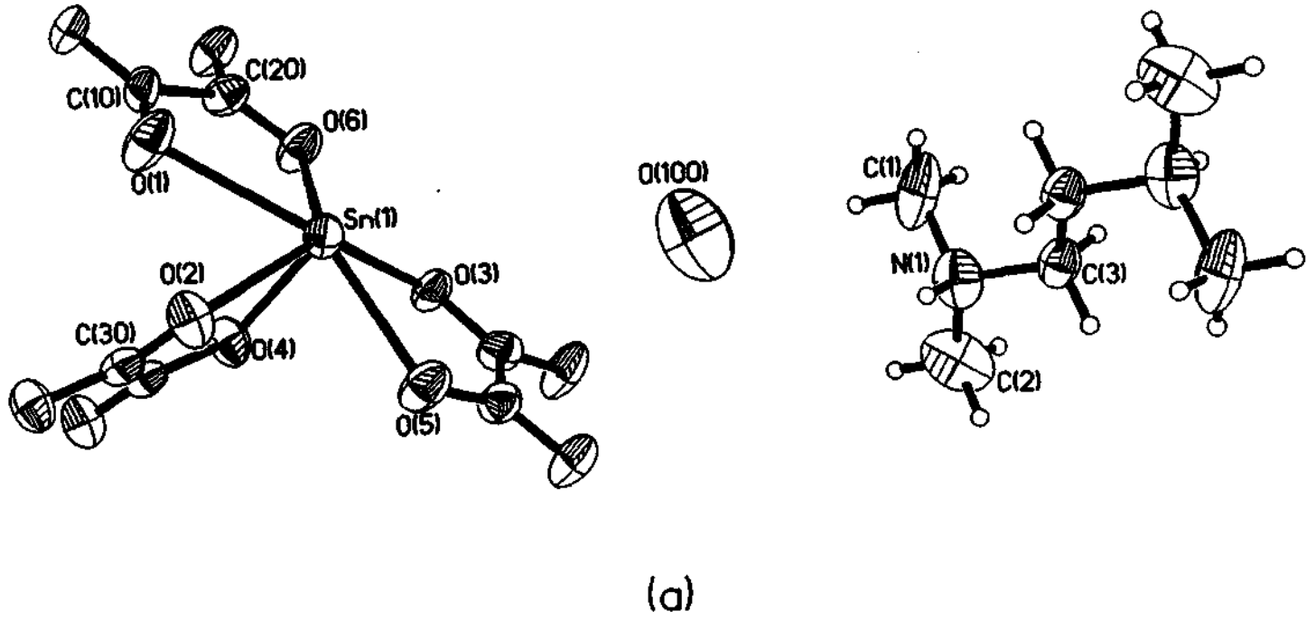

(a)

Figure 4.2.1

(a) ORTEP plot of $[(CH_3)_2NH(CH_2)_2NH(CH_3)_2]^{2+}$ $[Sn_2(C_2O_4)_3]^{2-}$ H_2O showing the connectivity (asymmetric unit is labeled). Thermal ellipsoids are given at 50% probability.

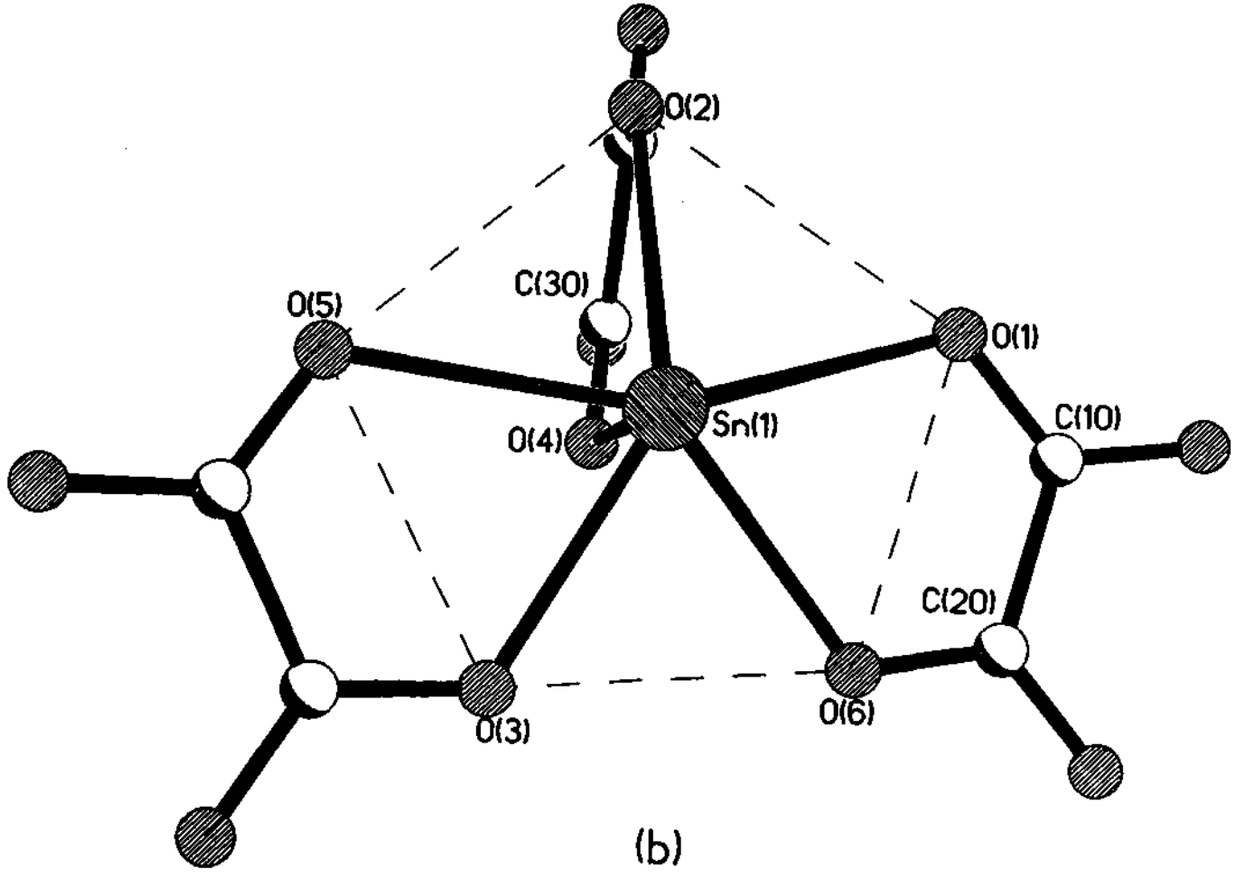

Figure 4.2.1

(b) View showing the stereochemistry around Sn.

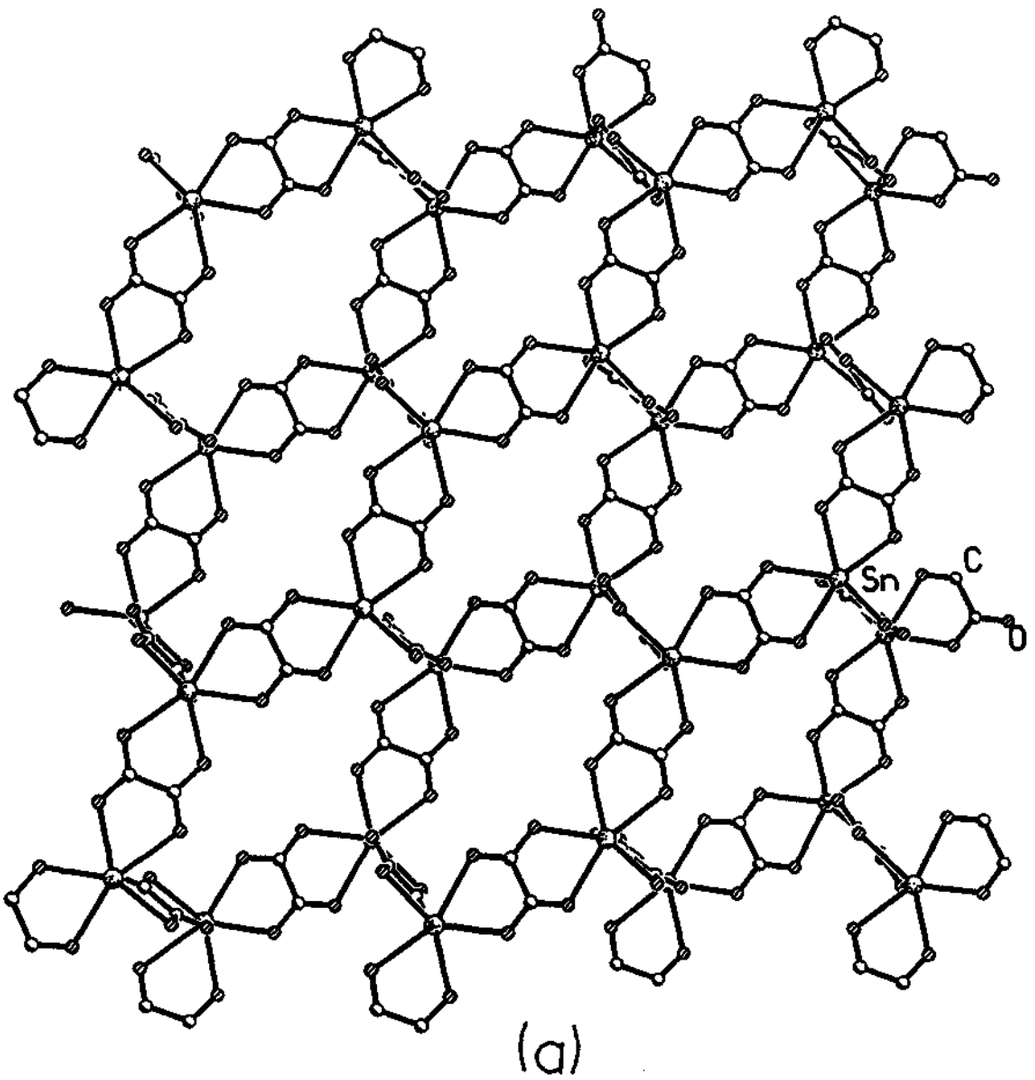

Figure 4.2.2

(a) Structure of $[(CH_3)_2NH(CH_2)_2NH(CH_3)_2]^{2+}[Sn_2(C_2O_4)_3]^{2-}H_2O$ along the a axis showing the 12-membered aperture within one singe layer.

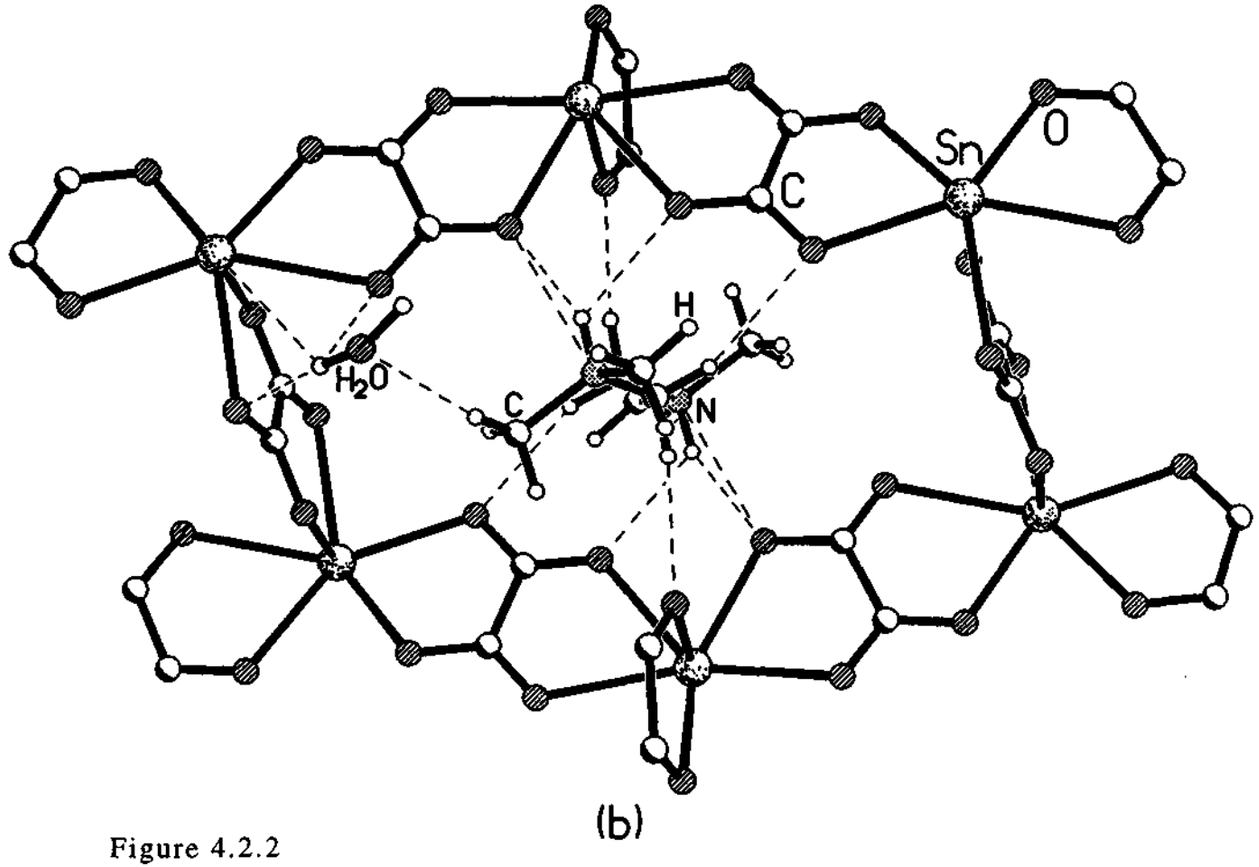

Figure 4.2.2

(b) Figure showing the hydrogen bond interaction of the amine and water molecules with the framework within a 12-membered aperture.

– C – O bond angles are in the range 65.4 - 149.9° and 124.4 - 125.0°, respectively (Table 4.2.4).

4.2.2 Initial characterization of the tin oxalate

TGA of the tin oxalate was carried out in static air from room temperature to 900° C. The weight loss occurs in two steps. A sharp mass loss of about 18% at 300°C corresponds to the loss of the amine along with the hydrogen bonded water moleclules (calc. 21.3%) and the loss of about 16% in the region360-440°C corresponds to the loss of carbon dioxide from the oxalate group. The powder XRD patterns of the decomposed products indicated a poorly crystalline nature with very weak reflections corresponding to SnO (JCPDS: 13-111).

Since the synthesis involves kinetically controlled solvent-mediated reactions, there is no apparent correlation between the starting composition and the stoichiometry of the solid product. The material is a member of the family of low-dimensional framework solids, essentially possessing two-dimensional layered architectures. The layers in the material have oxalate 8- and 12-membered apertures. The entire framework has only hexa-coordinated Sn. The hexa coordinated tin atoms in these oxalates have an unusual coordination, akin to the classic 14-electron systems such as $[IF_6]^-$. This feature is observed in a previous tin(II) oxalate structure as well[32].

4.2.3 Role of lone-pairs in the structure

The lone-pairs of the tin atoms play an important role in the

structure. The stereoactive lone-pairs manifest themselves in the lattice by creating open spaces such as the space between the two layers in these tin oxalates. Similar lone-pair positionings have been observed in many of the layered tin(II) phosphate and related materials.[83,84] In such an arrangement the direct interaction between the lone pairs gets avoided, enhancing the stability of the structure. This situation is reminiscent of $[XeF_5]^+$ type systems where other donor groups approach the Xe atoms obliquely to avoid the lone pair repulsions.[71]

The coordination environment of Sn(II) atoms in phosphates and oxalates presents an interesting comparison. Most of the tin(II) phosphates have three- or four- coordination, forming a trigonal pyramidal SnO_3 or distorted square-pyramidal SnO_4 moieties.[20-24] In the oxalate under discussion, we have higher coordination number. This is probably because the average charge per oxygen on the oxalate (0.5) is less than that on the phosphate (0.75) and more oxalate oxygens are therefore needed to satisfy the valence of tin.

It is to be noted that the tin oxalate under discussion was synthesized by an adjustment of the pH of the synthetic mixture (different phases are formed at lower pH[74,24,77] and the synthesis was effected at near neutral pH. We believe that the phosphoric acid in the initial synthesis mixture essentially acts as a mineralizer, similar to F^- ions in some of the phosphate-based framework solids reported in the literature,[78,85] rather than forming part of the framework (synthesis of

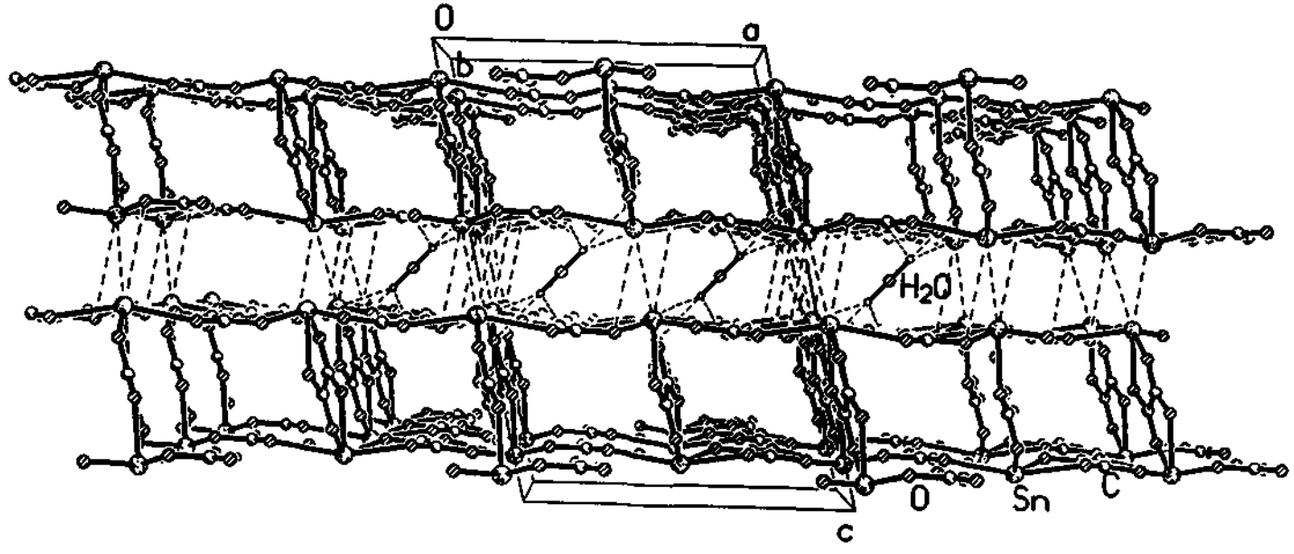

Figure 4.2.3

Structure of $[(CH_3)_2NH(CH_2)_2NH(CH_3)_2]^{2+}[Sn_2(C_2O_4)_3]^{2-}H_2O$ along the b axis showing the 8-membered aperture and the interactions between the water molecules and the framework layers. Note that the dotted lines also show the interactions between the tin atoms (lone-pair interactions) (amine molecules are not shown for clarity).

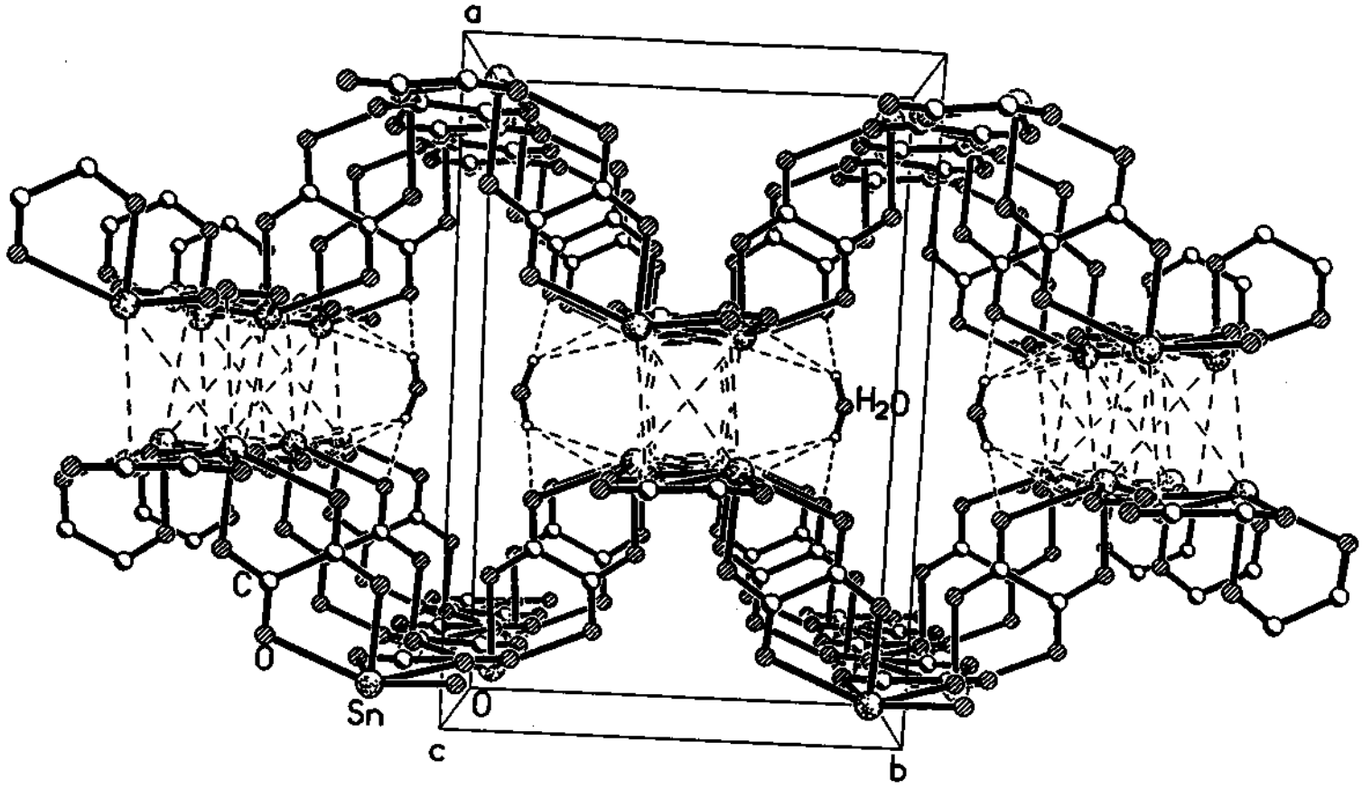

Figure 4.2.4

Structure of $[(CH_3)_2NH(CH_2)_2NH(CH_3)_2]^{2+}[Sn_2(C_2O_4)_3]^{2-}H_2O$ along the c axis showing the layers and the water molecules. Dotted lines represent the various interactions between the layers and the guest species (see text).

phosphate framework materials is generally carried out under acidic conditions). We are presently pursuing this approach further, by exploring the effect of HCl and other additives on the oxalate structures obtained by hydrothermal methods.

Based on the structure of the tin oxalate obtained, and the hydrogen bond and lone-pair interactions present in them, a tentative mechanism for the formation of these materials may be proposed. Interaction between the protonated amine and water with the framework in the tin oxalate leads only to hexa-coordinated tin atoms and 12-membered apertures. While the energy changes involved in the inter-conversions of the rings are likely to be minimal, further work is necessary to understand the mechanism of formation of the variety of open-framework structures in the presence of SDA.

4.2.4 Conclusions

The present study shows that anew open-framework tin(II) oxalates can be synthesized by employing various structure-directing amines. It is noteworthy that the oxalate presented has an unusual coordination for Sn resembling the classic 14 electron systems such as $[IF_6]^-$. The unique coordination environment of Sn(II) described here suggests that it would be profitable to explore this lead further by investigating other Sn(II) dicarboxylates synthesized under similar conditions. Dicarboxylates of other metals are also likely to yield interesting coordination environments and new open-framework structures.

Table 4.2.1 Crystal data and structure refinement parameters for $[(CH_3)_2NH(CH_2)_2NH(CH_3)_2]^{2+}[Sn_2(C_2O_4)_3]^{2-}H_2O$.

Parameters	$[(CH_3)_2NH(CH_2)_2NH(CH_3)_2]^{2+}[Sn_2(C_2O_4)_3]^{2-}H_2O$
Empirical formula	$Sn_2O_{13}C_{12}N_2H_{20}$
Crystal system	Monoclinic
Space group	C2/c (No. 15)
Crystal size (mm)	0.06 x 0.08 x 0.2
a (Å)	16.567(8)
b (Å)	10.851(6)
c (Å)	11.652(6)
β (°)	102.62(3)
Volume ($Å^3$)	2038.6(2)
Z	4
Formula mass	637.4(1)
ρ_{calc} (gcm^{-3})	2.825
λ (MoKα) Å	0.71073
μ (mm^{-1})	5.813
θ range	2.26 – 23.29
Total data collected	4180
Index ranges	$-18 \le h \le 15$, $-12 \le k \le 9$, $-12 \le l \le 12$
Unique data	1466
Observed data ($I > 2\sigma(I)$)	1042
Refinement method	Full-matrix least-squares on $\|F^2\|$
R_{merg}	0.059
R indexes [$I > 2\sigma(I)$]	$R_1 = 0.043^a$, $wR_2 = 0.10^b$
R (all data)	$R_1 = 0.080$, $wR_2 = 0.13$
Goodness of fit ($S_{obs.}$)	1.08
Goodness of fit ($S_{all.}$)	1.05
No. of variables	136
Largest difference map peak and hole $eÅ^{-3}$	0.790 and –1.014

$^a R_1 = \sum ||F_o|-|F_c|| / \sum |F_o|$; $^b wR_2 = \{ \sum[w(F_o^2 - F_c^2)^2] / \sum[w(F_o^2)^2]\}^{1/2}$, $w = 1/[\sigma^2(F_o)^2 + (aP)^2 + bP]$, $P = [\max.(F_o^2,0) + 2(F_c)^2]/3$, where a=0.0433 and b = 0.0 for $[(CH_3)_2NH(CH_2)_2NH(CH_3)_2]^{2+}[Sn_2(C_2O_4)_3]^{2-}H_2O$.

Table 4.2.2 Atomic coordinates (x 10^4) and equ4alent isotropic displacement parameters ($Å^2$ x 10^3) for, $[(CH_3)_2NH(CH_2)_2NH(CH_3)_2]^{2+}[Sn_2(C_2O_4)_3]^{2-}H_2O$

Atom	x	Y	z	U(eq)[#]
Sn(1)	5941(1)	-6076(1)	-15(1)	33(1)
O(1)	6205(4)	-3441(5)	2910(5)	51(2)
O(2)	6551(3)	-8197(5)	-5(5)	39(1)
O(3)	6224(3)	-4276(5)	1167(5)	35(1)
O(4)	7285(3)	-5947(5)	276(5)	36(1)
O(5)	6187(4)	-6533(5)	2097(5)	45(2)
O(6)	6062(4)	-4273(5)	-1203(5)	42(2)
O(100)	5000	-1337(12)	2500	141(6)
C(10)	6199(5)	-4336(8)	2259(8)	35(2)
C(20)	6139(5)	-5647(8)	2749(8)	34(2)
C(30)	7284(5)	-8133(7)	-79(7)	29(2)
N(1)	3548(5)	-1912(8)	4837(8)	51(2)
C(1)	3345(7)	-1182(9)	3695(9)	74(3)
C(2)	4236(7)	-1327(9)	5714(11)	80(4)
C(3)	2816(5)	-2051(7)	5354(8)	41(2)

[#] U(eq) is defined as one third of the trace of the orthogonalized U_{ij} tensor.

Table 4.2.3 Selected bond distances in $[(CH_3)_2NH(CH_2)_2NH(CH_3)_2]^{2+}[Sn_2(C_2O_4)_3]^{2-}H_2O$

Moiety	Distance (Å)	Moiety	Distance (Å)
		Framework	
Sn(1) – O(1) #1	2.596(6)	Sn(1) – O(2)	2.513(6)
Sn(1) – O(3)	2.375(5)	Sn(1) – O(4)	2.182(5)
Sn(1) – O(5)	2.450(6)	Sn(1) – O(6)	2.427(5)
C(10) – O(1)	1.230(10)	C(10) – O(3)	1.280(10)
C(20) – O(5)	1.237(9)	C(20) #1 – O(6)	1.255(9)
C(30) – O(2)	1.237(8)	C(30) #2 – O(4)	1.277(9)
C(10) – C(20)	1.543(11)	C(30) – C(30) #2	1.54(2)
		Organic moiety	
C(1) – N(1)	1.518(12)	C(2) – N(1)	1.494(13)
C(3) – N(1)	1.475(10)	C(3) – C(3) #3	1.53(2)

#1 x, -y-1, z-1/2 #2 -x+3/2, -y-3/2, -z #3 -x+1/2. –y-1/2, -z+1

Table 4.2.4 Selected bond angles in, $[(CH_3)_2NH(CH_2)_2NH(CH_3)_2]^{2+}[Sn_2(C_2O_4)_3]^{2-}H_2O$

Moiety	Angle (°)	Moiety	Angle (°)
Framework			
O(1) $^{\#1}$ – Sn(1) – O(2)	70.7(2)	O(1) $^{\#1}$ – Sn(1) – O(3)	130.6(2)
O(1) $^{\#1}$ – Sn(1) – O(4)	77.5(2)	O(1) $^{\#1}$ – Sn(1) – O(5)	149.9(2)
O(1) $^{\#1}$ – Sn(1) – O(6)	65.4(2)	O(2) – Sn(1) – O(3)	136.2(2)
O(2) – Sn(1) – O(4)	70.3(2)	O(2) – Sn(1) – O(5)	80.3(2)
O(2) – Sn(1) – O(6)	131.1(2)	O(3) – Sn(1) – O(4)	78.0(2)
O(3) – Sn(1) – O(5)	67.6(2)	O(3) – Sn(1) – O(6)	68.6(2)
O(4) – Sn(1) – O(5)	85.3(2)	O(4) – Sn(1) – O(6)	80.1(2)
O(5) – Sn(1) – O(6)	135.8(2)	O(1) – C(10) – O(3)	124.9(7)
O(5) – C(20) – O(6) $^{\#3}$	125.0(8)	O(2) – C(30) –O(4) $^{\#2}$	124.4(7)
O(1) – C(10) – C(20)	119.5(8)	O(2) – C(30) – C(30) $^{\#2}$	118.6(10)
O(3) – C(10) – C(20)	115.6(8)	O(4) $^{\#2}$ – C(30) – C(30) $^{\#2}$	117.0(9)
O(5) – C(20) – C(10)	118.2(8)	O(6) $^{\#3}$ – C(20) – C(10)	116.8(8)
Organic Moiety			
C(1) – N(1) – C(2)	111.4(8)	C(1) – N(1) – C(3)	111.4(8)
C(2) – N(1) – C(3)	109.8(8)	N(1) – C(3) – C(3) $^{\#4}$	111.9(9)

#1 x, -y-1, z-1/2 #2 -x+3/2, -y-3/2, -z #3 x, -y-1, z+1/2 #4 -x+1/2, -y-1/2, -z+1

Table 4.2.5 Important hydrogen bond distances and angles in $[(CH_3)_2NH(CH_2)_2NH(CH_3)_2]^{2+}$ $[Sn_2(C_2O_4)_3]^{2-}H_2O$

Moiety	Distance (Å)	Moiety	Angle (°)
O(3) – H(7)	2.143(1)	O(3) – H(7) – N(1)	158.5(1)
O(2) – H(101)	2.380(1)	O(2) – H(101) – O(100)	174.3(1)
O(100) – H(3)#	2.395(1)	O(100) – H(3) – C(1)	167.5(1)
O(5) – H(8)	2.497(1)	O(5) – H(8) – C(3)	160.4(1)
O(4) – H(9)	2.434(1)	O(4) – H(9) – C(3)	162.3(1)

Interlayer

4.3 Amine Oxalates and their reactions with Zn^{II} ions

4.3.1 Structure of amine oxalates

In order to study the reaction of the amine oxalates with zinc ions, we have first prepared the oxalates of several amines including those of propylamine (PRO), ethylenediamine (ENO), piperazine (PIPO), imidazole (IMO), guanidine (GUO), and 1,4-diazabicyclo[2,2,2]octane (DABCO-O). An examination of the structures showed that there was strong N-H...O hydrogen bonding between the oxalate and the amine in all the amine oxalates. In most of the amine oxalates, one of the carboxyl groups transfer a proton to the amino nitrogen, leaving the other carboxyl group free to form a linear hydrogen bonded chain as shown in structure A (Fig.4.3.1a). In DABCO-O, the amine forms two N-H...O bonds linking the distorted cyclic carboxylic dimers; the dimers here are formed by the carboxyls in the anti confirmation as shown in structure B (Fig.4.3.1b). The N...O and O...O distances in the amine oxalates are all around 2.5Å and the N-H...O and O-H...O bonds angles in all the amine oxalates are > 150°. Figure 4.3.1

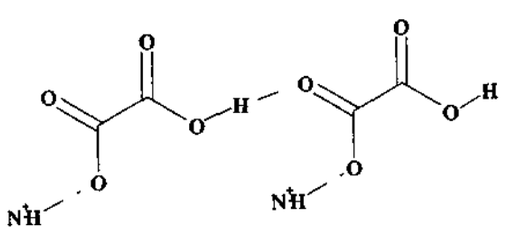

(A)

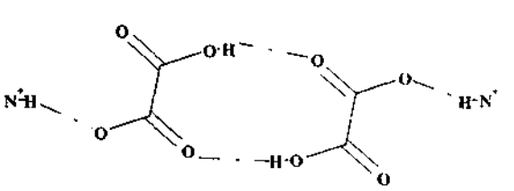

(B)

Table4.3.9 Composition and lattice parameters of the amine oxalates synthesized.

Composition	Cell	Product	Code

1 Oxalic acid:
1 Propylamine:
25 Water
	a=21.6428 (6); b = 5.6737(2);
	c=14.3086 (1) Å;
	β=115.63 (8)°;
	V=1584.148 (2)Å^3;
	Sp.gr.=C2/c
		$[[C_3NH_{10}]^+$.
		$[HC_2O_4]^-$ H_2O
			PRO

2 Oxalic acid;
1 Ethylenediamine;
25 Water
	a=18.004 (9); b=5.679 (2);
	c=13.986 (4) Å;
	β=126.766 (6)°;
	V=1144.4 (2)Å^3;
	Sp.gr.= C2/ c
		$0.5[CH_2NH_3]_2^+$
		$[HC_2O_4]^-$. H_2O
			ENO

2 Oxalic acid;
1Piperazine; 25 Water
	a=15.9626 (6); b=5.7156 (2);
	c=12.354 (1) Å;
	β=108.074 (10)°;V=1071.48(6)Å^3;
	Sp.gr.=C2/ c
		$0.5[C_4N_2H_{12}]^+$
		$[HC_2O_4]^-$
			PIPO

1 Oxalaic acid:
1imidazole: 25 Water
	a=5.6972 (6); b=17.5396 (2);
	c=6.8169 (1) Å;
	β=105.593 (8)°;
	V = 656.1(2)Å^3; Sp.gr.= $P2_1/n$
		$[C_3N_2H_5]^+$
		$[HC_2O_4]^-$
			IMO

2 Oxalic acid:
1Guanidine: 25 Water
	a=6.6991 (9); b=10.5524(6);
	c=10.2243 (2)Å;
	β=103.766(5);
	V = 702.0 (2); Sp.gr. = $P2_1/c$
		$[CN_3H_6]^+$
		$[HC_2O_4]^-.H_2O$
			GUO

2 Oxalic acid: 1DABCO: 25 Water	a=6.9710(6); b=9.6065(10); c= 10.6328 (1) Å; α =91.25(10)°; β=107.51(10)°; γ = 109.35 (10)°; V = 634.8 (11)Å^3; Sp.gr. = $P2_1/n$	$2[HC_2O_4]^-$ $[C_6N_2H_{14}]^+$	DABCO-O

* All synthesis were done at 85° C.

4.3.2 Hydrogen Bonds in Amine Oxalates

All the amine oxalates form N-H...O hydrogen bonds. The carboxylic groups generally form linear O-H...O hydrogen bonds or dimeric O-H...O hydrogen bonds (cyclic dimer), the exception being the guanidinium oxalate. In the N-H...O hydrogen bonds the N...O distances are in the range 2.60-2.93Å and the N-H...O bond angles are in the range 148-177°. In all compounds O-H...O hydrogen bonds are observed

between the monohydrogen oxalate units, the exception being the guanidinium-oxalate. The O...O distances in these O-H...O hydrogen bonds lies in the range 2.56-2.75Å, while the O-H...O bond angles vary from 157° to 172°. In C-H...O hydrogen bonds C...O distances are generally in the range 3.32-3.48Å, again the exception being the guanidinium oxalate. In imidazolium oxalate the C-H...O hydrogen bonds are very weak. We list the various D...A hydrogen bond distances and D-H...A angles in (Table 4.3.13). It is interesting to note that in none of the case amines form any hydrogen bonds between them.

In PRO, ENO, PIPO and IMO the O-H...O hydrogen bonds between the carboxylate moieties result in linear chains of anionic oxalates (See Fig.4.3.1a). In DABCO-O a very unusual orientation of the carboxylic hydrogen is observed, which has been reported only in a very few carboxylates (see Fig.4.3.1b). In PIPO and IMO classic bifurcated N-H...O bonds forming a $R^2_1(5)$ ring system is present. Especially in the case of DABCO Oxalate the N-H...O, C-H...O hydrogen bonds form distinct ring systems namely, $R^2_2(8)$ characteristic of oxalic acid and carboxylates, $R^2_1(5)$ ring by the bifurcated N-H...O bonds and the $R^2_2(5)$ ring by the C-H...O bonds. In guanidine molecules there is no evidence of any considerable O-H...O or C-H...O hydrogen bonds. The tables of atomic coordinates and bond lengths of amine oxalates are not presented for brevity.

4.3.3 Reactions of Amine Oxalate with Zinc

The amine oxalates were reacted with Zn^{II} ions under hydrothermal conditions. The structure of $[CN_3H_6]_2[Zn(H_2O)_2(C_2O_4)_2]$ is that of a monomer consisting of two oxalate units directly linked to Zn atoms, which are also bonded to two water molecules. The monomeric zinc oxalate units are held by strong hydrogen bonds with the monoprotonated amine (Fig. 4.3.2a). In $[C_4N_2H_{12}]_3[Zn_2(C_2O_4)_5].8H_2O$, two Zn atoms are joined by one oxalate unit, leaving two terminal oxalates and thereby forming a dimeric unit. The dimeric zinc oxalate is hydrogen bonded to the diprotonated amine (Fig. 4.3.2b). In $[C_6N_2H_{14}][Zn(C_2O_4)_2].3H_2O$, the connectivity between Zn and the oxalate units is such as to form a one-dimensional chain with each Zn possessing a terminal oxalate unit. The diprotonated amine is situated in between these chains and interacts with the terminal oxalate via hydrogen bonds (Fig. 4.3.3a). Zinc oxalate dihydrate, $[Zn(C_2O_4)(H_2O)_2]$, with a chain architecture has been known earlie[82], but this is the first example of a chain zinc oxalate synthesized with the structure-directing amine. The $[C_4N_2H_{12}][Zn_2(C_2O_4)_3].4H_2O$ has a two-dimensional layer structure involving the honeycomb motif as in many of the divalent metal oxalates. The diprotonated amine sits in the middle of a 12-membered ring (6 Zn and 6 oxalate units) as shown in Fig.4.3.3b. In $[C_3NH_{10}]_2[Zn_2(C_2O_4)_3].3H_2O$, the connectivity between Zn and the oxalates units give rise to a three-dimensional structure, consisting of a 20-membered aperture which on projection forms a 12-

membered square channels. The amine sits in the middle of the channels. $[C_3NH_{10}]_2[Zn_2(C_2O_4)_3].3H_2O$ was recently synthesized by employing the conventional hydrothermal procedure and the structure described in section 4.1.1 in this chapter.

What is significant in the present study is that zinc oxalates with one-, two- and three-dimensional architectures, in addition to the monomeric and dimeric oxalates, could be synthesized by using amine oxalates. In Fig. 4.3.5, we have presented the various types of structures obtained by us to demonstrate the similarities and relationships. We can derive the structure of the dimer from that of the monomer, the chain from the dimer, and the layer from the chain. Just as the four-membered ring monomeric phosphate unit plays a crucial role in the building of framework phosphates[40,41,168], it is possible that the monomeric and dimeric oxalates are involved in the construction of the extended oxalate framework structures. We are pursuing the synthesis of a variety of amine dicarboxylates and their reactions with metal ions.

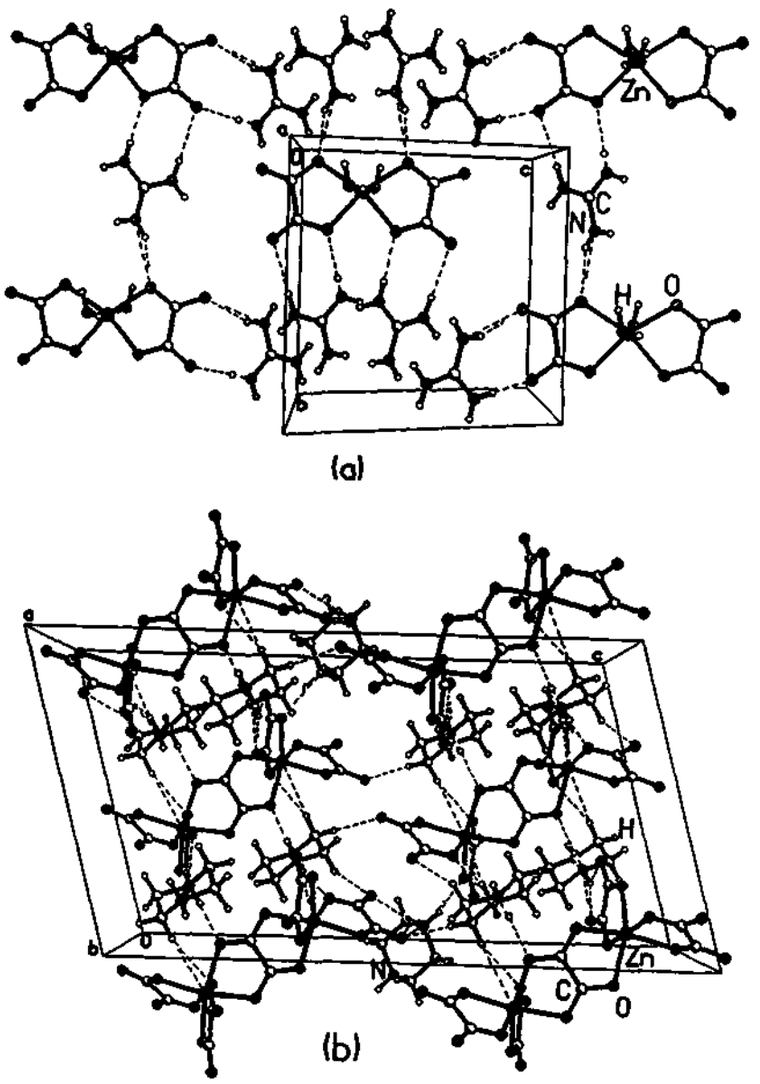

Figure 4.3.2

(a) Structure of the monomer, along the [100] direction. Dotted lines represent hydrogen bond interactions.

(b) Structure of the dimer, along the [010] direction. The dimer and the amine alternate in a plane. Water molecules are omitted for clarity. Dotted lines are hydrogen bond interactions.

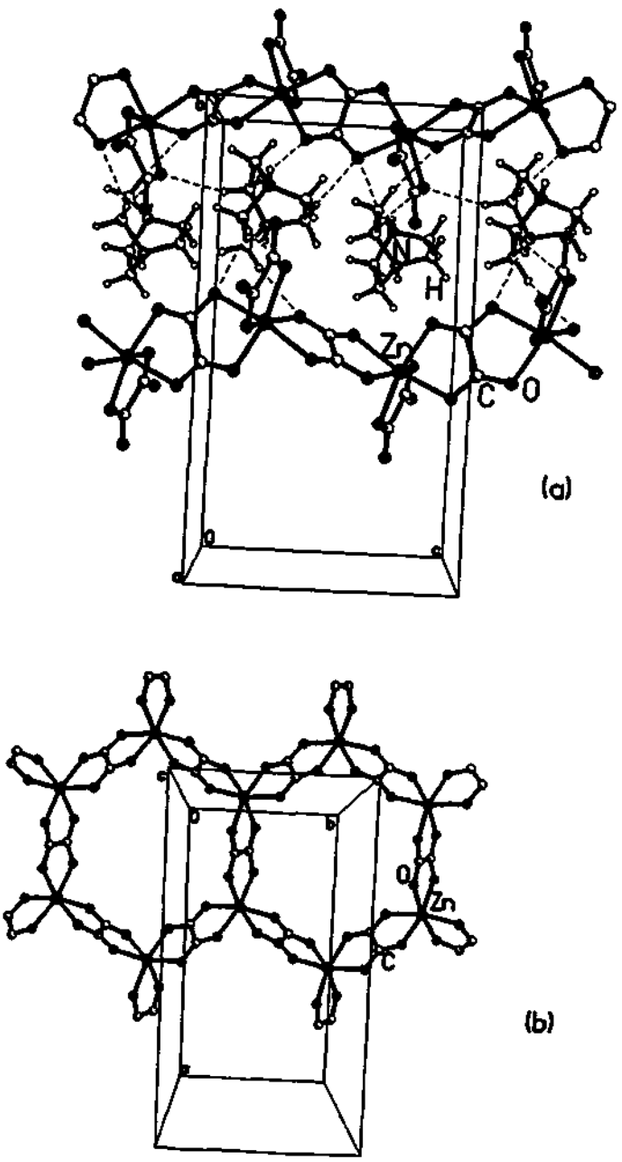

Figure 4.3.3.

(a) Structure of the linear chain, along the [100] direction. The oxalate chains are separated by the amine.

(b) Structure of the layer structure, along the [001] direction showing the honeycomb architecture. The amine and water molecules are not shown.

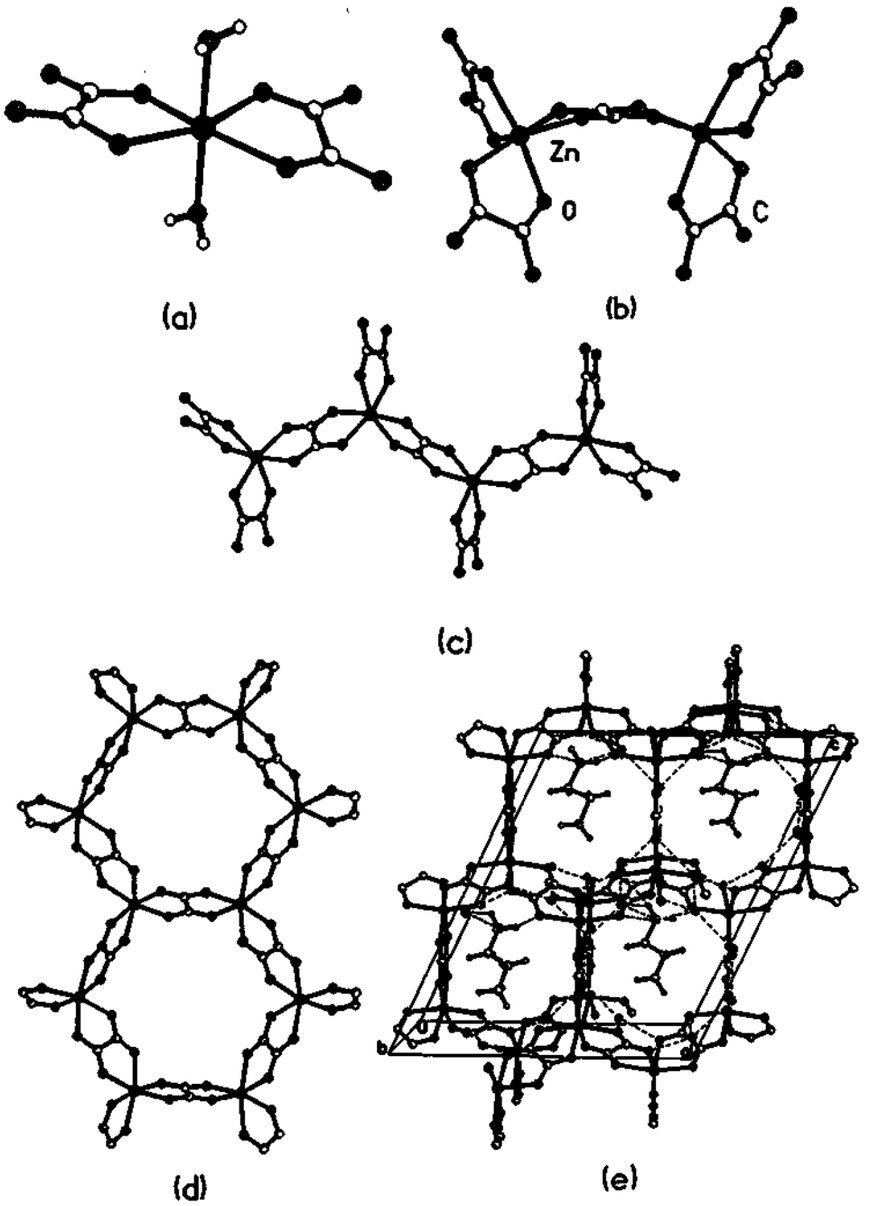

Figure 4.3.4

Figure showing the various structure types obtained in the present study: (a) monomer, (b) dimer, (c) one-dimensional chain, (d) two-dimensional layer and (e) three-dimensional structure. Note the close relationships between them.

Table 4.3.1 Crystal data and structure refinement for zinc oxalate monomer with guanidine.

Parameter	Monomer
Empirical formula	$C_3H_8N_3O_5Zn_{0.5}$
Crystal system	Monoclinic
Space group	C2/c
Crystal size (mm)	0.2× 0.1× 0.1 mm
a (Å)	14.170(2)
b (Å)	10.1285(2)
c (Å)	11.3243(4)
α (°)	90
β (°)	115.4(3)
γ (°)	90
Volume (Å^3)	1468.1 (9)
Z	8
Formula mass	198.81
ρ_{calc} (gcm^{-3})	1.799
λ (MoKα) Å	0.71073
μ (mm^{-1})	1.739
θ range	2.56 to 23.26°
Total data collected	3002
Index ranges	-15 ≤ h ≤ 15, -11 ≤ k ≤ 11, -12 ≤ l ≤12
Unique data	1051
Observed data (σ >2σ(I))	1053
Refinement method	Full-matrix least-squares on $\|F^2\|$
R indices [I >2σ(I)]	R_1 = 0.0437, wR2 = 0.0970
R indices (all data)	R_1 = 0.0558, wR_2 = 0.1073
Goodness of fit (S)	1.138
No. of variables	138
Largest difference map peak and hole eÅ^{-3}	0.402 and –0.547

[a] $w=1/[\sigma^2(F_0)^2+(0.0197P)^2+10.2010P]$ where $P=[F_0^2+2F_c^2]/3$.

[b] $w=1/[\sigma^2(F_0)^2+(0.0619P)^2]$ where $P=[F_0^2+2F_c^2]/3$

Table 4.3.2 Crystal data and structure refinement for zinc oxalate dimer with piperazine.

Parameter	Dimer
Empirical formula	$C_{11}H_{18}N_3O_{14}Zn$
Crystal system	Monoclinic
Space group	C2/c
Crystal size (mm)	0.2× 0.1× 0.1 mm
a (Å)	13.789(2)
b (Å)	11.524(2)
c (Å)	25.412(4)
α (°)	90
β (°)	105.19(3)
γ (°)	90
Volume ($Å^3$)	3897.2 (9)
Z	8
Formula mass	481.65
ρ_{calc} (gcm^{-3})	1.642
λ (MoKα) Å	0.71073
μ (mm^{-1})	1.337
θ range	2.34to 23.28°
Total data collected	7750
Index ranges	$-15 \leq h \leq 14$, $-11 \leq k \leq 12$, $-17 \leq l \leq 28$
Unique data	2757
Observed data ($\sigma > 2\sigma(I)$)	2758
Refinement method	Full-matrix least-squares on $\|F^2\|$
R indices [$I > 2\sigma(I)$]	$R_1 = 0.0418$, wR2 = 0.1158
R indices (all data)	$R_1 = 0.0520$, $wR_2 = 0.1243$
Goodness of fit (S)	1.109
No. of variables	262
Largest difference map peak and hole $eÅ^{-3}$	0.638 and –0.535

[a] $w=1/[\sigma^2(F_0)^2+(0.0197P)^2+10.2010P]$ where $P=[F_0^2+2F_c^2]/3$.

[b] $w=1/[\sigma^2(F_0)^2+(0.0619P)^2]$ where $P=[F_0^2+2F_c^2]/3$

Table 4.3.3 Crystal data and structure refinement for zinc oxalate chain with DABCO

Parameter	Chain
Empirical formula	$C_{10}H_{20}N_2O_{11}Zn$
Crystal system	Monoclinic
Space group	$P2_1/n$
Crystal size (mm)	0.08× 0.08× 0.14 mm
a (Å)	9.4328 (2)
b (Å)	16.8608 (2)
c (Å)	9.7878 (4)
α (°)	90
β (°)	91.37(3)
γ (°)	90
Volume ($Å^3$)	1556.1 (9)
Z	4
Formula mass	409.65
ρ_{calc} (gcm^{-3})	1.749
λ (MoKα) Å	0.71073
μ (mm^{-1})	1.641
θ range	2.41 to 23.30°
Total data collected	6499
Index ranges	$-10 \le h \le 9$, $-18 \le k \le 12$, $-9 \le l \le 10$
Unique data	2236
Observed data ($\sigma > 2\sigma(I)$)	2246
Refinement method	Full-matrix least-squares on $]F^2]$
R indices [$I > 2\sigma(I)$]	$R_1 = 0.0482$, wR2 = 0.1040
R indices (all data)	$R_1 = 0.1001$, $wR_2 = 0.1293$
Goodness of fit (S)	0.990
No. of variables	241
Largest difference map peak and hole $eÅ^{-3}$	0.695 and –0.708

[a] $w=1/[\sigma^2(F_0)^2+(0.0197P)^2+10.2010P]$ where $P=[F_0^2+2F_c^2]/3$.

[b] $w=1/[\sigma^2(F_0)^2+(0.0619P)^2]$ where $P=[F_0^2+2F_c^2]/3$

Table 4.3.4 Crystal data and structure refinement for layered zinc oxalate with piperazine

Parameter	Layered
Empirical formula	$C_{10}H_{20}N_2O_{16}Zn_2$
Crystal system	Monoclinic
Space group	C2/c
Crystal size (mm)	0.2× 0.1× 0.1 mm
a (Å)	16.7253 (2)
b (Å)	9.2540 (2)
c (Å)	31.2982 (4)
α (°)	90
β (°)	98.59(3)
γ (°)	90
Volume ($Å^3$)	4789.9 (9)
Z	4
Formula mass	555.1
ρ_{calc} (gcm^{-3})	0.881
λ (MoKα) Å	0.71073
μ (mm^{-1})	1.043
θ range	1.32 to 23.29°
Total data collected	9600
Index ranges	$-18 \le h \le 13$, $-10 \le k \le 10$, $-30 \le l \le 34$
Unique data	3439
Observed data ($\sigma > 2\sigma(I)$)	3439
Refinement method	Full-matrix least-squares on $\|F^2\|$
R indices [$I > 2\sigma(I)$]	$R_1 = 0.0539$, wR2 = 0.1347
R indices (all data)	$R_1 = 0.0920$, $wR_2 = 0.1612$
Goodness of fit (S)	1.064
No. of variables	326
Largest difference map peak and hole $eÅ^{-3}$	0.266 and –0.875

[a] $w=1/[\sigma^2(F_0)^2+(0.0197P)^2+10.2010P]$ where $P=[F_0^2+2F_c^2]/3$.

[b] $w=1/[\sigma^2(F_0)^2+(0.0619P)^2]$ where $P=[F_0^2+2F_c^2]/3$

Table 4.3.5 Atomic coordinates [$\times 10^4$] and equivalent isotropic displacement parameters [$Å^2 \times 10^3$] for zinc oxalate monomer with guanidine.

Moiety	x	y	z	U(eq) #
Zn(1)	5000(4)	8287(1)	7500(2)	28(1)
O(1)	4236(3)	6782(3)	6182(3)	34(1)
O(2)	5775(2)	9379(3)	9231(3)	32(1)
O(3)	6304(3)	8454(4)	7005(4)	32(1)
C(1)	3767(3)	7156(4)	5016(5)	27(1)
O(4)	3273(3)	6400(3)	4070(3)	38(1)
C(2)	6190(3)	8667(5)	10242(5)	28(1)
O(5)	6550(3)	9039(3)	11393(3)	41(1)
C(10)	3769(3)	3251(4)	6037(4)	31(1)
N(1)	3946(4)	3563(5)	5017(5)	43(1)
N(2)	3648(4)	4191(5)	6779(5)	43(1)
N(3)	3690(4)	1997(4)	6327(5)	43(1)

U(eq) is defined as one third of the trace of orthogonalized U_{ij} tensor.

Table 4.3.6. Atomic coordinates [$\times 10^4$] and equivalent isotropic displacement parameters [$Å^2 \times 10^3$] for zinc oxalate dimer with piperazine.

Moiety	x	y	z	U(eq) #
Zn(1)	1164(1)	10949(1)	8537(1)	27(1)
O(1)	1770(2)	12488(3)	8864(1)	39(1)
O(2)	706(2)	9275(3)	8303(1)	36(1)
O(3)	1310(3)	7523(3)	8211(2)	65(1)
C(1)	1575(3)	12766(4)	9313(2)	31(1)
C(2)	1413(3)	8564(4)	8341(2)	36(1)
O(4)	750(2)	10925(3)	9273(1)	35(1)
O(5)	2557(2)	10100(3)	8716(1)	36(1)
O(6)	616(2)	12164(3)	9928(1)	40(1)
O(7)	1849(3)	13662(3)	9575(1)	47(1)
O(8)	3224(3)	8410(3)	8573(2)	57(1)
C(3)	922(3)	11879(4)	9529(2)	28(1)
C(4)	2508(3)	9048(4)	8563(2)	34(1)
O(9)	-345(2)	11474(3)	8117(1)	30(1)
O(10)	1312(2)	11460(3)	7742(1)	34(1)
C(5)	-478(3)	11468(3)	7604(2)	26(1)
C(6)	8144(5)	10271(5)	8899(2)	57(2)
C(7)	7236(4)	10132(5)	7927(2)	50(1)
N(1)	7838(3)	10299(3)	8369(2)	49(1)
C(8)	7828(4)	9068(4)	7873(2)	42(1)
C(9)	8734(4)	9211(5)	8847(2)	50(1)
N(2)	8159(3)	8439(3)	8403(2)	36(1)
C(10)	10143(4)	5663(5)	9543(2)	42(1)
C(11)	9061(4)	4391(4)	9914(2)	43(1)
N(3)	9132(3)	5498(3)	9627(2)	38(1)
O(100)	1074(3)	8706(4)	9789(2)	71(1)
O(200)	9409(3)	6772(4)	8146(3)	94(2)
O(300)	4780(4)	9326(4)	8114(3)	114(2)
O(400)	2210(9)	7183(10)	9434(4)	216(5)

U (eq) is defined as one third of the trace of orthogonalized U_{ij} tensor.

Table 4.3.7. Atomic coordinates [$\times 10^4$] and equivalent isotropic displacement parameters [$Å^2 \times 10^3$] for zinc oxalate chain with DABCO.

Moiety	x	y	z	U(eq) #
Zn(1)	993(1)	4542(1)	2514(1)	36(1)
O(1)	-780(4)	4417(2)	3710(4)	41(1)
O(2)	441(4)	5568(2)	1437(4)	37(1)
O(3)	3119(4)	4614(2)	1978(4)	39(1)
O(4)	1712(4)	3416(2)	3144(4)	42(1)
O(5)	293(4)	4046(2)	634(4)	38(1)
O(6)	1604(4)	5239(2)	4250(4)	42(1)
C(1)	-682(6)	4758(4)	4844(6)	34(2)
C(2)	3768(7)	3983(4)	2159(6)	41(2)
C(3)	2945(7)	3275(4)	2764(6)	39(2)
C(4)	-39(6)	4562(4)	-237(6)	30(1)
O(7)	3554(5)	2618(3)	2802(5)	67(2)
O(8)	5035(5)	3863(3)	1887(6)	76(2)
O(100)	4397(8)	5834(6)	4865(10)	86(2)
O(200)	1533(7)	1396(5)	3152(8)	67(2)
O(300)	6779(7)	5027(4)	873(7)	77(2)
N(2)	-1201(5)	1749(3)	2341(5)	42(1)
N(1)	-3396(5)	2545(3)	2220(5)	44(1)
C(10)	-2237(7)	2990(4)	1552(7)	46(2)
C(9)	-983(7)	2448(4)	1436(7)	50(2)
C(8)	-2383(7)	1251(4)	1736(7)	47(2)
C(7)	-3660(7)	1777(4)	1507(6)	46(2)
C(6)	-1553(8)	2004(5)	3715(6)	60(2)
C(5)	-3007(7)	2394(5)	3682(6)	55(2)

U (eq) is defined as one third of the trace of orthogonalized U_{ij} tensor.

Table 4.3.8. Atomic coordinates [$\times 10^4$] and equivalent isotropic displacement parameters [$Å^2 \times 10^3$] for layered zinc oxalate with piperazine.

Moiety	x	y	z	U(eq) #
Zn(1)	4770(1)	1345(1)	3612(1)	30(1)
Zn(2)	6513(1)	-3641(1)	3596(1)	28(1)
O(1)	3911(3)	692(5)	3988(2)	33(1)
O(2)	3709(3)	1951(6)	3210(2)	34(1)
O(3)	5736(3)	245(6)	3978(2)	38(1)
O(4)	5003(3)	3267(5)	3967(2)	36(1)
O(5)	5519(3)	2440(5)	3234(2)	37(1)
O(6)	4793(3)	-575(5)	3243(2)	34(1)
O(7)	6467(3)	-1768(5)	3955(2)	35(1)
O(8)	7569(3)	-4337(6)	3977(2)	34(1)
O(9)	6252(3)	-5545(5)	3239(2)	33(1)
O(10)	7371(3)	-2969(6)	3211(2)	33(1)
O(11)	5580(3)	-2504(5)	3199(2)	33(1)
O(12)	5724(3)	-4700(5)	3968(2)	33(1)
C(1)	8198(4)	-4028(7)	3821(2)	28(2)
C(2)	8078(5)	-3263(7)	3379(2)	26(2)
C(3)	5913(4)	-920(8)	3809(2)	30(2)
C(4)	5472(4)	4104(8)	3816(2)	27(2)
C(5)	5779(4)	3628(8)	3395(2)	29(2)
C(6)	5384(4)	-1364(8)	3378(2)	28(2)
O(100)	3702(4)	693(7)	2321(2)	59(2)
O(200)	6662(4)	-5685(9)	905(2)	78(2)
O(300)	5124(9)	1273(18)	4938(8)	294(11)
O(400)	4874(8)	-3950(14)	4677(4)	173(5)
C(7)	6203(5)	-4451(9)	1891(3)	42(2)
C(8)	6204(5)	-3811(9)	2332(3)	42(2)
C(9)	7109(5)	-1903(9)	2140(3)	44(2)
C(10)	7060(6)	-2580(10)	1701(3)	52(2)
C(11)	6879(7)	-3585(10)	4949(3)	66(3)
C(12)	7368(5)	-1110(8)	4806(2)	33(2)
C(13)	6984(9)	2204(14)	5313(4)	92(4)
C(14)	7123(9)	2577(13)	4572(4)	94(4)
N(1)	6361(4)	-2232(7)	2326(2)	36(2)

N(2)	6938(4)	-4139(8)	1711(2)	44(2)
N(3)	6690(7)	-1939(12)	4954(3)	108(4)
N(4)	6819(6)	1634(10)	4884(3)	83(3)

U(eq) is defined as one third of the trace of orthogonalized U_{ij} tensor.

Table 4.3.9 Selected bond lengths and bond angles of zinc oxalate monomer with guanidine.

Moiety	Distance (Å)	Moiety	Angle (°)
Zn(1)-O(1)	2.083(3)	O(2)#1-Zn(1)-O(2)	116.6(2)
Zn(1)-O(1)#1	2.083(3)	O(1)-Zn(1)-O(3)	96.39(14)
Zn(1)-O(2)#1	2.103(3)	O(1)#1-Zn(1)-O(3)	90.2(2)
Zn(1)-O(2)	2.103(3)	O(2)#1-Zn(1)-O(3)	83.08(14)
Zn(1)-O(3)	2.155(4)	O(2)-Zn(1)-O(3)	92.19(13)
Zn(1)-O(3)#1	2.155(4)	O(1)-Zn(1)-O(3)#1	90.2(2)
O(1)-C(1)	1.255(5)	O(1)#1-Zn(1)-O(3)#1	96.39(14)
O(2)-C(2)	1.264(5)	O(2)#1-Zn(1)-O(3)#1	92.19(13)
C(1)-O(4)	1.257(5)	O(2)-Zn(1)-O(3)#1	83.08(14)
C(1)-C(2)#1	1.564(6)	O(3)-Zn(1)-O(3)#1	171.0(2)
C(2)-O(5)	1.237(5)	C(1)-O(1)-Zn(1)	114.3(3)
C(2)-C(1)#1	1.564(6)	C(2)-O(2)-Zn(1)	113.5(3)
C(10)-N(1)	1.321(7)	O(1)-C(1)-O(4)	124.3(4)
C(10)-N(2)	1.328(6)	O(1)-C(1)-C(2)#1	116.5(4)
C(10)-N(3)	1.329(6)	O(4)-C(1)-C(2)#1	119.2(4)
Moiety	Angle (°)	O(5)-C(2)-O(2)	127.0(4)
O(1)-Zn(1)-O(1)#1	85.9(2)	O(5)-C(2)-C(1)#1	117.6(4)
O(1)-Zn(1)-O(2)#1	79.26(11)	O(2)-C(2)-C(1)#1	115.4(4)
O(1)#1-Zn(1)-O(2)#1	162.87(12)	N(1)-C(10)-N(2)	120.4(5)
O(1)-Zn(1)-O(2)	162.87(12)	N(1)-C(10)-N(3)	120.8(5)
O(1)#1-Zn(1)-O(2)	79.26(11)	N(2)-C(10)-N(3)	118.8(5)

Symmetry transformations used to generate equivalent atoms :

#1 -x+1, y, -z+3/2

Table 4.3.10. Selected bond lengths and angles of zinc oxalate dimer with piperazine oxalate.

Moiety	Distance (Å)	Moiety	Angle (°)
Zn(1)-O(1)	2.043(3)	O(2)-Zn(1)-O(9)	86.40(12)
Zn(1)-O(2)	2.069(3)	O(4)-Zn(1)-O(9)	89.58(12)
Zn(1)-O(4)	2.093(3)	O(5)-Zn(1)-O(9)	161.16(11)
Zn(1)-O(5)	2.097(3)	O(1)-Zn(1)-O(10)	90.85(12)
Zn(1)-O(9)	2.160(3)	O(2)-Zn(1)-O(10)	94.69(13)
Zn(1)-O(10)	2.164(3)	O(4)-Zn(1)-O(10)	162.14(12)
O(1)-C(1)	1.279(5)	O(5)-Zn(1)-O(10)	91.35(12)
O(2)-C(2)	1.257(5)	O(9)-Zn(1)-O(10)	77.14(10)
O(3)-C(2)	1.243(6)	C(1)-O(1)-Zn(1)	114.9(3)
C(1)-O(7)	1.233(5)	C(2)-O(2)-Zn(1)	114.4(3)
C(1)-C(3)	1.555(6)	O(7)-C(1)-O(1)	125.9(4)
C(2)-C(4)	1.569(6)	O(7)-C(1)-C(3)	118.9(4)
O(4)-C(3)	1.268(5)	O(1)-C(1)-C(3)	115.3(4)
O(5)-C(4)	1.270(5)	O(3)-C(2)-O(2)	125.2(4)
O(6)-C(3)	1.242(5)	O(3)-C(2)-C(4)	118.1(4)
O(8)-C(4)	1.226(6)	O(2)-C(2)-C(4)	116.7(4)
O(9)-C(5)	1.267(5)	C(3)-O(4)-Zn(1)	112.9(3)
O(10)-C(5)#1	1.252(5)	C(4)-O(5)-Zn(1)	114.0(3)
C(5)-O(10)#1	1.252(5)	O(6)-C(3)-O(4)	126.2(4)
C(5)-C(5)#1	1.544(8)	O(6)-C(3)-C(1)	117.9(4)
C(6)-N(1)	1.488(7)	O(4)-C(3)-C(1)	115.9(4)
C(6)-C(9)	1.492(8)	O(8)-C(4)-O(5)	126.0(4)
C(7)-N(1)	1.498(7)	O(8)-C(4)-C(2)	119.2(4)
C(7)-C(8)	1.499(7)	O(5)-C(4)-C(2)	114.7(4)
C(8)-N(2)	1.491(6)	C(5)-O(9)-Zn(1)	111.6(2)
C(9)-N(2)	1.492(6)	C(5)#1-O(10)-Zn(1)	111.3(3)
C(10)-N(3)	1.478(6)	O(10)#1-C(5)-O(9)	125.6(4)
C(10)-C(11)#2	1.523(7)	O(10)#1-C(5)-C(5)#1	118.0(5)
C(11)-N(3)	1.485(6)	O(9)-C(5)-C(5)#1	116.4(5)
C(11)-C(10)#2	1.523(7)	N(1)-C(6)-C(9)	110.5(4)
Moiety	Angle (°)	N(1)-C(7)-C(8)	110.1(4)
O1)-Zn(1)-O(2)	171.34(11)	N(2)-C(8)-C(7)	111.2(4)
O(2)-Zn(1)-O(4)	96.36(11)	N(2)-C(9)-C(6)	111.2(4)
O(1)-Zn(1)-O(5)	93.59 (12)	C(8)-N(2)-C(9)	111.6(4)

O(2)-Zn(1)-O(5)	79.64(13)	N(3)-C(10)-C(11)#2	110.2(4)
O(4)-Zn(1)-O(5)	104.41(12)	N(3)-C(11)-C(10)#2	110.8(4)
O(1)-Zn(1)-O(9)	101.35(13)	C(10)-N(3)-C(11)	111.6(4)

Symmetry transformations used to generate equivalent atoms :

#1 –x, y, -z+3/2 #2 –x+2, -y+1, -z+2

Table 4.3.11. Selected bond distances and bond angles of chain-like zinc oxalate with DABCO

Moiety	Distance (Å)	Moiety	Angle (°)
Zn(1)-O(1)	2.074(4)	O(3)-Zn(1)-O(5)	94.9(2)
Zn(1)-O(2)	2.085(4)	O(4)-Zn(1)-O(5)	89.4(2)
Zn(1)-O(3)	2.089(4)	O(1)-Zn(1)-O(6)	79.2(2)
Zn(1)-O(4)	2.103(4)	O(2)-Zn(1)-O(6)	90.3(2)
Zn(1)-O(5)	2.112(4)	O(3)-Zn(1)-O(6)	85.7(2)
Zn(1)-O(6)	2.134(4)	O(4)-Zn(1)-O(6)	100.6(2)
O(1)-C(1)	1.253(7)	O(5)-Zn(1)-O(6)	169.9(2)
O(2)-C(4)#1	1.245(6)	C(1)-O(1)-Zn(1)	114.2(4)
O(3)-C(2)	1.238(7)	C(4)#1-O(2)-Zn(1)	113.4(4)
O(4)-C(3)	1.252(6)	C(2)-O(3)-Zn(1)	112.9(4)
O(5)-C(4)	1.252(7)	C(3)-O(4)-Zn(1)	112.3(4)
O(6)-C(1)#2	1.257(7)	C(4)-O(5)-Zn(1)	112.7(3)
C(1)-O(6)#2	1.257(7)	C(1)#2-O(6)-Zn(1)	112.6(4)
C(1)-C(1)#2	1.546(11)	O(1)-C(1)-O(6)#2	126.1(5)
C(2)-O(8)	1.248(7)	O(1)-C(1)-C(1)#2	117.4(7)
C(2)-C(3)	1.549(9)	O(6)#2-C(1)-C(1)#2	116.5(7)
C(3)-O(7)	1.248(7)	O(3)-C(2)-O(8)	125.6(6)
C(4)-O(2)#1	1.245(6)	O(3)-C(2)-C(3)	117.8(6)
C(4)-C(4)#1	1.550(12)	O(8)-C(2)-C(3)	116.6(6)
N(2)-C(6)	1.457(7)	O(7)-C(3)-O(4)	126.2(6)
N(2)-C(9)	1.492(7)	O(7)-C(3)-C(2)	117.4(6)
N(2)-C(8)	1.506(7)	O(4)-C(3)-C(2)	116.4(6)
N(1)-C(7)	1.489(8)	O(2)#1-C(4)-O(5)	125.9(5)
N(1)-C(10)	1.490(7)	O(2)#1-C(4)-C(4)#1	117.5(7)
N(1)-C(5)	1.490(8)	O(5)-C(4)-C(4)#1	116.6(6)
C(10)-C(9)	1.500(8)	C(6)-N(2)-C(9)	110.7(5)
C(8)-C(7)	1.509(8)	C(6)-N(2)-C(8)	110.2(5)
C(6)-C(5)	1.521(9)	C(9)-N(2)-C(8)	108.6(5)
Moiety	Angle (°)	C(7)-N(1)-C(10)	110.4(5)
O(1)-Zn(1)-O(2)	100.1(2)	C(7)-N(1)-C(5)	109.6(5)
O(1)-Zn(1)-O(3)	159.9(2)	C(10)-N(1)-C(5)	110.0(5)
O(2)-Zn(1)-O(3)	93.1(2)	N(1)-C(10)-C(9)	108.4(5)
O(1)-Zn(1)-O(4)	90.1(2)	N(2)-C(9)-C(10)	108.4(5)

O(2)-Zn(1)-O(4)	166.3(2)	N(2)-C(8)-C(7)	108.1(5)
O(3)-Zn(1)-O(4)	79.7(2)	N(1)-C(7)-C(8)	108.5(5)
O(1)-Zn(1)-O(5)	102.2(2)	N(2)-C(6)-C(5)	109.4(5)
O(2)-Zn(1)-O(5)	79.6(2)	N(1)-C(5)-C(6)	107.2(5)

Symmetry transformations used to generate equivalent atoms :

#1 –x, -y+1, -z #2 –x, -y+1, -z+1

Table 4.3.12. Selected bond lengths and bond angles of layered zinc oxalate with piperazine.

Moiety	Distance (Å)	Moiety	Angle (°)
Zn(1)-O(1)	2.079(5)	O(4)-Zn(1)-O(6)	168.1(2)
Zn(1)-O(2)	2.092(5)	O(5)-Zn(1)-O(6)	92.1(2)
Zn(1)-O(3)	2.100(5)	O(7)-Zn(2)-O(8)	92.6(2)
Zn(1)-O(4)	2.103(5)	O(7)-Zn(2)-O(9)	165.8(2)
Zn(1)-O(5)	2.107(5)	O(8)-Zn(2)-O(9)	97.9(2)
Zn(1)-O(6)	2.123(5)	O(7)-Zn(2)-O(10)	98.5(2)
Zn(2)-O(7)	2.074(5)	O(8)-Zn(2)-O(10)	80.1(2)
Zn(2)-O(8)	2.082(5)	O(9)-Zn(2)-O(10)	92.8(2)
Zn(2)-O(9)	2.098(5)	O(7)-Zn(2)-O(11)	79.6(2)
Zn(2)-O(10)	2.101(5)	O(8)-Zn(2)-O(11)	167.4(2)
Zn(2)-O(11)	2.123(5)	O(9)-Zn(2)-O(11)	91.6(2)
Zn(2)-O(12)	2.126(5)	O(10)-Zn(2)-O(11)	91.3(2)
O(1)-C(1)#1	1.257(8)	O(7)-Zn(2)-O(12)	90.6(2)
O(2)-C(2)#1	1.264(8)	O(8)-Zn(2)-O(12)	94.9(2)
O(3)-C(3)	1.256(9)	O(9)-Zn(2)-O(12)	78.9(2)
O(4)-C(4)	1.244(8)	O(10)-Zn(2)-O(12)	169.7(2)
O(5)-C(5)	1.259(9)	O(11)-Zn(2)-O(12)	94.9(2)
O(6)-C(6)	1.251(8)	C(1)#1-O(1)-Zn(1)	113.3(5)
O(7)-C(3)	1.248(9)	C(2)#1-O(2)-Zn(1)	113.1(4)
O(8)-C(1)	1.257(8)	C(3)-O(3)-Zn(1)	113.4(5)
O(9)-C(5)#2	1 250(9)	C(4)-O(4)-Zn(1)	113.8(5)
O(10)-C(2)	1.251(8)	C(5)-O(5)-Zn(1)	113.2(5)
O(11)-C(6)	1.260(8)	C(6)-O(6)-Zn(1)	112.5(4)
O(12)-C(4)#2	1.253(8)	C(3)-O(7)-Zn(2)	114.3(5)
C(1)-O(1)#3	1.257(8)	C(1)-O(8)-Zn(2)	113.1(4)
C(1)-C(2)	1.540(11)	C(5)#2-O(9)-Zn(2)	113.6(5)
C(2)-O(2)#3	1.264(8)	C(2)-O(10)-Zn(2)	112.2(4)
C(3)-C(6)	1.554(10)	C(6)-O(11)-Zn(2)	111.9(4)
C(4)-O(12)#4	1.253(8)	C(4)#2-O(12)-Zn(2)	113.6(5)
C(4)-C(5)	1.548(10)	O(1)#3-C(1)-O(8)	126.0(7)
C(5)-O(9)#4	1.250(9)	O(1)#3-C(1)-C(2)	117.2(7)
C(7)-N(2)	1.457(10)	O(8)-C(1)-C(2)	116.8(6)
C(7)-C(8)	1.500(11)	O(10)-C(2)-O(2)#3	125.8(7)
C(8)-N(1)	1.486(10)	O(10)-C(2)-C(1)	117.8(7)
C(9)-N(1)	1.488(10)	O(2)#3-C(2)-C(1)	116.3(6)
C(9)-C(10)	1.502(11)	O(7)-C(3)-O(3)	126.4(7)
C(10)-N(2)	1.458(11)	O(7)-C(3)-C(6)	116.6(7)
C(11)-C(12)#5	1.403(12)	O(3)-C(3)-C(6)	117.0(7)

C(11)-N(3)	1.555(14)	O(4)-C(4)-O(12)#4	126.9(7)
C(12)-C(11)#5	1.403(12)	O(4)-C(4)-C(5)	117.1(6)
C(12)-N(3)	1.498(13)	O(12)#4-C(4)-C(5)	116.0(6)
C(13)-N(4)	1.429(14)	O(9)#4-C(5)-O(5)	125.4(7)
C(13)-C(14)#6	1.50(2)	O(9)#4-C(5)-C(4)	117.9(7)
C(14)-N(4)	1.458(14)	O(5)-C(5)-C(4)	116.7(7)
C(14)-C(13)#6	1.50(2)	O(6)-C(6)-O(11)	125.7(7)
Moiety	Angle (°)	O(6)-C(6)-C(3)	117.3(7)
O(1)-Zn(1)-O(2)	79.8(2)	O(11)-C(6)-C(3)	117.1(6)
O(1)-Zn(1)-O(3)	95.1(2)	N(2)-C(7)-C(8)	113.1(7)
O(2)-Zn(1)-O(3)	166.5(2)	N(1)-C(8)-C(7)	110.7(7)
O(1)-Zn(1)-O(4)	92.0(2)	N(1)-C(9)-C(10)	109.8(7)
O(2)-Zn(1)-O(4)	99.5(2)	N(2)-C(10)-C(9)	112.5(7)
O(3)-Zn(1)-O(4)	93.1(2)	C(12)#5-C(11)-N(3)	111.0(8)
O(1)-Zn(1)-O(5)	167.8(2)	C(11)#5-C(12)-N(3)	112.8(7)
O(2)-Zn(1)-O(5)	93.2(2)	N(4)-C(13)-C(14)#6	108.8(11)
O(3)-Zn(1)-O(5)	93.8(2)	N(4)-C(14)-C(13)#6	110.7(9)
O(4)-Zn(1)-O(5)	79.1(2)	C(8)-N(1)-C(9)	111.5(6)
O(1)-Zn(1)-O(6)	97.8(2)	C(7)-N(2)-C(10)	109.5(6)
O(2)-Zn(1)-O(6)	88.9(2)	C(12)-N(3)-C(11)	109.6(9)
O(3)-Zn(1)-O(6)	79.4(2)	C(13)-N(4)-C(14)	111.7(9)

Symmetry transformations used to generate equivalent atoms :

#1 x-1/2, y+1/2, z #2 x, y-1, z #3 x+1/2, y-1/2, z #4 x, y+1, z

#5 –x+3/2, -y-1/2, -z+1 #6 –x+3/2, -y+1/2, -z+1

Table 4.3.13 H-Bond distances and angles of Amine-Oxalates

Compound	N...O (Å)	N-H..O (°)	O...O(Å)	O-H..O (°)	C...O(Å)	C-H..O (°)
Propylamine[a]	2.868(4)	142	2.580(2)	176	3.427	147
	2.862(6)	172	-	-	-	-
Ethylenediamine[a]	2.835(5)	174.0(5)	2.567(6)	169.0(6)	3.327(8)	134(5)
	2.832(7)	148.0(5)	-	-	-	-
1,4-Diaminobutane[a]	2.826(9)	153.2(6)	2.581(8)	172.0(4)	3.452(10)	146.2(9)
	2.881(8)	176.0(7)	2.568(8)	172.0(3)	3.480(10)	148.4(8)
	2.862(9)	169.7(7)	-	-	3.452(10)	151.6(8)
	2.795(9)	151.4(6)	-	-	-	-
Piperazine[a]	2.816(19)	150.0(2)	2.563(16)	172.0(2)	3.431(2)	163.0(17)
	2.784(2)	158.0(2)	-	-	3.328(2)	159.0(18)
	-	-	-	-	3.373(2)	158.0(19)
DABCO[b]	2.619(3)	152.0(2)	2.619(3)	158.0(3)	3.393(3)	165.0(2)
	2.619(3)	148.8(19)	2.741(3)	157.0(3)	3.359(3)	141.0(18)
	-	-	-	-	3.419(3)	153.1(18)
Guanidine[c]	2.881(5)	177.0(4)	-	-	-	-
	2.923(5)	171.0(4)	-	-	-	-
Imidazole[d]	2.766(3)	163.7(3)	2.595(3)	172.0(3)	3.203(4)	141.0(4)
	2.725(3)	155.0(3)	-	-	3.353(7)	142.0(4)
	-	-	-	-	-	-

(a) Linear chains are formed by oxalate moieties.
(b) Dimer units are formed by oxalate moieties as in oxalic acid.
(c) Amine and oxalate units alternate in the layer resulting in only N-H..O type H-bonds.
(d) Linear chains formed by oxalates are so arranged that C-H..O type H-bonds turn out to be stronger than N-H..O type H-bonds, which is unusual.

4.4 A zinc phosphate with open-architecture

4.4.1 Structure of the zinc phosphate

To arrive at the oxidation states of the various species involved as well as to find out about the extent of protonation of the amine molecules, extensive bond-valence sum analysis[86] was undertaken. The calculations indicate that the valence states of Zn, P and O to be +2, +5 and –2 respectively. The oxygens O(41) and O(42) are formally water molecules and are found to be terminal. Similar terminal water molecules have been observed earlier in open-framework zinc phosphate materials[16].

The asymmetric unit of the zinc phosphate consists of 85 non-hydrogen atoms (Fig. 4.4.1). The structure involves a network of ZnO_4, ZnO_3N and PO_4 tetrahedra in which vertices are shared. The network between these polyhedra produces an adamantane type unit, made of 3- and four-membered rings, connected in various ways forming the channels. We present the structure of the zinc phosphate, under discussion, viewed along two different directions in Figures 4.4.2 and 4.4.3. Along the a axis, there are four-membered rings made of two Zn and two P atoms with the P atoms connected to ZnO_4 units and the Zn atoms to PO_4 units, giving rise to a spherical, basic building block (see inset in Fig. 4.4.2). The building blocks are connected to each other by Zn – O – Zn linkages (which form a 3-membered ring) and ZnO_3N tetrahedra. The connectivity between the various units gives rise to two

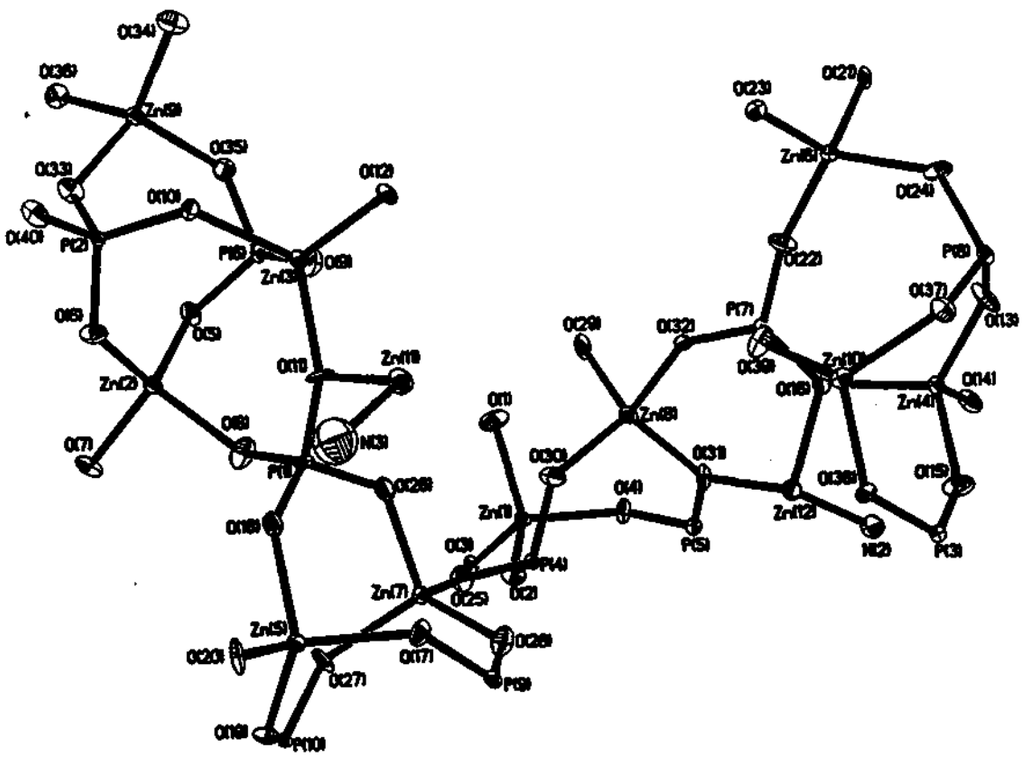

Figure 4.4.1

ORTEP plot of the framework of $[NH_3(CH_2)_3NH_3]_2[NH_3(CH_2)_3NH_2]_2[Zn_{12}(OH_2)_2(PO_4)_{10}]H_2O$. The thermal ellipsoids are given at 50% probability. The zinc atoms Zn(11) and Zn(12), are disordered (the disordered positions are not shown).

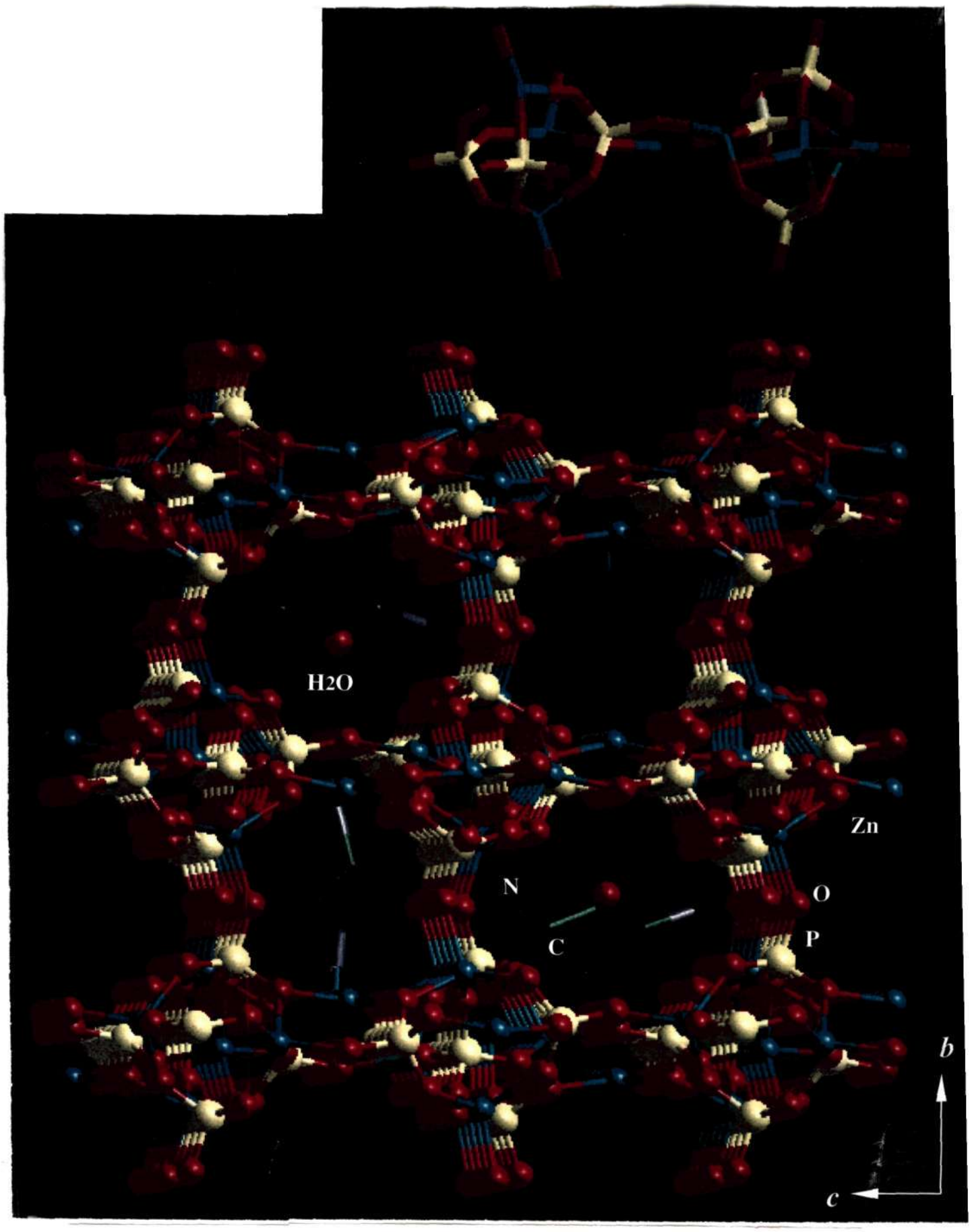

Fig. 4.4.2

Structure of $[NH_3(CH_2)_3NH_3]_2$ $[NH_3(CH_2)_3NH_2]_2$ $[(Zn_{12}(OH_2)_2(PO_4)_{10}].H_2O$ along the [100] direction showing the different channels. The bonded and free amine molecules occupy different channels. Note that the water molecules (not bound to Zn center) also occupy the 10-membered channel along with the free amine. The inset shows the spherical building block.

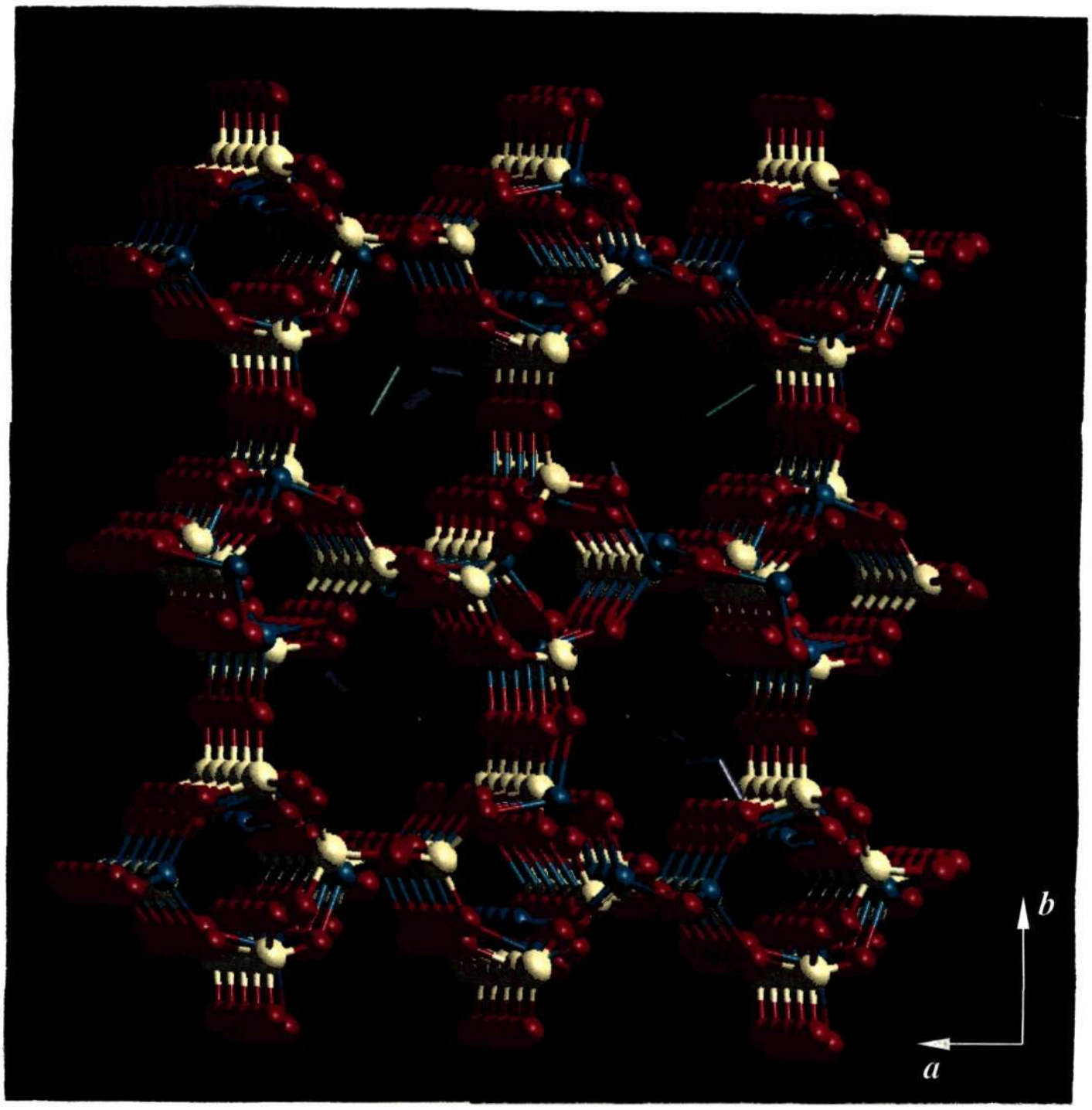

Figure 4.4.3
Structure of $[NH_3(CH_2)_3NH_3]_2$ $[NH_3(CH_2)_3NH_2]_2$ $[(Zn_{12}(OH_2)_2(PO_4)_{10}].H_2O$ along the [001] direction showing the channels. Note that both bonded and free amine molecules occupy the same channels (free amine molecules are situated at the center of the channels). Water molecules are omitted for clarity.

distinct channels along the c and a axes as can be seen in figures 4.4.2 and 4.4.3. The protonated 1,3-DAP and water molecules fill the channels.

4.4.2 Dual role of amine in the structure

Two distinct types of amine molecules (two of each type) are present in the channels of this material – a di-protonated amine and a mono-protonated amine acting as the ligand to zinc. For purpose of convenience, we designate these two amine species as "free" and "bonded" respectively.

Along the c-axis, the bonded and free amine molecules are both located within the channels made by 10-membered rings. The position of the bonded amine molecule causes the channels to be marginally different in shape and dimensions [(5.7 x 7.5 Å) and (5.6 x 8.1 Å)] (Fig.4.4.3). Along the a-axis, however the two types of amine molecules occupy distinctly different channels. The bonded amine sits in the middle of an 8-membered channel (5.1 x 5.9 Å), whereas the free-amine occupies an elliptical 10-membered channel (7.9 x 7.0 Å) (atom-atom contact distances not including the van der Waals radii) as shown in Fig. 4.4.2. The free water molecule is also located in the 10-membered channel containing the free amine (Fig. 4.4.2). Solids where different amine molecules occupy different channels are known[87]. What we find in the zinc phosphate is, however, different, and unique in two respects. First, the same amine occupies two different channels and second, there are two types of the amine molecules, free and bonded, each present in a separate

channel in one of the directions. The presence of different types of amines is also reflected in the shapes of the 8- and 10-membered channels along the a-axis. These channels are reminiscent of aluminosilicate zeolites[2]. The framework density (FD: number of tetrahedral atoms per 1000 $Å^3$) of the material is 16.6, a value in the middle range of FD values, indicating a degree of openness comparable to the aluminophosphates and aluminosilicates[2].

Of the 42 oxygen atoms in the asymmetric unit, eight make trigonal connection with two Zn atoms and one P atom (~20%) forming a three-membered ring, two are terminal oxygens (water molecules) and the remainder of the oxygens form Zn – O – P linkages. The three-coordinated oxygen atom results in the formation of three-membered rings in this material. The three-coordinated oxygen atom leads to the formation short Zn – O – Zn linkages in this material, the third coordination being always to a P atom. Such a trigonal coordination of the oxygen atom in the Zn –O – Zn bridge is an electrostatic valence requirement of the bridging oxygen atoms. Thus, it can not be concluded that the presence of three-coordinated oxygen bridges tends to give rise to more dense frameworks. There are other examples of such electrostatic valence requirements of oxygens that have been reported in the literature[86,2,88,15]. The trigonal and tetrahedral coordination of oxygen atoms observed in the structures[86,2,88] suggests that these bridges occur when divalent tetrahedral atoms are involved. It may be expected that the

presence of such features in the zinc phosphate system would lead to novel open-framework architectures that have no structural counterparts in aluminosilicates or aluminophosphates.

A few observations on the important structural parameters in this zinc phosphate would be in order. The bond distances and angles in zinc phosphate, under discussion, show typical values. The Zn – O bond distances are in the range 1.867 – 2.12 Å (ave. 1.956 Å) and O – Zn – O bond angles in the range 98.5 – 132.3° (ave. 109.7°), in agreement with the values found in similar structures. The P – O distances and O – P – O angles are also in the expected range. The longest Zn – O/N distance and the largest O – Zn – O/N angle are found with the oxygens involved in three-coordination and the nitrogen atoms bonded to Zn. Two of the zinc atoms [Zn(11) and Zn(12)]are disordered and bound to a water molecule [terminal oxygen, O(41) and O(42)] in the structure, just as in other zinc phosphate materials[16]. The water molecules O(41) and O(42) have the same occupancies as that of Zn(11) and Zn(12) to which they are attached (Table 4.4.3). We have not been able to identify the other disordered position of the water molecules from the difference Fourier maps.

4.4.3 Hydrogen bonds in the zinc phosphate

As typical of many open-framework structures, the zinc phosphate structure also possesses large number of hydrogen bond interactions. The selected important hydrogen bond interactions are: O(6) ... H(1) = 2.128(1)Å, O(6) ... H(1)-N(5) = 163.3(2)°; O(28) ... H(11) = 2.065(1)Å,

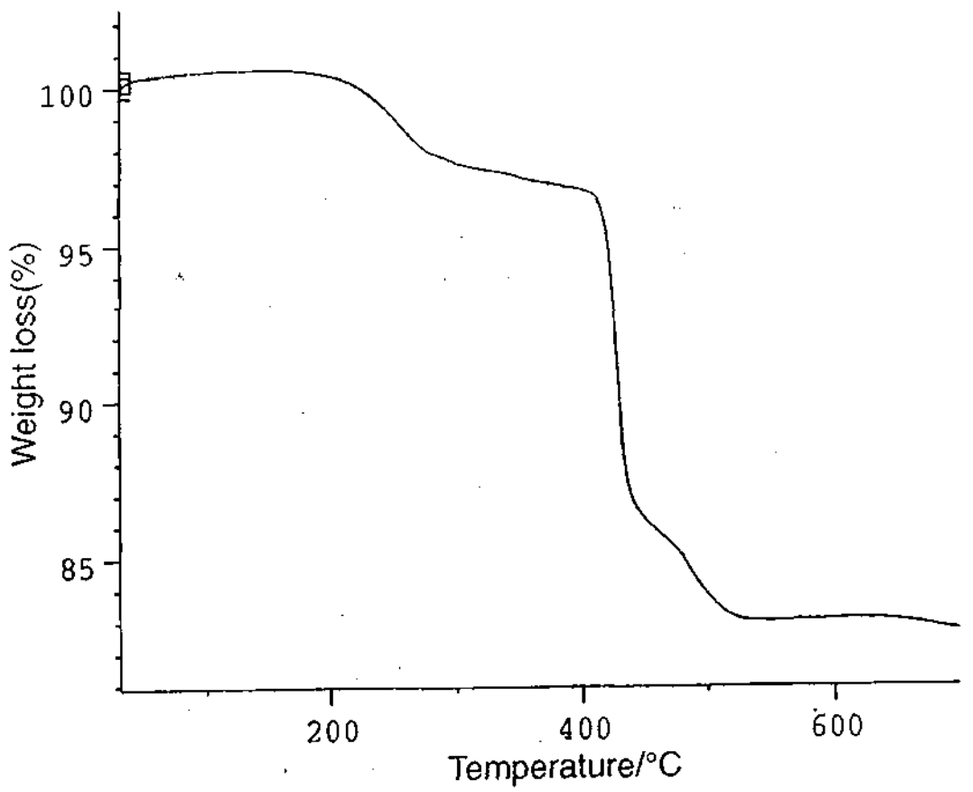

Figure 4.4.4

Thermogravimetric analysis of $[NH_3(CH_2)_3NH_3]_2$ $[NH_3(CH_2)_3NH_2]_2$ $[(Zn_{12}(OH_2)_2(PO_4)_{10}]$. H_2O in flowing nitrogen at 5°C min^{-1}.

O(28) ...H(11)-N(6) = 159.9(1)°; O(30) ...H(13) = 1.906(1)Å, O(30) ... H(13)-N(7) = 157.6(1)°. The above indicates that extensive hydrogen bond interactions involving the free amine and the framework oxygens are prominent. Similar hydrogen bond interactions have been observed in many of the open-framework phosphates.[2,16,23,30]

4.4.4 Initial characterization of the zinc phosphate

Thermogravimetric analysis (TGA) was carried out under nitrogen atmosphere indicated three mass losses in the range 25°C to 700°C as show in Figure 4.4.4. The first mass loss of 2.6% around 250°C corresponds to the loss of some adsorbed and the free as well as bound water molecules (Calc. 2.8%). The second mass loss with a broad tail amount to a total loss of 14.4 % in the range 400 – 500°C corresponds to the loss of the bound and free amine molecules (Calc. 15.6%). The decomposed sampled was found to be poorly crystalline (powder XRD) and corresponds to a dense zinc phosphate, $Zn_2P_2O_7$, (JCPDS: 43-0488), indicating the loss of framework structure with the loss of the amine.

4.4.5 Conclusions

The present study establishes the structure of an interesting zinc phosphate where the amine simultaneously performs two roles, that of a metal ligand and of a space-filling or structure directing molecule. Such a structure has not been encountered in any of the open-framework materials reported hitherto. It is possible that the structure of discussed zinc phosphate and of the zinc phosphate where the amine acts as a

structure-directing ligand[23], are intermediate structures that occur between 3-dimensional open-framework phosphates and a starting "precursor" chain phosphate. The observation of such structures point the need to investigate the role of the amines in the formation of open-framework structures more closely, and to explore the varieties of structures that may exist wherein the amine plays different roles.

Table 4.4.1 Summary of crystal data, intensity measurements and structure refinement parameters for $[NH_3(CH_2)_3NH_3]_2[NH_3(CH_2)_3NH_2]_2[(Zn_{12}(OH_2)_2(PO_4)_{10}]H_2O$ (I)

Parameter	Compound I
Empirical formula	$Zn_{12}P_{10}O_{43}C_{12}N_8H_{52}$
Crystal system	Monoclinic
Space group	Pn (no. 7)
Crystal size (mm)	0.08 x 0.08 x 0.1
a (Å)	13.092(2)
b (Å)	14.272(2)
c (Å)	14.220(1)
α (°)	90.0
β (°)	90.3(2)
γ (°)	90.0
Volume ($Å^3$)	2656.9(1)
Z	2
Formula mass	1927.6
ρ_{calc} (gcm^{-3})	2.73
λ (MoKα) Å	0.71073
μ (mm^{-1})	6.6
θ range	1.43 – 23.27
Total data collected	10808
Index ranges	$-14 \le h \le 12$, $-15 \le k \le 15$, $-15 \le l \le 15$
Unique data	5571
Observed data ($\sigma > 2\sigma(I)$)	5332
Refinement method	Full-matrix least-squares on $\|F^2\|$
R indices [$I > 2\sigma(I)$]	$R = 0.037$, $R_w = 0.10$
R indices (all data)	$R = 0.04$, $R_w = 0.11$
Goodness of fit (S)	1.16
No. of variables	745
Largest difference map peak and hole $eÅ^{-3}$	1.18 and –0.76

Table 4.4.2 Atomic coordinates [x 10^4] and equivalent isotropic displacement parameters [$Å^2$ x 10^3] for

$[NH_3(CH_2)_3NH_3]_2[NH_3(CH_2)_3NH_2]_2[(Zn_{12}(OH_2)_2(PO_4)_{10}]H_2O$

Atom	x	Y	Z	U(eq)
Zn(1)	7572(1)	25309(1)	6699(1)	13(1)
Zn(2)	10423(1)	19757(1)	6680(1)	15(1)
Zn(3)	10839(1)	20142(1)	4204(1)	14(1)
Zn(4)	6679(1)	26243(1)	792(1)	15(1)
Zn(5)	6480(1)	18775(1)	5107(1)	13(1)
Zn(6)	9782(1)	25158(1)	226(1)	16(1)
Zn(7)	6674(1)	21316(1)	5393(1)	13(1)
Zn(8)	8076(1)	24961(1)	4232(1)	16(1)
Zn(9)	13630(1)	20120(1)	5704(1)	17(1)
Zn(10)	6954(1)	23725(1)	469(1)	17(1)
Zn(11)#1	8708(2)	19562(2)	3019(2)	26(1)
Zn(12)#1	6245(2)	25725(2)	2928(2)	21(1)
Zn(11A)#2	7097(4)	19162(4)	2987(4)	26(2)
Zn(12A)#2	4817(5)	25040(4)	2905(5)	38(2)
P(1)	8603(3)	19975(2)	5119(3)	13(1)
P(2)	11923(3)	18579(2)	5465(3)	12(1)
P(3)	4820(3)	24764(2)	752(3)	15(1)
P(4)	6717(3)	23602(2)	5482(2)	11(1)
P(5)	6496(3)	26452(2)	5026(2)	13(1)
P(6)	11689(3)	21444(2)	5885(2)	11(1)
P(7)	8235(3)	24988(2)	1932(2)	13(1)
P(8)	7712(3)	25312(2)	-977(2)	15(1)
P(9)	5209(3)	20275(2)	3972(2)	13(1)
P(10)	5670(3)	19842(2)	6869(2)	11(1)
O(1)	9034(9)	25307(7)	6527(8)	38(3)
O(2)	6784(7)	24232(6)	6347(7)	25(2)
O(3)	7370(7)	25528(6)	8027(6)	22(2)
O(4)	7145(7)	26364(6)	5901(7)	24(2)
O(5)	11306(7)	20820(6)	6698(7)	22(2)
O(6)	10982(7)	18614(6)	6105(7)	22(2)
O(7)	9924(7)	19544(6)	7934(6)	22(2)
O(8)	9145(9)	20064(7)	6038(8)	32(3)
O(9)	11106(8)	21230(6)	4974(7)	28(2)
O(10)	11755(7)	19128(6)	4528(7)	25(2)
O(11)	9373(7)	19854(7)	4306(7)	21(2)
O(12)	10971(7)	20420(6)	2882(6)	19(2)
O(13)	7372(8)	29120(6)	-345(7)	31(3)
O(14)	6452(8)	27529(6)	1157(7)	26(2)
O(15)	5325(8)	25734(6)	789(8)	33(3)
O(16)	7320(7)	25692(6)	1916(6)	19(2)
O(17)	5994(7)	19472(7)	4012(6)	24(2)
O(18)	7927(7)	19111(6)	5099(7)	20(2)
O(19)	5717(7)	18982(6)	6242(7)	21(2)
O(20)	6451(8)	17482(6)	4702(6)	24(2)
O(21)	10675(7)	26224(6)	-31(6)	20(2)
O(22)	9152(8)	25405(7)	1444(7)	29(2)
O(23)	10413(7)	23910(6)	185(7)	22(2)
O(24)	8904(8)	25236(8)	-914(8)	35(3)
O(25)	6803(7)	22578(6)	5786(7)	26(2)
O(26)	7993(7)	20878(6)	4923(7)	23(2)

O(27)	6425(8)	20593(6)	6540(7)	28(2)
O(28)	5664(8)	21177(6)	4404(7)	25(2)
O(29)	9314(8)	25403(8)	4783(8)	36(3)
O(30)	7626(7)	23799(6)	4821(7)	26(2)
O(31)	6974(7)	25892(6)	4190(6)	21(2)
O(32)	8527(7)	24793(6)	2945(6)	20(2)
O(33)	12828(7)	19000(6)	6004(7)	25(2)
O(34)	14247(9)	19994(7)	4501(8)	34(3)
O(35)	12852(8)	21309(6)	5764(8)	27(2)
O(36)	14573(8)	20199(6)	6839(7)	24(2)
O(37)	7219(8)	24392(7)	-682(7)	28(2)
O(38)	5592(7)	23982(6)	937(7)	23(2)
O(39)	7898(8)	24073(6)	1472(8)	31(3)
O(40)	12183(8)	17578(6)	5217(7)	27(2)
O(41)[#1]	7664(11)	20455(9)	2896(9)	24(3)
O(42)[#1]	5798(12)	24343(10)	2968(10)	27(3)
O(100)	11669(22)	17698(39)	-2115(35)	295(21)
		Free Amine		
N(8)	9364(9)	22614(7)	1366(8)	22(3)
N(7)	9281(10)	22613(8)	4850(11)	36(3)
C(12)	9913(13)	22904(10)	2232(11)	33(4)
C(11)	9370(12)	22554(9)	3110(12)	24(3)
C(10)	9881(11)	22901(10)	3988(11)	28(3)
N(6)	8920(10)	17559(8)	9535(10)	34(3)
N(5)	8961(10)	17637(8)	6039(8)	28(3)
C(9)	8364(12)	17826(9)	8664(11)	27(3)
C(8)	8920(13)	17503(10)	7809(14)	36(4)
C(7)	8437(12)	17940(9)	6941(10)	28(3)
		Bonded Amine		
N(4)	10536(9)	15959(8)	3043(9)	30(3)
N(3)	8146(15)	18170(13)	2972(14)	76(5)
C(6)	10766(15)	16934(12)	3062(13)	53(5)
C(5)	9875(34)	17464(27)	3411(30)	153(15)
C(4)[#1]	8916(27)	17521(21)	3362(23)	68(9)
C(4A)[#2]	9345(31)	17481(26)	2611(29)	14(9)
N(2)[#1]	5441(14)	26936(12)	2828(12)	27(4)
N(2A)[#2]	4988(33)	26564(27)	2905(28)	27(9)
N(1)	3033(9)	29262(8)	2863(15)	30(3)
C(3)	4216(18)	26819(14)	2863(15)	66(6)
C(2)	3705(22)	27622(17)	3274(20)	87(8)
C(1)	3484(29)	29224(25)	2606(27)	136(12)

[#1] Disordered atoms with Site Occupancy Factor (SOF) = 0.689

[#2] Disordered atoms with Site Occupancy Factor (SOF) = 0.311

Table 4.4.3 Powder X-ray diffraction data for $[NH_3(CH_2)_3NH_3]_2[NH_3(CH_2)_3NH_2]_2[(Zn_{12}(OH_2)_2(PO_4)_{10}]H_2O$

d_{obs} (Å)	d_{calc} (Å)	I_{rel}	h k l
9.4750	9.6058	6.8	1 0 1
7.0847	7.1097	100	0 2 2
5.6831	5.7127	4.9	1 1 2
4.7579	4.7572	10.0	0 3 0
4.4251	4.4491	8.3	1 0 3
4.2235	4.2475	4.6	1 1 3
3.9621	3.9538	20.1	0 3 2
3.7616	3.7754	3.8	1 2 3
3.7053	3.7117	4.3	2 3 1
3.5497	3.5549	10.5	0 0 4
3.3605	3.3742	7.3	2 2 3
3.1746	3.1819	15.0	0 2 4
3.1119	3.1163, 3.1169	18.6	4 1 –1, 2 0 4
3.0346	3.0452	38.8	2 1 4
2.9635	2.9671	10.3	4 0 2
2.8523	2.8563, 2.8543, 2.8506	11.3	2 2 4, 0 5 0, 0 4 3
2.7666	2.7622	7.9	3 4 0
2.7141	2.7133, 2.7131	6.3	3 4 –1, 3 1 –4
2.6414	2.6471, 2.6418, 2.6402	6.0	4 3 1, 0 2 5, 4 1 3
2.5602	2.5652, 2.5610	6.4	3 2 4, 2 1 5
2.5187	2.5183, 2.5175, 2.5143	6.4	0 4 4,4 3 2, 4 2 3
2.4021	2.4048, 2.4024, 2.4016, 2.4014	10.5	1 5 –3, 1 5 3, 1 3 –5, 4 0 4
2.3903	2.3901	9.7	3 4 –3
2.3156	2.3196	3.5	5 2 2
2.2661	2.2664, 2.2663, 2.2650	7.8	3 5 –2, 5 3 –1, 3 2 –5
2.2277	2.2257, 2.2245, 2.2239, 2.2223	3.7	0 5 4, 2 0 6, 0 4 5, 1 6 2
2.0071	2.0090, 2.0057, 2.0053, 2.0050	3.8	1 0 –7, 1 0 7, 3 6 –2, 6 2 –2
1.9752	1.9769, 1.9741	10.7	0 6 4, 0 4 6
1.9487	1.9477	3.3	2 7 0

4.5 Open-framework tin(II) phosphates

4.5.1 Structure of the open-framework tin phosphates

Two new tin(II) phosphates, $[NH_3(CH_2)_3NH_3]^{2+}2[SnPO_4]^-$ and $[NH_3CH_2CH(OH)CH_2NH_3]^{2+}2[SnPO_4]^-$, have been synthesized by hydrothermal methods and the structures have been determined by single crystal methods. Since the synthesis involves kinetically controlled solven-mediated reactions, there is no apparent correlation between the starting composition and the stoichiometry of the solid product. Both tin phosphates have identical structures forming layers that are intercalated by the structure-directing organic amine molecules. The structure of the DAP and the DAHP containing tin phosphates are based on a network of strictly alternating SnO_3 and PO_4 units. The SnO_3 and PO_4 units form infinite layers with the framework formula $[SnPO_4]^-$. Charge neutrality is achieved by the incorporation of the organic amine in its diprotonated form; there are 0.5 $[amine]^{2+}$ ions per framework formula unit. The asymmetric unit contains 9 and 10 independent non-hydrogen atoms for $[NH_3(CH_2)_3NH_3]^{2+}2[SnPO_4]^-$ and $[NH_3(CH_2CHOHCH_2)NH_3]^{2+}2[SnPO_4]^-$ respectively (Fig. 4.5.1a and b). The Sn atoms are coordinated to three oxygens and occupy the vertex of a trigonal pyramid; the lone pair presumably occupies the fourth vertex of the tetrahedron.

The structure of both the tin phosphates under discussion is constructed by the networking of SnO_3 and PO_4 units forming infinite

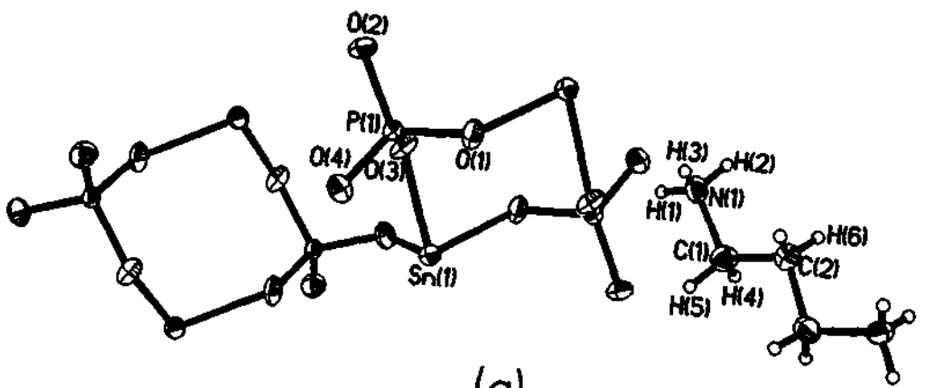

(a)

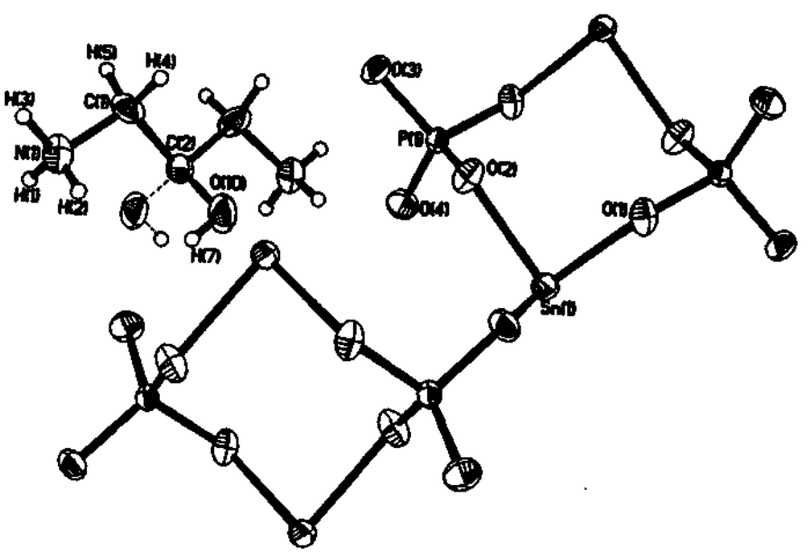

(b)

Figure 4.5.1

(a) ORTEP Plot of $[NH_3(CH_2)_3NH_3]^{2+}2[SnPO_4]^-$

(b) ORTEP plot of $[NH_3CH_2CH(OH)CH_2NH_3]^{2+}2[SnPO_4]^-$; the dotted line represents the other position of the –OH group of the amine. In both the materials, the asymmetric unit is labelled.

layers that are anionic. The connectivity between these moieties create four- and eight- membered rings along the a-axis formed by the T atoms (T = Sn, P) (Fig. 4.5.2). Each four-membered ring is attached to four 8-membered rings and each 8-membred ring is connected to four four-membrred rings. One of the basic building unit present in many of the tin phosphates and other related materials, viz., $M_2P_2O_4$ units (M = Sn in the present case)[77] is also seen in both materials. The structure-directing amine molecules (DAH in $[NH_3(CH_2)_3NH_3]^{2+}2[SnPO_4]^-$ and DAHP in $[NH_3(CH_2CHOHCH_2)NH_3]^{2+}2[SnPO_4]^-$ are located in between the layers (Figs. 4.5.3a,b and 4.5.4). The individual layers are held together by the doubly protonated DAP molecules in $[NH_3(CH_2)_3NH_3]^{2+}2[SnPO_4]^-$ (Fig. 4.5.3a,b) and DAHP molecules in $[NH_3(CH_2CHOHCH_2)NH_3]^{2+}2[SnPO_4]^-$ (Fig. 4.5.4), through hydrogen bonding. Both tin phosphates described here, thus, represent another example of framework solids possessing alternating anionic and cationic layers. It is interesting to note that both materials have a unique architecture constructed by the minimum basic structural motif, i.e, one SnO_3 and one PO_4 unit (see Fig. 4.5.1), that is needed for the formation of a open-framework tin phosphate material.

The Sn – O bond lengths are in the range from 2.081 – 2.131Å (ave. 2.113Å for $[NH_3(CH_2)_3NH_3]^{2+}2[SnPO_4]^-$ and 2.109Å for $[NH_3(CH_2CHOHCH_2)NH_3]^{2+}2[SnPO_4]^-$) and the O – Sn – O bond angles are between 83.4 and 89.8° (ave. 86.7° for $[NH_3(CH_2)_3NH_3]^{2+}2[SnPO_4]^-$ and $[NH_3(CH_2CHOHCH_2)NH_3]^{2+}2[SnPO_4]^-$), which is typical of three

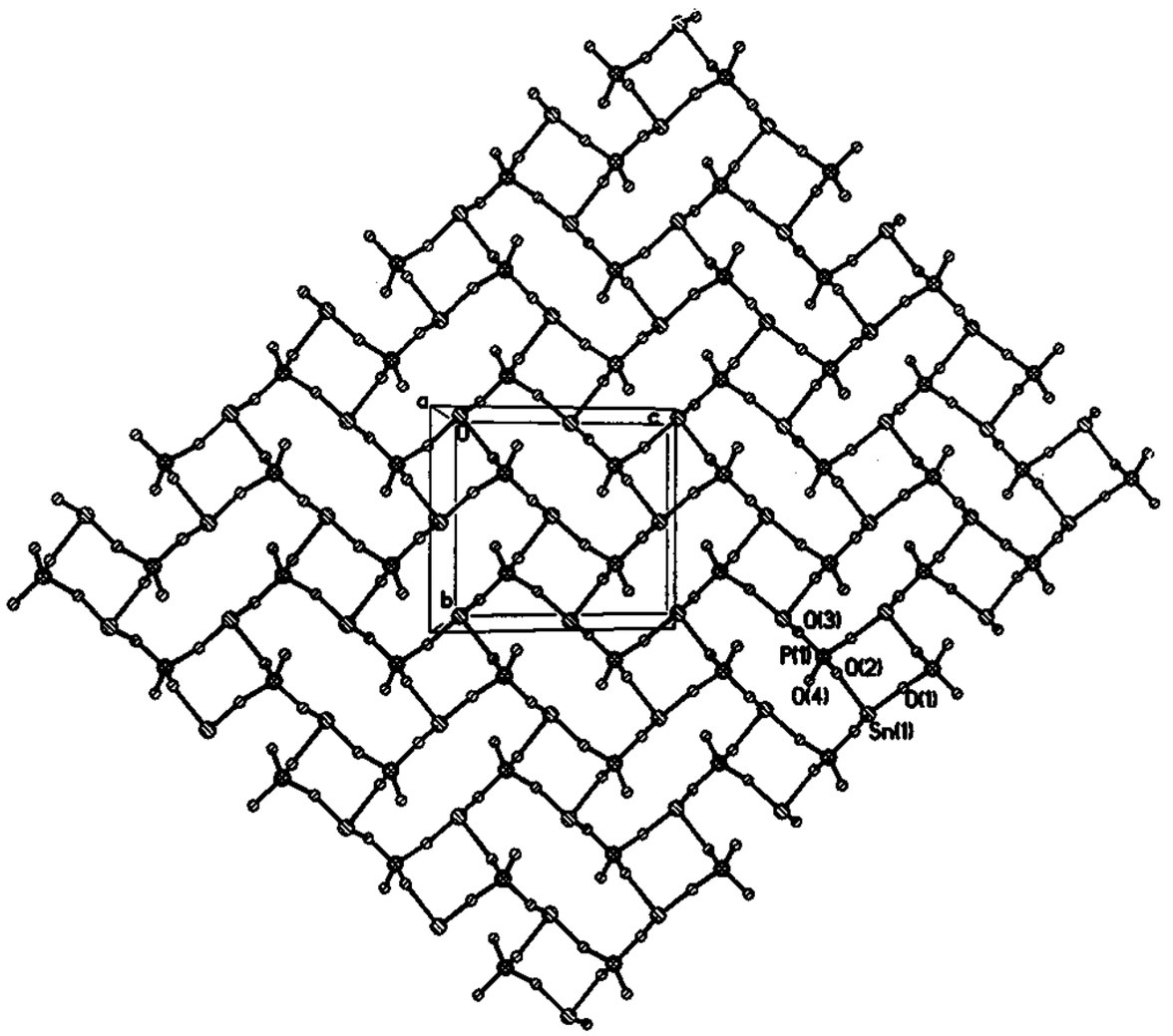

Figure 4.5.2

Structure showing the connectivity within a single layer along [100] direction. Please note that four 4-membered rings surround one 8-membered ring and vice versa.

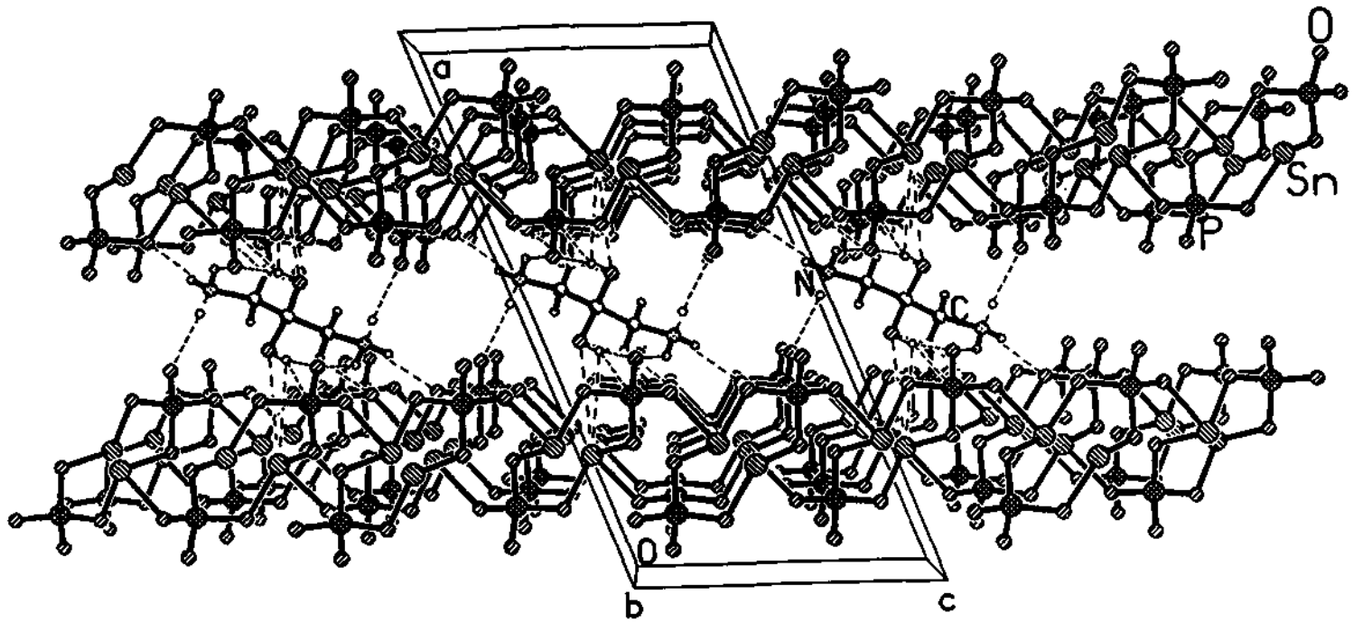

Figure 4.5.3

(a) Structure of $[NH_3(CH_2)_3NH_3]^{2+}2[SnPO_4]^-$ along the *b* axis showing the layers and the position of the amines. The dotted lines show the hydrogen bonding.

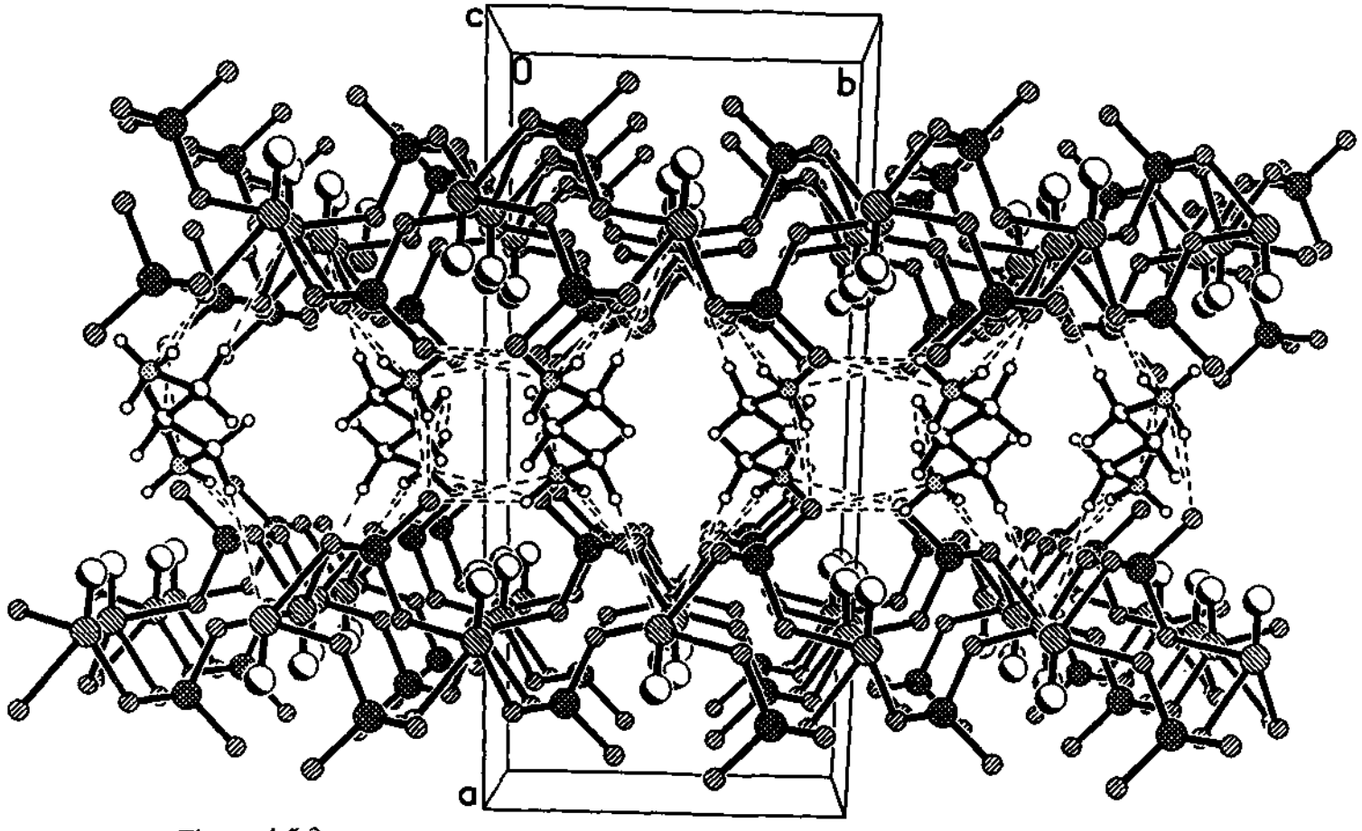

Figure 4.5.3

(b) Structure of $[NH_3(CH_2)_3NH_3]^{2+}2[SnPO_4]^-$ along the *c* axis showing the layers and the position of the amines. The dotted lines show the hydrogen bonding interactions. Please note that the lone pair of electrons of Sn(II) point perpendicular to the layers.

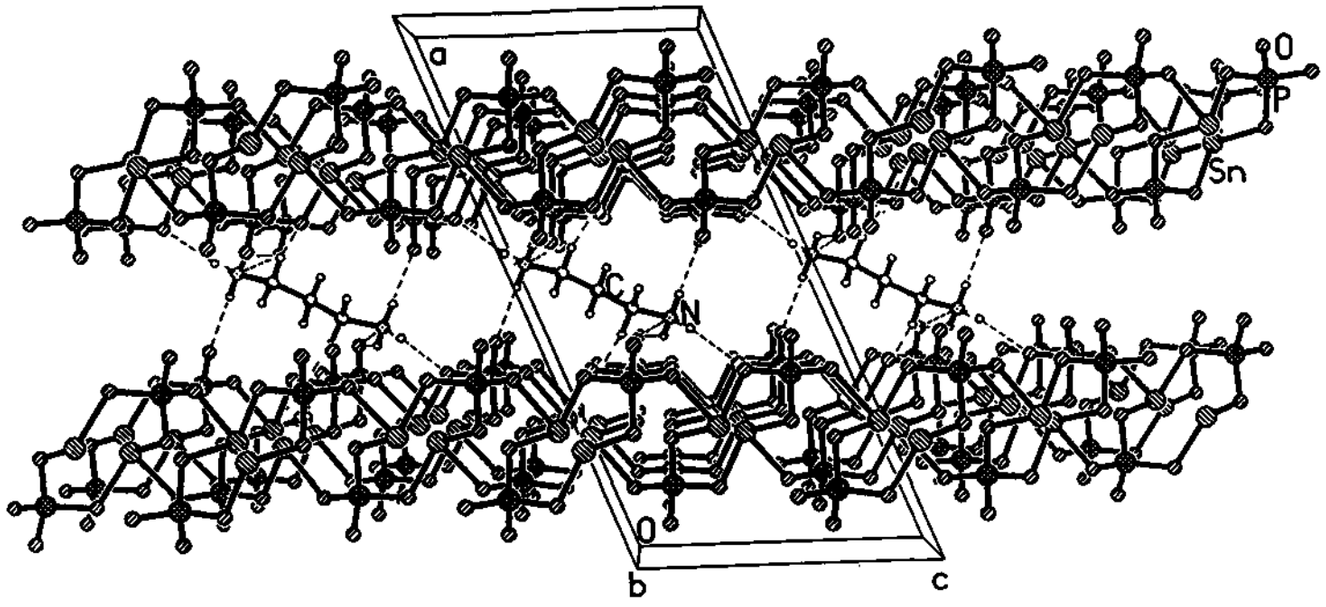

Figure 4.5.4

Structure of $[NH_3CH_2CH(OH)CH_2NH_3]^{2+}2[SnPO_4]^-$ along the *b* axis showing the interaction between the layers and the amine. The dotted lines show the hydrogen bonding between the amine and the framework.

coordinate Sn(II)[24-28,77] (Tables 4 and 6). The Sn atoms are linked to P via the oxygen links. The P – O distances are in the range 1.503 and 1.564Å (ave. 1.537Å for $[NH_3(CH_2)_3NH_3]^{2+}2[SnPO_4]^-$ and 1.538Å for $[NH_3(CH_2CHOHCH_2)NH_3]^{2+}2[SnPO_4]^-$). The P – O(4) distance of 1.503Å that is observed in both materials is formally the P=O double bond. Terminal P=O groups in, for example $H_3PO_4.0.5H_2O$, are 1.485 and 1.495Å in length[89]. The O – P – O bond angles are in the range 106.8 – 112.3° (ave. 109.4° for $[NH_3(CH_2)_3NH_3]^{2+}2[SnPO_4]^-$ and 109.5° for $[NH_3(CH_2CHOHCH_2)NH_3]^{2+}2[SnPO_4]^-$). The largest bond angles are observed for bonds involving the P=O linkage (109.4 – 112.3°) indicating the multiple-bond nature of the P=O bonds. These values are in agreement with other phosphate-based open-framework structures[2,24-28].

4.5.2 Role of the lone-pair electrons in the structure

The lone pair of electrons which are associated with Sn(II) play an important role in the structures of these materials. The stereoactive lone-pair manifest themselves in the lattice by creating open-space between the two layers in these tin phosphates. As can be seen from Fig. 4.5.3a, the lone-pair of electrons of Sn(II) points perpendicular to the plane of the layers. Similar lone-pair positionings have been observed in many of the layered tin(II) phosphates and related materials[83,84].

4.5.3 Hydrogen bonds in the structure

Multipoint hydrogen bonding interactions have helped in the structural stability, and possibly in the formation, of many of the open-framework materials that have low dimensional character and a large number of examples exist in the literature[26, 28]. In both the tin phosphate structures, the hydrogens of the amine molecule interact strongly with the framework oxygens, especially with the double bonded oxygen. The important hydrogen bonding interactions are: H(3) – O(4) = 1.909Å; O(4) – H(3) – N(1) = 158.8° for $[NH_3(CH_2)_3NH_3]^{2+}2[SnPO_4]^-$ and H(1) – O(4) = 1.944Å; O(4) – H(1) – N(1) = 152.5° for compound $[NH_3(CH_2CHOHCH_2)NH_3]^{2+}2[SnPO_4]^-$. In the case of compound containing DAHP, the –OH group attached to the amine molecule also participates in both intra- as well as inter-layer hydrogen bonding. The inter-molecular hydrogen bonding with framework oxygens are nearly planar: H(7) – O(4) = 1.793Å; O(4) – H(7) – O(10) = 160.9°. Complete hydrogen bonding interactions are presented in Table 4.5.7. The tin phosphates described here, thus, illustrate the importance of multipoint hydrogen bonding in the stability of two-dimensional solids.

4.5.4 Initial characterization of the tin phosphates

The thermogravimetric analysis (TGA) carried out on $[NH_3(CH_2)_3NH_3]^{2+}2[SnPO_4]^-$ and $[NH_3(CH_2CHOHCH_2)NH_3]^{2+}2[SnPO_4]^-$ indicate that there is only one mass loss in the region of 350-400°C in both cases. The mass loss of 15% observed for the one with DAP as SDA

and a loss of 17% for the one with DAHP as SDA corresponds to the loss of amine in both the cases (calc. 15.2% for $[NH_3(CH_2)_3NH_3]^{2+}2[SnPO_4]^-$ and 17.8% for $[NH_3(CH_2CHOHCH_2)NH_3]^{2+}2[SnPO_4]^-$). The loss of the amine molecule renders the material to lose the layered architecture. The powder XRD pattern of the sample calcined at 450°C in air for 24h indicate that the resultant solid is amorphous with very weak reflections.

The structures of both the compounds discussed have similar features to other previously known layered phosphates; aluminum phosphates, antimony phosphates and zirconium phosphates. Of particular interest is the similarity to the layered aluminum phosphates reported by Chippindale *et al.*[90] and the phosphatoantimonates reported by Piffard *et al.*[91-93]. In the case of the former, the macroanionic sheets (made of AlO_4 and PO_4 moieties) are held together by strong hydrogen bonded interactions involving the double bonded oxygens of the phosphate groups and the organic template molecules. In the case of the later, the layers are made up of corner shared PO_4 tetrahedra and SbO_6 octahedra. The interlamellar space is occupied by Na^+ or K^+ ions which are easily replaced by protons (H^+) by washing with dilute acids. The interlamellar space is also filled with H_2O molecules during the proton exchange. Similar structural features are also seen in the so called α-ZrP (α-$Zr(HPO_4)_2.H_2O$) structure[26]. The present structures have many of the interesting structural features common to the aforementioned layered phosphate structures. The presence of trigonal pyramidal SnO_3 and

tetrahedral PO_4 units linking to form the layers and the interactions with the organic amine molecule renders the unique architecture seen in these materials.

4.5.5 Conclusions

The synthesis of two new layered tin(II) phosphate materials consisting of alternating inorganic-organic layers has been accomplished. These materials, together with previously reported Sn(II) phosphate and phosphonate solids, illustrates profound structural influences of relatively minor modifications in reaction conditions and/or changes in the starting souce for the tin. The present solids represent another example illustrating the importance of multipoint hydrogen bonding in the synthesis and stability of open-framework materials. The stereoactive lone-pair of electrons of Sn(II) manifest themselves in the structure and points perpendicular to the plane of the layers. Our continuing research on tin phosphates indicates that other related structures are formed under hydrothermal conditions using other structure directing agents. While the isolation of a two-dimensional solid with strictly alternating SnO_3 and PO_4 moieties provide information about the stereochemical consequences of the Sn(II) lone pair electrons, further evaluation is required to exploit the structure-directing influences of this unit in the presence of other organic amines in the synthesis of potentially open-framework phosphate materials.

Table 4.5.1 Crystal data and structure refinement parameters for $[NH_3(CH_2)_3NH_3]^{2+}2[SnPO_4]^-$ and $[(NH_3)_2(CH_2)_2CH(OH)]^{2+}2[SnPO_4]^-$

Parameters	$[NH_3(CH_2)_3NH_3]^{2+}2[SnPO_4]^-$	$[(NH_3)_2(CH_2)_2CH(OH)]^{2+}2[SnPO_4]^-$
Empirical formula	$Sn_2P_2O_8C_3N_2H_{12}$	$Sn_2P_2O_9C_3N_2H_{12}$
Crystal system	Monoclinic	Monoclinic
Space group	C2/c	C2/c
Crystal size (mm)	0.06 x 0.1 x 0.14	0.06 x 0.12 x 0.16
a (Å)	18.097(1)	18.133(1)
b (Å)	7.889(1)	7.858(1)
c (Å)	9.151(1)	9.344(1)
α (°)	90.0	90.0
β (°)	111.84(1)	111.3(1)
γ (°)	90.0	90.0
Volume (Å^3)	1212.6(2)	1240.5(1)
Z	4	4
Formula mass	501.9	517.9
ρ_{calc} (gcm^{-3})	2.118	2.58
λ (MoKα) Å	0.71073	0.71073
μ (mm^{-1})	3.31	5.31
θ range	2.42 – 23.26°	2.41 – 23.28°
Total data collected	2412	2549
Index ranges	$-16 \le h \le 20$, $-8 \le k \le 8$, $-10 \le l \le 5$	$-19 \le h \le 20$, $-8 \le k \le 8$, $-10 \le l \le 7$
Unique data	873	898
Observed data ($\sigma > 2\sigma(I)$)	791	867
Refinement method	Full-matrix least-squares on $\lvert F^2 \rvert$	Full-matrix least-squares on $\lvert F^2 \rvert$
R indices [$I > 2\sigma(I)$]	R = 0.026, R_w = 0.059	R = 0.039, R_w = 0.11
R indices (all data)	R = 0.033, R_w = 0.061[#1]	R = 0.040, R_w = 0.11[#2]
Goodness of fit (S)	1.11	1.28
No. of variables	83	89
Largest difference map peak and hole eÅ^{-3}	0.656 and -0.575	1.442 and -1.093

#1 $W = 1/[\sigma^2(F_O)^2 + (0.0197P)^2 + 10.2010P]$ where $P = [F_O^2 + 2F_C^2]/3$

#2 $W = 1/[\sigma^2(F_O)^2 + (0.0619P)^2]$ where $P = [F_O^2 + 2F_C^2]/3$

Table 4.5.2 Atomic coordinates (x 10^4) and equivalent isotropic thermal parameters (Å x 10^3) for non-hydrogen atoms in $[NH_3(CH_2)_3NH_3]^{2+}2[SnPO_4]^-$

Atom	x	y	z	U(eq)[#]
Sn(1)	2612(1)	-5136(1)	-381(1)	18(1)
P(1)	3448(1)	-2684(2)	2613(2)	15(1)
O(1)	3544(2)	-3652(5)	1203(4)	22(1)
O(2)	3510(2)	-3974(5)	3902(5)	22(1)
O(3)	2598(2)	-1918(5)	1996(4)	24(1)
O(4)	4076(2)	-1332(5)	3184(5)	24(1)
N(1)	5564(3)	-1981(6)	5420(6)	26(1)
C(1)	5363(4)	-3017(8)	6585(7)	30(2)
C(2)	5000	-1924(12)	7500	29(2)

[#] U(eq) is defined as one third of the trace of the orthoganalized U_{ij} tensor

Table 4.5.3 Selected bond distances and bond angles for $[NH_3(CH_2)_3NH_3]^{2+}2[SnPO_4]^-$

Moiety	Distance (Å)	Moiety	Angle (°)
Sn(1) – O(1)	2.122(4)	O(1) – Sn(1) – O(2)$^{\#1}$	83.4(2)
Sn(1) – O(2)$^{\#1}$	2.088(4)	O(1) – Sn(1) – O(3)$^{\#3}$	86.9(2)
Sn(1) – O(3)$^{\#2}$	2.130(4)	O(2)$^{\#1}$ – Sn(1) – O(3)$^{\#2}$	89.8(2)
P(1) – O(1)	1.563(4)	O(1) – P(1) – O(2)	108.2(2)
P(1) – O(2)	1.530(4)	O(1) – P(1) – O(3)	106.8(2)
P(1) – O(3)	1.551(4)	O(2) – P(1) – O(3)	108.5(2)
P(1) – O(4)	1.503(4)	O(1) – P(1) – O(4)	109.4(2)
		O(2) – P(1) – O(4)	112.0(2)
		O(3) – P(1) – O(4)	111.7(2)
		Organic Moiety	
N(1) – C(1)	1.492(8)	N(1) – C(1) – C(2)	110.8(5)
C(1) – C(2)	1.512(8)	C(1) – C(2) – C(1)$^{\#4}$	110.5(8)
C(2) – C(1)$^{\#4}$	1.512(8)		

Symmetry transformations used to generate equivalent atoms
$^{\#1}$ x, -y-1, z-1/2; $^{\#2}$ –x+1/2, -y-1/2, -z; $^{\#3}$x, -y-1, z+1/2; $^{\#4}$ –x+1, y, -z+3/2

Table 4.5.4 Atomic coordinates (x 10^4) and equivalent isotropic thermal parameters (Å x 10^3) for non-hydrogen atoms in $[NH_3CH_2CH(OH)CH_2NH_3]^{2+}2[SnPO_4]^-$

Atom	x	y	z	U(eq)[#]
Sn(1)	2630(1)	-5165(1)	-430(1)	20(1)
P(1)	3457(1)	-2745(2)	2517(2)	16(1)
O(1)	3552(2)	-3698(5)	1126(4)	24(1)
O(2)	3503(2)	-4079(5)	3749(5)	27(1)
O(3)	2617(2)	-1960(5)	1949(4)	23(1)
O(4)	4094(2)	-1419(6)	3098(5)	29(1)
O(10)[#]	5601(5)	-1005(11)	8467(9)	41(3)
N(1)	5535(3)	-2017(7)	5422(6)	30(1)
C(1)	5323(4)	-3080(10)	6559(8)	31(2)
C(2)	5000	-1937(12)	7500	23(2)

site occupancy factor (SOF) = 0.5

[#] U(eq) is defined as one third of the trace of the orthoganalized U_{ij} tensor

Table 4.5.5 Selected bond distances and bond angles for $[NH_3CH_2CH(OH)CH_2NH_3]^{2+}2[SnPO_4]^-$

Moiety	Distance (Å)	Moiety	Angle (°)
Sn(1) – O(1)	2.114(4)	O(1) – Sn(1) – O(2)$^{\#1}$	87.3(2)
Sn(1) – O(2)$^{\#1}$	2.131(4)	O(1) – Sn(1) – O(3)$^{\#2}$	83.8(2)
Sn(1) – O(3)$^{\#2}$	2.081(4)	O(2)$^{\#1}$ – Sn(1) – O(3)$^{\#2}$	89.0(2)
P(1) – O(1)	1.564(4)	O(1) – P(1) – O(2)	107.4(2)
P(1) – O(2)	1.548(4)	O(1) – P(1) – O(3)	107.7(2)
P(1) – O(3)	1.536(4)	O(2) – P(1) – O(3)	107.9(2)
P(1) – O(4)	1.503(4)	O(1) – P(1) – O(4)	109.3(2)
O(3) – Sn(1)$^{\#3}$	2.081(4)	O(2) – P(1) – O(4)	112.3(2)
O(3) – Sn(1)$^{\#2}$	2.131(4)	O(3) – P(1) – O(4)	112.1(2)
		Organic Moiety	
N(1) – C(1)	1.507(9)	N(1) – C(1) – C(2)	109.4(7)
C(1) – C(2)	1.516(10)	C(1)$^{\#4}$ – C(2) – C(1)	107.3(9)
C(2) – C(1)$^{\#4}$	1.516(10)	C(1)$^{\#4}$ – C(2) – O(10)$^{\#4}$	108.8(5)
C(2) – O(10)$^{\#4}$	1.351(10)	C(1) – C(2) – O(10)$^{\#4}$	108.7(4)

#1 x, -y-1, z-1/2; #2 -x+1/2, -y-1/2, -z; #3 x, -y-1, z+1/2; #4 -x+1, y, -z+3/2

Table 4.5.6 Important Hydrogen bond distances and angles for both tin phosphates

$[NH_3(CH_2)_3NH_3]^{2+}2[SnPO_4]^-$			
Moiety	Distance (Å)	Moiety	Angle (°)
O(1) – H(1)	2.017(1)	O(1) – H(1) – N(1)	165.3(1)
O(4) – H(2)	2.140(1)	O(4) – H(2) – N(1)	139.5(1)
O(4) – H(3)	1.909(1)	O(4) – H(3) – N(1)	158.8(1)
$[NH_3CH_2CH(OH)CH_2NH_3]^{2+}2[SnPO_4]^-$			
O(4) – H(1)	1.944(1)	O(4) – H(1) – N(1)	152.6(1)
O(4) – H(2)	2.290(2)	O(4) – H(2) – N(1)	136.3(1)
O(1) – H(3)	2.024(1)	O(1) – H(3) – N(1)	161.8(2)
O(1) – H(4)	2.591(1)	O(1) – H(4) – C(1)	150.9(1)
O(3) – H(4)	2.541(1)	O(3) – H(4) – C(1)	122.4(1)
O(4) – H(7)[&]	1.793(1)	O(4) – H(7) – O(10)[&]	160.8(1)

[&]Intra-layer

Table 4.5.7 Powder X-ray diffraction data for compound ,$[NH_3(CH_2)_3NH_3]^{2+}2[SnPO_4]^-$

d_{obs} (Å)	d_{calc} (Å)	I_{rel}	h k l
8.4064	8.3990	100	*2 0 0*
4.5625	4.5660	11.4	*3 1 0*
4.2023	4.1995	11.7	*4 0 0*
3.9312	3.9337	12.3	*1 1 -2*
3.7652	3.7681	18.5	*4 0 -2*
3.5748	3.5702	31.2	*2 2 0*
3.3242	3.3246	12.9	*2 0 2*
2.9723	2.9743	21.4	*2 2 -2*
2.8902	2.8901	26.9	*0 2 2*
2.7982	2.7997	4.8	*6 0 0*
2.5427	2.5420	15.1	*2 2 2*
2.4084	2.4101	6.4	*7 1 -2*
2.2662	2.2691	1.6	*2 0 -4*
2.2393	2.2323	1.8	*3 3 -2*
2.1965	2.1971	4.6	*3 1 -4*
2.1281	2.1295	4.0	*1 1 -4*
	2.1271	1.2	*5 3 -1*
2.1008	2.0998	3.7	*8 0 0*
2.0165	2.0179	4.3	*6 0 2*
1.9698	1.9721	2.1	*0 4 0*
1.9413	1.9436	7.1	*9 1 -2*
	1.9408	8.7	*7 1 -4*
1.8607	1.8618	1.1	*6 2 -4*

References

1. J.M. Thomas, *Angew.Chem.Int.Ed.Engl.*, 1999, **38**, 3588.
2. A.K. Cheetham, G. Férey and T. Loiseau, *Angew. Chem. Int. Ed Engl.*,1999, **38**, 3268; W.M. Meier, D.H. Olsen, C. Baerlocher, *Atlas of Zeolite Structure Types, Elsevier London*, 1996.
3. R.M. Barrer, *J. Chem. Soc.* 1948, 127; R.M. Barrer, *"Hydrothermal Chemistry of Zeolites"*, Academic Press (London), 1982.
4. W. Lowenstein, *Amer. Mineral.*, 1954, **39**, 92.
5. D. McConnell, *Min. Mag,*. 1964, **33**, 799.
6. D. McConnell, *Amer. Mineral.*, 1952, **37**, 609.
7. E.M. Flanigen and R.W. Grose, *"Molecular Sieves and Zeolites-1"*, *Amer. Chem. Soc. Adv. Chem. Series*, 1971.
8. S.T. Wilson, B.M. Lok, C.A. Messina, T.R. Cannan and E.M. Flanigen, *J. Am. Chem. Soc.*, 1982, **104**, 1146.
9. B.M. Lok, C.A. Messina, R.L. Patton, R.T. Gajek, T.R. Cannan and E.M. Flanigen, *J. Am. Chem. Soc.*, 1984, **106**, 6092.
10. E.M. Flanigen, B.M. Lok, R.L. Patton and S.T. Wilson, *Pure & Appl. Chem.*, 1986, **58**, 1351;
11. E.M. Flanigen, R.L. Patton and S.T. Wilson, *Stud. Surf. Sci. Catal.*, 1988, **37**, 13.
12. J.M. Bennet, J.P. Cohen, E.M. Flanigen, J.J. Pluth and J.V. Smith, *ACS Symp. Series*, 1983, **218**, 109.
13. W.T.A. Harrison, Z. Bircsak, L. Hannooman and Z. Zhang, *J. Solid State Chem.*,1998, **136**, 93.
14. W.T.A. Harrison and L. Hannooman, *Angew. Chem. Int. Ed. Engl.*,1997, **36**, 641.
15. P. Feng, X. Bu, G.D. Stucky, *Angew. Chem. Int. Engl. Ed.*, 1995, **34**, 1745.
16. X. Bu, P. Feng and G.D. Stucky, *J. Solid State Chem.*, 1996, **125**, 243.
17. S. Neeraj and S. Natarajan, *Int. J. Inorg. Mater.*, 1999, **1**, 317.
18. W.T.A. Harrison, M.L.F. Phillips, *Chem. Commun.*, 1996, 2771.
19. W.T.A. Harrison and M.L.F. Phillips, *Chem. Mater.*, 1997, **9**, 1837.
20. G.Y. Yang and C. Sevov, *J. Am. Chem. Soc.*, 1999, **121**, 8389.
21. S. Neeraj, S. Natarajan and C.N.R. Rao, *Chem. Commun.*, 1999, 165.
22. S. Neeraj, S. Natarajan and C.N.R. Rao, *Chem. Mater.*, 1999, **11**, 1390.
23. S. Neeraj, S. Natarajan and C.N.R. Rao, *New J. Chem.*, 1999, 303.

24. S. Natarajan, M.P. Attfield and A.K. Cheetham, *Angew. Chem. Int. Ed. Engl.*, 1997, **36**, 978.
25. S. Natarajan and A.K. Cheetham, *J. Solid State Chem.*, 1998, **140**, 435.
26. S. Ayyappan, X. Bu, A.K. Cheetham, S. Natarajan and C.N.R. Rao, *Chem. Commun.*, 1998, 2181.
27. S. Natarajan, M. Eswaramoorthy, A.K. Cheetham and C.N.R. Rao, *Chem. Commun.*, 1998, 1561.
28. S. Natarajan, S. Ayyappan, A.K. Cheetham, C.N.R. Rao, *Chem. Mater.*, 1998, **10**, 1627.
29. F. Serpaggi and G. Ferey, *J. Mater. Chem.*, 1998, **8**, 2737; F. Serpaggi, G. Férey, *J. Mater. Chem.*, 1998, **8**, 2749.
30. G. Ferey, *C.R.Acad.Sci.Ser.C1*, 1998, 1.
31. C. Livage, C. Egger, M. Nogues and G. Ferey, *J. Mater. Chem.*, 1998, **8**, 2743.
32. S. Ayyappan, A.K. Cheetham, S. Natarajan and C.N.R. Rao, *Chem. Mater.*, 1998, **10**, 3746.
33. M.E. Davis and R.F. Lobo, *Chem.Mater.*, 1992, **4**, 756.
34. M.E. Davis, C. Saldarriaga, C. Montes, J.M. Garces and C. Crowder, *Nature*, 1988, **331**, 698.
35. J.M. Thomas, R.H. Jones, R. Xu, J. Chen, A.M. Chippindale, *J. Solid State Chem.*, 1993, **102**, 204.
36. R.M. Dessau, J.L. Schlenker and J.B. Higgins, *Zeolites*, 1990, **10**, 522.
37. M. Estermann, L.B. McCusker, C. Baerlocher, A. Merrouche and H. Kessler, *Nature, London*, 1991, **352**, 320.
38. T. Loiseau and G. Ferey, *J. Solid State Chem.*, 1994, **111**, 403.
39. T. Loiseau and G. Ferey, *J. Mater. Chem.*, 1996, **6**, 1073.
40. S. Oliver, A. Kuperman, A. Lough and G.A. Ozin, *Chem. Mater.*, 1996, **8**,2391.
41. S. Oliver, A. Kuperman and G.A. Ozin, *Angew. Chem. Int. Ed. Engl.*, 1998, **37**, 46.
42. S. Oliver, A. Kuperman and G.A. Ozin, *Angew. Chem. Int. Ed Engl.*, 1998, **110**, 48.
43. S. Neeraj, S. Natarajan and C.N.R. Rao, *Angew. Chem. Int. Ed. Engl.*, 1999, **38**, 3480.
44. P. Feng, X. Bu, G.D. Stucky, *Angew. Chem. Int. Engl. Ed.*, 1995, **107**, 1911.
45. A.G. Oblad, *J. Oil and Gas*, 1972, **70**, 84.
46. J. Haggin, *C&E News*, 1993, 30.
47. M. Iwamoto, H. Yahiro, K. Tanda and N. Mizuno, *J. Phys. Chem.*, 1991, **95**, 3727.

48. G. Pergo, C. Bellussi, C. Corno, M. Taramasso and F. Buonomo. *In new Developments in Zeolite Science and Technology.*

49. N.Y. Chen and W. Garwood, *J. Catal.*, 1978, **52**, 453.

50. P.E. Hathaway and M.E. Davis, *J. Catal.*, 1988, **116**, 253.

51. F.P. Gortsema, B. Beshty, J.J. Friedmann, D. Matsumoto, J.J. Sharkey, G. Wildmann, T.J. Blacklock and S.H. Pan. *Catalysis of Organic Reactions.*

52. J.M. Newsam, M.M.J. Tracey, W.T. Koetsier and C.B. de Gruyer, *Proc. Roy. Soc. (london)*, 1988, **A420**, 375.

53. J.M. Thomas, *Angew. Chem. Int. Ed. Engl.*, 1988, **27**, 1673.

54. L.J. King, D.O. Campbell, E.D. Collins, J.B. Knauer and R.M. Wallace, *Proc. of Sixth Intl. Zeolite Conf., Butterworth,* 1984.

55. T.R. Gaffney, *Current Opinion in Solid State and Material Science,* 1996, **1**, 69.

56. D.M. Ruthven, *Principles of Adorption and Adsorption Processes, Wiley Interscience (1984).*

57. S. Romero, A. Mosset and J.C. Trombe, *Euro. J. Solid State Inorg. Chem.*, 1997, **34**, 209; V. Kiritsis, A. Michaelides, S. Skoulika, S. Golhen and L. Ouahab, *Inorg. Chem.*, 1998, **37**, 3407.

58. H.W. Schmalle, P. Schneuwly, J. Ensling, P. Gutlich and S. Decurtins, *J. Am. Chem. Soc.*, 1994, **116**, 9521 and references therein.

59. S. Decurtins, H.W. Schmalle, H.R. Oswald, A. Linden, J. Ensling, P. Gütlich and A. Hauser, *Inorg. Chem.*, 1993, 32, 1888 and the references therein.

60. C. Mathoniere, S.G. Carling, D. Yusheng and P. Day, *J. Chem. Soc. Chem. Commun.*, 1994, 1551.

61. R. Wang, Y. Zhang, H. Hu, R.R. Frausto and A. Clearfield, *Chem. Mater.*, 1992, **4**, 864 and references therein.

62. C.L. Bowes and G.A. Ozin, *Adv. Mater.*, 1996, **8**, 13 and references therein.

63. G.H. Bonavia, R.C. Haushalter, S. Lu, C.J. O'Connor and J. Zubieta, *J. Solid State Chem.*, 1997, **132**, 144.

64. Clearfield, *Chem. Mater.*, 1998, **10**, 2801 and references therein; D.M. Poojary, H.L. Hu, F.L. Campbell and A. Clearfield, *Acta Crystallogr.*, 1993, **B49**, 996.

65. D. Riou, G. Férey, *J. Mater. Chem.*, 1998, **8**, 2733; B. Zhang, D.M. Poojary and A. Clearfield, *A. Inorg. Chem.*, 1998, **37**, 1844.

66. P.J. Zapf, D.J. Rose, R.C. Haushalter and J. Zubieta, *J. Solid State Chem.*, 1996, **125**, 182; *J. Solid State Chem.*, 1997, **132**, 438 and references therein.

66. P.J. Zapf, D.J. Rose, R.C. Haushalter and J. Zubieta, *J. Solid State Chem.*, 1996, **125**, 182; *J. Solid State Chem.*, 1997, **132**, 438 and references therein.

67. P. Losier and M.J. Zaworotko, *Angew. Chem. Int. Ed. Engl.*, 1996, **35**, 2779; M.J. Zaworotko, *Chem. Soc. Rev.*, 1994, 283.

68. O.M. Yaghi and H. Li, *Angew. Chem. Int. Ed. Engl.*, 1995, **34**, 207; O.M. Yaghi and H. Li, *J. Am. Chem. Soc.*, 1995, **117**, 10401; O.M. Yaghi and H. Li, *Nature*, 1995, **378**, 703.

69. V.R. Pedireddi, S. Chatterjee, A. Ranganathan and C.N.R. Rao, *J. Am. Chem. Soc.*, 1997, **119**, 10867.

70. D. Hagrman, C.J. Warren, R.C. Haushalter, C. Seip, C.J. O'Connor, Jr.R.S. Rarig, K.M. Johnson. III, Jr.R.L. LaBuca, J. Zubieta, *Chem. Mater.*, 1998, **10**, 3294.

71. N.N. Greenwood and A. Earnshaw, *Chemistry of Elements, Pergamon Press, New York*, 1993.

72. S.P. Farrell, T.W. Hambley and P.A. Lay, *Inorg. Chem.*, 1995, **34**, 757.

73. S. Kitagawa, T. Okubo, S. Kawata, M. Kondo, M. Katada, and H. Kobayashi, *Inorg. Chem.*, 1995, **34**, 4790.

74. S. Natarajan and A.K. Cheetham, *Chem. Commun.*, 1997, 1089.

75. Q. Gao, N. Guillou, M. Nogues, A.K. Cheetham and G. Ferey, *Chem. Mater.*, 1999, **11**, 2937; D. Riou and G. Ferey, *J. Mater. Chem.*, 1998, **8**, 2733; D. Riou, C. Serre and G. Ferey, *Microporous and Mesoporous Mater.*, 1998, **23**, 23.

76. G.B. Hix, D.S. Wragg, I. Bull, R.E. Morris and P.A. Wright, *Chem. Commun.*, 1999, 2421.

77. S. Ayyappan, A.K. Cheetham, S. Natarajan and C.N.R. Rao. *J. Solid State Chem.*, 1998, **139**, 207.

78. J.M. Thomas, R.H. Jones, R. Xu, J. Chen, A.M. Chippindale, S. Natarajan and A.K. Cheetham, *J. Chem. Soc. Chem. Commun.*, 1992, 929.

79. A.Choudhury, S. Natarajan and C.N.R. Rao, *Chem. Mater.*, 1999, **11**, 2316.

80. Q. Huo, R. Xu, S. Li, Z. Ma, J.M. Thomas, R.H. Jones, A.M. Chippindale, *J. Chem. Soc. Chem. Commun.*, 1992, 875.

81. A.Choudhury , S. Natarajan and C.N.R. Rao, *J. Solid State Chem.*, 1999, **146**, 538.

82. R. Deyrieux, C. Bero and A. Penelous, *Bull. Soc. Chim. Fr.*, 1973, 25.

83. R.C. McDonald, K. Eriks, *Inorg. Chem.*, 1980, **19**, 1237.

84. T.H. Jordan, L.W. Schroeder, B. Dickens, W.E.Brown, *Inorg. Chem.*, 1976, **15**, 1810.

87. S.J. Weigel, S.C. Weston, A.K. Cheetham and G.D. Stucky, *Chem. Mater.*, 1997, **9**, 1293; S.J. Weigel, J.C. Gabriel, E.G. Puebla, A.M. Bravo, N.J. Henson, L.M. Bull and A.K. Cheetham, *J. Am. Chem. Soc.*, 1996, **118**, 2427.

88. T. Song, M.B. Hursthouse, J. Chen, J. Xu, K.M. Abdul Malik, R.H. Jones, R. Xu and J.M. Thomas, *Adv. Mater.*, 1994, **6**, 679.

89. Dickens, E. Prince, L.W. Schroeder and T.H. Jordan, *Acta Crystallogr.*, 1974, **B30**, 1470.

90. A.M. Chippindale, V.A. Powell, L.M. Bull, R.H. Jones, A.K. Cheetham, J.M. Thomas, R. Xu, *J. Solid State Chem.*, 1992, **96**, 199.

91. Y. Piffard, A. Lachgar and M. Tournoux, *Rev. de. Chim. Miner.*, 1985, **22**, 101.

92. Y. Piffard, V. Verbeare, S. Oyetola, S. Courant and M. Tournoux, *Eur. J. Solid State Inorg. Chem.*, 1989, **26**, 113.

93. Y. Piffard, S. Oyetola, S. Courant and A. Lachgar, *J. Solid State Chem.*, 1985, **60**, 209.

94. U. Costantino, R. Vivani, V. Zima and E. Cernoskova, *J. Solid State Chem.*, 1997, **132**, 17 and references therein.